BACTERIAL CELLULOSE/THERMOPLASTIC POLYMER NANOCOMPOSITES

By

ELVIE ESCORRO BROWN

A thesis submitted in partial fulfillment of
the requirements for the degree of

MASTER OF SCIENCE IN CHEMICAL ENGINEERING

WASHINGTON STATE UNIVERSITY
Department of Chemical Engineering

MAY 2007

To the Faculty of Washington State University:

The members of the Committee appointed to examine the thesis of ELVIE ESCORRO BROWN find it satisfactory and recommend that it be accepted.

_____
Chair

_____

_____

ACKNOWLEDGMENT

Firstly, I would like to thank my advisor, Marie-Pierre Laborie for giving me the chance to work on a very interesting project. She has given me the freedom to explore on my own but her brilliant ideas and guidance never left me adrift. I am very grateful to my committee, James Lee and Eric Aston who shared their knowledge and imparted significant assistance in finishing my research. A special thanks goes to Bernard Van Wie for encouraging me to try M.S. degree, I never thought I'd go this far.

All of the WMEL personnel have become important to me not only for the help in my project but also for the friendship. For the two years that I was here, I bonded with impeccably wonderful people. Thank you very much and I hope to keep the communications with you.

I thank International Marketing Program for Agricultural Commodities and Trade (IMPACT) for providing financial support for my research and also for featuring me in their newsletter. I also would like to thank Society of Women Engineers (SWE) for the support during my first year of MS degree.

I do believe that there should be a bigger word than 'thank you' for the man who's always been there for all my highs and lows and the reason why I'm in this country; my husband, Alan. His unfading support has given me the strength and enthusiasm (my own drive amazes me sometimes).

I would like to express my heartfelt gratitude to my Mom and Dad, Loretta and Earl Brown; my Mama who's in the Philippines, Benita Escorro and the rest of the family for the encouragement and pride. They made me believe in myself. Success is sweet because of all of these wonderful people.

Most importantly, I like to thank God for everything, for I believe that his sacred blessings put me where I am right now.

BACTERIAL CELLULOSE/THERMOPLASTIC POLYMER NANOCOMPOSITES

Abstract

by Elvie E. Brown, M.S.
Washington State University
May 2007

Chair: Marie Pierre Laborie

Bacterial cellulose (BC) has many applications in membranes, electronics, textiles and especially in the biomedical field. For bacterial cellulose to be more effectively utilized in these applications, it is imperative to fine-tune its properties.

This research aims at engineering the morphology, composition and structure of BC-thermoplastic polymer nanocomposites by augmenting the growth medium of the cellulose-producing bacterium, *Acetobacter xylinum*, with the thermoplastic polymer, thereby manipulating BC biogenesis. It is hypothesized that addition of the thermoplastic polymer into the medium allows the development of intermolecular interactions with the BC fibers during cellulose crystallization into nanofibers, yielding a thermoplastic nanocomposite reinforced with finely dispersed BC nanofibers.

Engineering of the nanocomposites was done by varying the type or the amount of polymer added to the medium. Varying polymers by addition of poly(ethylene oxide) (PEO) or poly(vinyl alcohol) (PVA) into the medium both produced nanocomposites with dispersed BC nanofibers and showed polymer melting point depression. However, BC/PVA nanocomposite demonstrates considerable miscibility and interaction when compared to BC-PEO material by forming hydrogen bonds and also by having single glass

transition and degradation temperatures. Varying the amount of polymer added into the medium varied all the characterized properties. BC fiber dispersity, polymer chemical composition and nanocomposite surface roughness increased as polymer amount in medium increased. Also, thermal and mechanical stability increased as BC loading in the nanocomposite increased. These variations of properties illustrated that BC/PEO and BC/PVA nanocomposites can be engineered by BC biogenesis manipulation.

TABLE OF CONTENTS

Page

LIST OF TABLES

Page

LIST OF FIGURES

Page

Dedication

For Alan

CHAPTER I: INTRODUCTION

Applications of Bacterial Cellulose

Bacterial Cellulose (BC) has gained attention in the research realm for the favorable properties it possesses; such as its remarkable mechanical properties in both dry and wet states, porosity, water absorbency, moldability, biodegrability and excellent biological affinity (Shoda and Sugano 2005). Because of these properties, BC has a wide range of potential applications including use as a separation medium for water treatment (Brown 1989, Choi et al 2004), a specialty carrier for battery fluids and fuel cells (Brown 1989), a mixing agent, a viscosity modifier (Brown 1989, Jonas and Farah 1998), light transmitting optical fibers (Brown 1989), a biological substrate medium (Brown 1989, Watanabe et al 1993), food or food substitute (Miranda et al 1965, Brown 1989, Jonas and Farah 1998), lint-free specialty clothing (Brown 1989), optoelectronics devices (Nogi et al 2005), paper (Jonas and Farah 1998, Shah and Brown 2005), stereo diaphragms (Jonas and Farah 1998) and immobilization matrices of proteins or chromatography substances (Jonas and Farah 1998, Sokolnicki et al 2006). The prevalent application of BC is in the biomedical field, as it is highly useful for wound dressing (Hamlyn et al 1997, Cienchanska 2004, Legeza et al 2004, Wan and Millon 2005, Czaja et al 2006); artificial skin (Jonas and Farah 1998, Czaja et al 2007); dental implants; vascular grafts; catheter covering dressing (Wan and Millon 2005); dialysis membrane (Wan and Millon 2005, Sokolnicki et al 2006); coatings for cardiovascular stents, cranial stents (Wan and Millon 2005), membranes for tissue-guided regeneration (Wan and Millon 2005, Czaja et al

2007), tissue replacement, controlled-drug release carriers (Wan and Millon 2005), vascular prosthetic devices (Charpentier et al 2006), a scaffold for tissue engineering (Czaja et al 2007), and as artificial blood vessels (Klemm et al 2001, Backdahl et al 2006, Wan et al 2006). For BC to be suitable for these diverse applications, some of its properties must be modified. Modification of BC had been accomplished in the applications listed in Table I-1.

Applications	BC Product Processing	Ideal/Obtained Properties	References
Vascular prosthetic device (to replace diseased arteries)	-BC films are used to coat surface-treated medical-grade polyesters.	-Minimizes blood clotting and increases biocompatibility. -Has high mechanical strength in wet state, substantial permeability to water and gases, high water retention and low surface roughness.	(Charpentier et al, 2006)
Wound care product (wounds such as thermal burns)	-BC sheets were impregnated with drugs known as SOD (procel-Super), porviargol(Procel-PA) and Inerpan. -Never-dried BC sheets are immersed in chitosan solution. -BC grown statically in a chitosan-modified medium.	-Highly nanoporous, allowing transfer of antibiotics or medicines while serving as a physical barrier against external infections. -Wound healing accelerated. -High mechanical properties in wet state	(Hamlyn et al 1997, Ciechanska 2004, Legeza et al 2004, Czaja et al 2006)
Artificial blood vessel in microsurgery	-BC grown in a static culture molded in BASYC® tubes (a hollow-shaped tube mimicking blood vessel shape).	-High mechanical strength in wet state enormous water retention values, low surface roughness of inner surface. -Highly moldable in situ. -Can sustain a mean tensile force of 800mN.	(Klemm et al, 2001)
Tissue-engineered blood vessels	-BC grown in a tubular-shaped mold.	-Young modulus should match carotid arteries, about 3MPa. -Inner side of tubular BC must be smoother compared to the outside.	(Backdahl et al, 2006)
Optically transparent reinforcement for optoelectronics industry (for transparent polymers used for displays)	-BC sheets are impregnated with acrylic resins.	-Highly transparent due to its nanoscale fibers free from light scattering. -Low thermal coefficient. -Mechanical strength 5 times that of engineered plastics.	(Nogi et al, 2005)
Substrate for mammalian cell culture	-BC membrane grown statically and electrically charged.	-High permeability	(Watanabe et al, 1993)

Applications	BC Product Processing	Ideal/Obtained Properties	References
Cation-exchange membrane for industrial wastewater treatment	-BC membranes are modified with cation-exchangeable acrylic acid	-Tensile strength of 12MPa and elongation of 6%	(Choi et al, 2004)
Electronic paper	-BC sheets are doped with conductors for embedding of electronic dyes.	-Paper has high reflectivity and contrast. -Improved conductivity in BC.	(Shah and Brown, 2005)
Encapsulation membrane system for living tissues or protein enzymes	-Statically grown BC membrane.	-BC have the appropriate mass transfer parameters and membrane morphology	(Sokolnicki et al, 2006)

Table I-1. Bacterial cellulose applications.

Table I-1 illustrates that for specific applications, specific properties must be met. Note that from the applications mentioned above, and in Table I-1, biomedical dominion has substantial utilization. The need for biomedical materials has grown significantly over the years (Anderson 2006, Jagur-Grodzinski 2006) and for this need, BC is highly regarded for it has the suitable properties especially for regenerative medicine (Czaja et al 2007). Yet for biomedical application, properties such as thermal stability, strength, porosity, roughness, morphology and density are crucial (Rezwan et al 2006). Fine-tuning of these properties is imperative for BC to conform to the substituted environment (Jagur-Grodzinski 2006, Rezwan et al 2006). Table I-1 cites some of the necessitated modifications for BC properties. In this research, modification is directed at the biogenesis of BC.

In the next section, the synthesis of BC by bacterium *Acetobacter xylinum* is discussed, to provide insight into the plausible property fine-tuning method of BC.

Biogenesis of BC

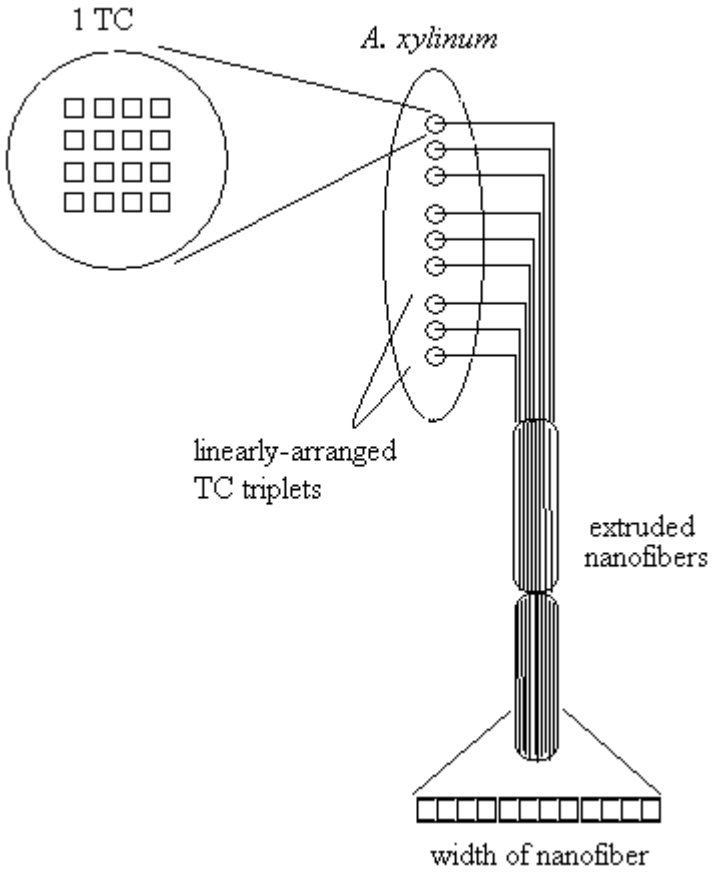

Figure I-1. Mechanism of BC formation by *Acetobacter xylinum*.

BC is a product of microbes' primary metabolic processes. It is produced by a species of Zoogloea, Sarcina, (Canale-Parola and Wolfe 1960), Salmonella, Rhizobium (Napoli et al 1975), Pseudomonas (Spiers et al 2003), Escherichia, Agrobacterium, (Matthysse et al 1995), Aerobacter, Achromobacter, Azotobacter, Alcaligenes, and Acetobacter. The most studied and most used BC-producing bacterium specie is *Acetobacter xylinum*, including the strains ATCC 23769, 10145, 53582, AX5 and many others (Klemm et al 2001). *Acetobacter xylinum* is an obligate aerobe bacterium usually

found in vinegar, alcoholic beverages, fruit juices, fruits, and vegetables, and most likely in rotting ones as well (Klemm et al 2001). The bacteria consume the sugar or carbohydrate from fruits as their main food. BC is formed on the air-liquid medium interface when the HS liquid medium (noted by Hestrin and Schramm, 1954, consisting of 2wt% D-glucose, 0.5wt% peptone, 0.5wt% yeast extract, 0.27wt% disodium phosphate, 0.115wt% citric acid) and distilled water is inoculated with a strain of *Acetobacter xylinum*. Glucose functions as the bacteria's carbon source, peptone as a nitrogen source, yeast extract as a vitamin source and citric acid and disodium phosphate as a buffer system for the medium.

The mechanism of BC formation by *Acetobacter xylinum* is depicted in Figure I-1 and implements as follows (Brown 1996). The bacterium extrudes linear glucan chains from its terminal complexes that are composed of few catalytic sites of extrusion. Approximately 10-100 linear glucan chains aggregate to form into twisting nanofibers. Some papers (Brown, 1976, Zaar 1977) refer to the different level of aggregated glucan chains as sub-elementary microfibrils or microfibrils, but this will be referred to collectively as nanofibers here. The nanofiber from a single bacterial cell with a rectangular cross section of 10-20 x 30-40Å aggregate further to form a ribbon with a diameter of about 70-80 nm. These ribbons are about 20μm long (Zaar 1977). The ribbons are spun into the liquid medium and intertwine with ribbons from other cells to form into a gelatinous suspension or pellicle (Brown 1996). The lateral dimension of BC increases as bacteria grow and as the population increases. During bacterial growth, new production sites for BC become available. Hence, the BC fibril or ribbon widens. At cell division, BC production sites are distributed between two daughter cells, which also increases BC

ribbon width (Zaar 1977). BC fibrils aggregate due to hydrogen bonding (Brett 2000) and Van der Waals forces. These forces cause the fibrils to interact, and they are held apart by adsorbed water layers. When the water layers evaporate, the hydroxyl groups of fibril chains associate irreversibly, and a highly crystalline cellulose sheet is formed (Colvin and Leppard 1977). When compared to plant cellulose, BC ribbons are only one one-hundredth in width (Shoda and Sugano 2005). The degree of polymerization (DP) of BC is usually between 2,000 and 6,000 (Jonas and Farah 1998). The morphology of BC depends on the growing culture environment. For a static culture, a leather-like pellicle of overlapping and intertwined ribbons forms (Jonas and Farah 1998). On the other hand, an agitated medium forms irregular BC granules and fibrous strands (Vandamme et al 1998).

The bacterium increases its population by consuming the glucose and oxygen initially dissolved in the liquid medium. When the oxygen has diminished, only the bacteria with access to air can continue their BC-producing activity. The bacteria below the surface are considered dormant, but can be reactivated by using the liquid as an inoculum for a new culture medium (Klemm et al 2001).

Given that BC is extruded as a very fine fibril, it is logical to start fine-tuning its morphology during biogenesis. These methods are examined in the next section.

Modification of BC

Alteration of BC morphology during its biogenesis is a concept adapted from researchers that use various polymers to investigate the facet of cellulose formation whether in plant cell wall or in BC (see Table I-2). As miscible polymers such as

hemicelluloses, cellulose derivatives and dyes are added into the BC-producing bacterium growth medium, the aggregation of nanofibers is altered due to the competitive adsorption of polymers in the medium. Polymerization and crystallization are separate mechanisms in BC biogenesis (Haigler et al 1980). Therefore, subsequent to BC polymerization, the polymer added in the medium can associate and co-crystallize with BC, producing an intimately blended composite material. The modification of bacterial cells is another way to alter BC morphology. However, this research concentrates on using miscible polymer to alter BC biogenesis.

Manipulating BC biogenesis can be a useful approach for fine-tuning BC properties to appropriate applications or for producing BC composites with tailored characteristics. A few researchers have undertaken this approach, including Ciechanska (2004), who fabricated modified BC by growing it in a chitosan-modified growth medium for wound dressing application, and Seifert et al (2004), who produced modified BC in a carboxymethylcellulose-, methylcellulose- and poly(vinyl alcohol)-modified medium to produce water-content-controlled BC for medically useful biomaterials. Biogenesis manipulation can presumably produce BC composites of nanoscale polymer interaction, given that BC fibrils and polymer can co-crystallize during ribbon formation and the fact that ribbon dimensions are in the nano scales. Moreover, the composites produced will have dispersed BC fibrils, as aggregation of the fibrils is controlled, which reduces dispersion (the major challenge in composite fabrication) (Stell, 1987).

Modification BC growth medium with:	**Resulting Properties or Modification (When Compared to Pure BC)**	**Reference**
Hemicellulose		
Xyloglucan	-Crystallite size of fibrils changed. -Aggregation of fibrillar units into ribbon assemblies broke down. -Lower stiffness or breaking stress. -Increased extensibility in uniaxial tension.	Uhlin et al 1995, Yamamoto et al 1996, Hirai et al 1998, Whitney et al 1999, Astley et al 2003
Xylan	-Ribbons were coherent, heavy bundles instead of flat and twisting. -Ribbon width decreased as aggregation of fibril subunits was controlled.	Uhlin et al, 1995
Pectin	-Increased extensibility and decreased breaking stress compared to pure BC.	Astley et al, 2003
Phosphomannan	-Fibrils are oriented in parallel. -Aggregation time of fibrils is delayed.	Ohad 1963, Ben-Hayyim and Ohad 1965, Uhlin et al 1995
Glucomannan, galactomannan	-Induced coalescence of fibrils and dramatic reduction of crystallinity.	Whitney et al 1998
Other Hemicellulosic polysaccharides: glucuronoxylan, arabinogalactan	-Crystallinity of BC was modified.	Iwata et al 1998
Cellulose derivatives		
Carboxymethyl Cellulose (CMC)	-In vivo cellulose ribbon formation prevented normal fasciation of fibril bundles into a typical ribbon. -Thinner ribbon width and smaller crystallite fibril size. -Aggregates and pellicle show birefringence, and contain crossed, superimposed layers of cellulose fibrils oriented in parallel. -Less resistant to stress.	Ohad 1963, Ben-Hayyim and Ohad 1965, Haigler et al 1982, Uhlin et al 1995, Yamamoto et al 1996, Hirai et al 1998
Cellulose derivatives (hydroxyethylcellulose, methylcellulose)	-In vivo cellulose ribbon formation was altered. -Fibril size was modified, and diameter was thinner.	Haigler et al 1982, Hirai et al 1998
Dyes		
Calcofluor White ST	-Morphology of BC is changed by preventing assembly of fibrils prohibiting crystallization, but BC is crystalline when dried.	Benziman et al 1980, Haigler et al 1980, Colvin and Witter 1983,
Congo Red	-Formation of the ribbon was prevented.	Colvin and Witter, 1983
Tinopal	-Support van der Waals force as initial step in cellulose crystallization.	Cousins and Brown, 1997
Antibiotics		
Nalidixic acid, chloramphenicol	-Elongates *A. xylinum* cells producing thicker, larger BC ribbons.	Yamanaka et al, 2000
Theinamycin, mecillinam	-Shortened *A. xylinum* cells producing thinner BC ribbons.	Yamanaka et al, 2000

Modification	Resulting Properties or modification (when compared to pure BC)	Reference
Others		
Dextransucrase and alternansucrase	-Produce soluble BC with new structure.	Doman et al, 1999
Lignin-carbohydrate complexes	-Crystallinity of BC modified. -BC is more resistant to alkali.	Iwata et al, 1998

Table I-2. Modification of BC Biogenesis.

Research Objectives

The aim of this study is to demonstrate that BC fiber-reinforced thermoplastic composites can be developed with engineered properties by growing BC in a growth medium that contains the thermoplastic polymer. The polymer is expected to disrupt the further aggregation of ribbons, producing very thin and long BC fibers that crystallize with the polymer and form into a nanocomposite. Reinforcement of polymer with nanoscale thin fibers produces superior composites with excellent properties (Coleman 2006) for the product. By including the thermoplastic polymer in the medium while BC was developing, the polymer interacts with BC in the nanoscale dimension. The produced nanocomposites are expected to be composed of dispersed fibers. Depending on the polymer miscibility with BC or the amount of polymer added to the medium, the nanocomposite morphology should be diverse, resulting in diverse properties; namely, density, strength, thermal properties, and composition. In other words, manipulation of growth medium composition may alter material properties leading to the engineering of a nanocomposite.

Two different polymers are used in this research, namely poly(ethylene oxide) (PEO) and poly(vinyl alcohol) (PVA). These two polymers have different molecular structures, one which has the ability to hydrogen-bond with cellulose and one which does

not. The difference in interaction between these polymers produces different trends in property modifications. Chapter II discusses the bacterial cellulose/PEO nanocomposite, while Chapter III discusses bacterial cellulose/PVA nanocomposites. For each polymer, different concentrations were applied in order to discover whether nanocomposite engineering can be accomplished with either polymer selection or polymer concentration variation.

In this project, two major hypothesis were proposed: that nanoscale dispersed BC reinforces thermoplastic polymer to form into a nanocomposite, and that engineered BC nanocomposites will be produced by BC biogenesis manipulation. Biotechnology and nanotechnology were employed to achieve and characterize BC composites of tailored properties. Characterization of nanoscale BC fibrils utilized Atomic Force Microscopy (AFM) and Transmission Electron Microscopy (TEM) for physical imaging. Compositional and molecular interaction analysis was accomplished with Thermogravimetric analysis (TGA) and Fourier Transform Infrared (FT-IR). Finally, thermal and mechanical properties were determined with Dynamic Scanning Calorimetry (DSC) and Dynamic Mechanical Analysis (DMA) instruments.

References

Anderson, J.M. (2006). The future of biomedical materials. *Journal of Materials Science: Materials in Medicine 17,* 1025-1028.

Astley, O.M., Chaliaud, E., Donald, A.M., & Gidley, M.J. (2003). Tensile deformation of bacterial cellulose composites. *International Journal of Biological Macromolecules 32*, 28-35.

Backdahl H., Helenius G., Bodin A., Nannmark U., Johansson B.R., Risberg B., & Gatenholm, P. (2006). Mechanical properties of bacterial cellulose and interactions with smooth muscle cells. *Biomaterials, 27*, 2141-2149.

Ben-Hayyim, G. & Ohad, I. (1965). Synthesis of Cellulose by *Acetobacter xylinum*. *Journal of Cell Biology, 25*, 191-207.

Benziman, M., Haigler, C.H., Brown, R.M., White, A.R. & Cooper, K.M. (1980). Cellulose Biogenesis: Polymerization and Crystallization are Coupled Processes in *Acetobacter xylinum*, *Proceedings of the National Academy of Sciences, 77,* 6678-6682.

Brett, C.T. (2000). Cellulose microfibrils in plants: Biosynthesis, deposition, and integration into the cell wall. *International Review of Cytology, 199*, 61-99.

Brown, R.M. Jr., Willison, J.H. & Richardson, C.L. (1976). Cellulose biosynthesis in *Acetobacter xylinum*: Visualization of the site of synthesis and direct measurement of the in vivo process. *Proceedings of the National Academy of Sciences, 73*, 4565-9.

Brown, R.M. Jr (1996). The biosynthesis of cellulose. *Journal of Macromolecular Science, Pure and Applied Chemistry, A33, 10*, 1345-1373.

Brown, R.M. (1989). Microbial cellulose as a building block resource for specialty products and processes therefore, *PCT Int. Appl. WO 8912107 A1*, 37.

Canale-Parol, E., & Wolfe, RS. (1960). Studies on *Sarcina Ventricula I.* Stock culture, *Journal of Bacteriology, 79*, 857-862 .

Charpentier, P.A., Maguire, A. & Wan, W. (2006). Surface modification of polyester to produce a bacterial cellulose-based vascular prosthetic device. *Applied Surface Science 252,* 6360-6367.

Choi, Y., Ahn, Y., Kang, M., Jun, H., Kim, I.S. & Moon, S. (2004). Preparation and characterization of acrylic acid-treated bacterial cellulose cation-exchange membrane, *Journal of Chemical Technology and Biotechnology 79*, 79-84.

Cienchanska, D. (2004). Multifunctional bacterial cellulose/chitosan composite materials for medical applications, *Fibres and Textiles in Eastern Europe, 12*, 69-72.

Coleman, J.N., Khan, U., & Gun'ko, Y.K. (2006). Mechanical reinforcement of polymers using carbon nanotubes. *Advanced Materials 18*, 689-706.

Colvin, J.R. & Leppard, G.G. (1977). The biosynthesis of cellulose by *Acetobacter xylinum* and Acetobacter acetigenus. *Canadian Journal of Microbiology*, 23, 701-709.

Colvin, J.R., Witter, D.E. (1983). Congo red and calcofluor white inhibition of *Acetobacter xylinum* cell growth of bacterial cellulose microfibril formation: Isolation and properties of a transient, extracellular glucan related to cellulose. *Protoplasma, 116,* 34-40.

Cousins, S.K. & Brown, R.M. Jr. (1997). X-ray diffraction and ultrastructural analyses of dye-altered celluloses support van der Waals forces as the initial step in cellulose crystallization. *Polymer*, 38, 897-902.

Czaja W., Krystynowicz A., Bielecki S., & Brown R.M. Jr. (2006). Microbial cellulose-the natural power to heal wounds. *Biomaterials*, 27, 145-51.

Czaja, W., Young, D.J., Kawechi, M. & Brown, R.M. Jr. (2007). The future prospects of microbial cellulose in biomedical applications, *Biomacromolecules*, 8, 1-12.

Doman, K., Kim, Y., Park, M. & Park, D.J. (1999). Modification of *Acetobacter Xylinum* bacterial cellulose using dextransucrase and alternansucrase. *Microbiol. Biotechnol., 9*, 704-708.

Haigler, C.H., Brown, R.M. Jr. & Benziman, M. (1980). Calcofluor White ST alters in vivo assembly of cellulose microfibrils. *Science*, 210, 903-905.

Haigler, C.H., White, A.R. & Brown, R.M. (1982). Alteration of in vivo cellulose ribbon assembly by carboxymethycellulose and other cellulose derivatives. *The Journal of Cell Biology*, 94, 64-69.

Hamlyn, P.F., Crighton, J., Dobb, M.G. & Tasker, A. (1997). Cellulose product. *UK Patent Application GB 2314856 A No. 9713991.9*.

Hestrin, S. & Schramm, M. (1954). Synthesis of cellulose by *Acetobacter Xylinum* 2. Preparation of freeze-dried cells capable of polymerizing glucose to cellulose. *Biochemical Journal*, 58, 345-352.

Hirai, A., Tsuji, M., Yamamoto, H. & Horii, F. (1998). In situ crystallization of bacterial cellulose III. Influences of different polymeric additives on the formation of microfibrils as revealed by transmission electron microscopy, *Cellulose*, 5, 201-213.

Iwata, T., Indrarti, L. & Azuma, J. (1998). Affinity of hemicellulose for cellulose produced by *Acetobacter Xylinum*. *Cellulose*, 5, 215-228.

Jagur-Grodzinski, J. (2006). Polymers for tissue engineering, medical devices, and regenerative medicine. Concise general review of recent studies. *Polymers for Advanced Technologies*, 17, 395-418.

Jonas, R. & Farah, L.F. (1998). Production and application of microbial cellulose. *Polymer Degradation and Stability*, 59, 101-106.

Joseph, G., Rowe, G.E., Margaritis, A. & Wan, W. (2003). Effects of polyacrylamide-co-acrylic acid on the cellulose production by *Acetobacter Xylinum*. *Journal of Chemical Technology and Biotechnology*, 78, 964-970.

Klemm, D., Schumann, D., Udhardt, U. & Marsch, S. (2001). Bacterial synthesized cellulose - artificial blood vessels for microsurgery. *Progress in Polymer Science,* 26, 1561-1603.

Legeza, V.I., Galenko-Yaroshevskii, V.P., Zinov'ev, E.V., Paramonov, B.A., Kreichman, G.S., Turkovskii, I.I., Gumenyuk, E.S., Karnovich, A.G. & Khripunov, A.K. (2004). Effects of new wound dressings on healing of thermal burns of the skin in acute radiation disease. *Bulletin of Experimental Biology and Medicine*, 138, 311-315.

Matthysse, A.G., Thomas, D. & White, A.R. (1995). Mechanisms of cellulose synthesis in *Agrobacterium tumefaciens*. *Journal of Bacteriology*, 177, 1076-1081.

Miranda, B.T., Miranda, S.R., Chan, L.P. & Saqueton, E.R. (1965). Some studies on nata. *Nat. Appl. Sci. Bull. (Univ. Philippines),* 19, 67-79.

Napoli, C., Dazzo, F. & Hubbell, D. (1975). Production of cellulose microfibrils by *Rhizobium*. *Applied Microbiology*, 30, 123-131.

Nogi, M., Handa, K., Nakagaito, A.N. & Yano, H. (2005). Optically transparent bionanofiber composites with low sensitivity to refractive index of the polymer matrix. *Applied Physics Letters* 87, 1-3.

Ohad, I. (1963). Biosynthesis of cellulose VII. The interaction of soluble carboxymethylcellulose with cellulose fibres. *Bulletin of Research Council Of Israel*, 11A, 279-285.

Rezwan, K., Chen, Q.Z., Blaker, J.J. & Boccaccini, A.R. (2006). Biodegradable and bioactive porous polymer/inorganic composite scaffolds for bone tissue engineering. *Biomaterials,* 27, 3413-3431.

Seifert, M., Hesse, S., Kabrelian, V. & Klemm, D. (2004). Controlling the water content of never dried and reswollen bacterial cellulose by the addition of water soluble polymers to the culture medium. *Journal of Polymer Science: Part A: Polymer Chemistry*, 42, 463-470.

Shah, J. & Brown, R.M. Jr. (2005). Towards electronic paper displays made from microbial cellulose. *Applied Microbiology and Biotechnology*, 66, 352-355.

Shoda, M. & Sugano, Y. (2005). Recent advances in bacterial cellulose production. *Biotechnology and Bioprocess Engineering*, 10, 1-8.

Sokolnicki, A.M., Fisher, R.J., Harrah, T.P. & Kaplan, D.L. (2006). Permeability of bacterial cellulose membranes. *Journal of Membrane Science,* 272, 15-27.

Spiers, A.J., Bohannon, J., Gehrig, S.M. & Rainey, P.B. (2003). Biofilm formation at the air-liquid interface by the *Pseudomonas fluorescens* SBW25 wrinkly spreader requires an acetylated form of cellulose. *Molecular Microbiology*, 50, 15-27.

Stell, G. & Rikvold, P.A. (1987). Polydispersity in fluids, dispersions, and composites; some theoretical results. *Chemical Engineering Communications*, 51, 233-60.

Uhlin, K.I., Atalla, R.H. & Thompson, N.S. (1995). Influence of hemicellulose on the aggregation patterns of bacterial cellulose. *Cellulose,* 2, 129-144.

Vandamme, E.J., De Baets, S., Vanbaelen, A., Joris, K. & De Wulf, P. (1998). Improved production of bacterial cellulose and its application potential. *Polymer Degradation and Stability*, 59, 93-99.

Wan, W.K. & Millon, L.E. (2005). Poly(vinyl alcohol)-bacterial cellulose nanocomposite. *U.S. Pat.Appl.,* Publ. US 2005037082 A1, 16.

Wan, W.K., Hutter, J.L., Millon, L. & Guhados, G. (2006). Bacterial cellulose and its nanocomposites for biomedical applications. *ACS Symposium Series,* 938, 221-241.

Watanabe K., Eto Y., Takano S., Nakamori S., Shibai H. & Yamanaka S. (1993). A new bacterial cellulose substrate for mammalian cell culture. *Cytotechnology*, 13, 107-114.

Whitney, E., Gothard, M., Mitchell, J. & Gidley, M. (1999). Roles of cellulose and xyloglucan in determining the mechanical properties of primary plant cell walls. *Plant Physiology*, 121, 657-663.

Whitney, S.E.C., Brigham, J.E., Darke, A.H., Reid, J.S.G. & Gidley, M.J. (1998). Structural aspects of the interaction of mannan-based polysaccharides with bacterial cellulose. *Carbohydrate Research,* 307, 299-309.

Yamamoto, H., Horii, F. & Hirai, A. (1996). In situ crystallization of bacterial cellulose II. Influences of different polymeric additives on the formation of cellulose I_α and I_β at the early stage of incubation. *Cellulose,* 3, 229-242.

Yamanaka, S., Ishihara, M. & Sugiyama, J. (2000). Structural modification of bacterial cellulose. *Cellulose*, 7, 213-225.

Zaar, K. (1977). The biogenesis of cellulose by *Acetobacter Xylinum*. *Cytobiologie European Journal Of Cell Biology*, 16, 1-15.

CHAPTER II: BIOENGINEERING OF BC/PEO NANOCOMPOSITES

Introduction

Bacterial cellulose (BC) has long been used in a variety of applications in the paper, food and electronic industries (Jonas and Farah 1998, Miranda et al 1965, Nishi et al 1990, Shah and Brown 2005, Yano et al 2005). Owing to its high porosity, water absorbance, mechanical properties, moldability and biocompatibility, bacterial cellulose has recently attracted a great deal of attention for its biomedical applications (Czaja et al, 2007). For instance, bacterial cellulose has been successfully used for wound dressings (Ciechanska et al 1998, Czaja et al 2006, Legeza et al 2005) and for vascular implants (Klemm et al 2001, Klemm et al 1999). The potential of BC for in vitro and in vivo tissue regeneration also continues to be explored and shows great promise (Backdahl et al 2006, Helenius et al 2006, Svensson et al 2005, Watanabe et al 1993).

For such biomedical applications, it is highly desirable to fine-tune the properties of the scaffold or implant to match the properties of the material it intends to regenerate or replace (Guilak et al, 2003). To that end, researchers have engaged in augmenting bacterial cellulose. For instance, bacterial cellulose has been soaked in hydroxyapatite to develop a composite scaffold for bone regeneration (Hong et al 2006, Wan et al 2006). Bacterial cellulose has also been augmented by immersion in solutions of polyacrylamide and gelatin yielding hydrogels with improved toughness (Yasuda et al, 2005). Similarly,

immersion of bacterial cellulose in polyvinyl alcohol has yielded hydrogels with a wide range of mechanical properties for use in cardiovascular implants (Millon et al, 2006).

Another means of altering the properties of bacterial cellulose has been to manipulate its biosynthesis in order to synthesize copolymers or miscible blends. Ciechanska (2004) produced bacterial cellulose in a chitosan-enriched medium, thus developing BC/chitosan copolymers with improved water absorbance and mechanical properties. Seifert et al (2004) added cellulose derivatives and polyvinyl alcohol in a culture medium yielding a composite material with improved water retention and ion absorption capacities.

The latter synthetic approach, in which bacterial cellulose is modified with a host polymer during biosynthesis, is particularly interesting because competitive adsorption of the host polymer present in the culture medium can alter the crystallization of cellulose, affording a range of morphologies (Haigler et al 1982, Hirai et al 1998, Uhlin et al 1995, Yamamoto et al 1996). In the case of *Acetobacter xylinum*, glucan chain sheets are extruded from the membrane enzymatic terminal complexes (Brown et al, 1976) into the aqueous medium where they crystallize into 3 to 7nm wide microfibrils of cellulose I_{α} primarily, which then aggregate into twisting ribbons with cross-sections 3-4nm x 70-140nm (Haigler et al 1980, Yamanaka et al 2000, Zaar 1977). When a compatible polymer is present in the culture medium, competitive adsorption of the host polymer onto the glucan chains hinders the crystallization into microfibrils and ribbons, resulting in smaller crystalline structures (Haigler et al, 1982). Many studies have investigated cellulose derivatives, hemicelluloses and pectins to shed light on the biogenesis of cellulose and the

plant cell wall (Haigler et al 1982, Hirai et al 1998, Uhlin et al 1995, Yamamoto et al 1996). As expected, BC biogenesis is altered when polymers are compatible, resulting in a range of microfibril and ribbon dimensions, crystalline allomorphs, and crystallinity indices.

It is therefore clear that fiber morphology can be tailored by adding a water-soluble polymer in the culture. In particular, this biotechnological tool could be used to develop bacterial cellulose reinforced thermoplastic nanocomposites, in which composition and morphology may be tailored to yield desirable properties for a specific application. Yet this potential to simultaneously tailor cellulose morphology and its dispersion into a polymer matrix for the manufacture of nanocomposites with improved properties has been largely unexploited.

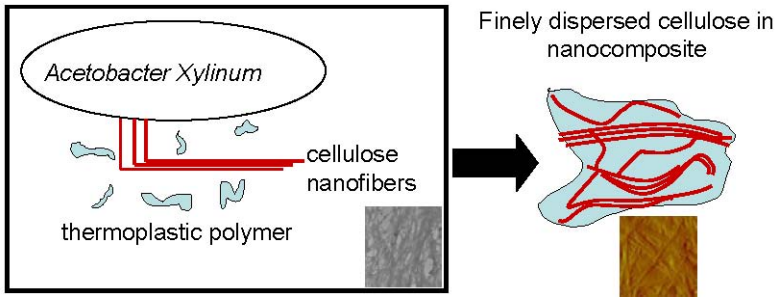

Bioengineering bacterial cellulose reinforced thermoplastic nanocomposites

This research aims to demonstrate that by modifying the culture conditions of bacterial cellulose with a thermoplastic polymer, polyethylene oxide (PEO), nanocomposites can be synthesized with a range of chemical compositions and morphologies. PEO is of particular interest, as it is biocompatible and water-soluble (seal

et al 2001). By tailoring the chemical composition and morphology of the BC/PEO nanocomposites, it is further hypothesized that properties can be fine-tuned. This goal is of significance not only for improved utilization of bacterial cellulose in biomedical applications, but also as a demonstration of how biotechnology and nanotechnology can be combined to afford greater flexibility in nanocomposite manufacture.

Materials and Methods

Production of the Starter Culture

Acetobacter xylinum of the strain 23769 was purchased from American Type Culture Collection. For the bacterium growth, the standard Hestrin-Schramm (HS) medium was prepared and pH was adjusted to 5.0 with hydrochloric acid (Hestrin and Schramm 1954). The starter culture was first autoclaved at 121ºC for 15 minutes and then inoculated with the bacterium strain in static conditions at 29º±1C in an incubator. After 1 week of production, the cellulose had materialized at the air-liquid interface and was sampled for preparing the BC/PEO products.

Production of Bacterial Cellulose into Polyethylene Oxide Modified Media

Polyethylene oxide (M_w=1.10^5 g/mol) was purchased from Fisher Scientific and added into the culture medium to produce 5 different culture media with PEO concentrations of 0.5, 1, 2, 3, and 5 w/w %. After 2 days of incubation in static cultures, some of the suspension material was used to start agitated cultures and develop a

homogeneous cellulose/PEO product. Under these conditions, strings of materials started appearing on the second day of growth, and were harvested by filtering with gauze on the seventh day.

Some of the material was prepared for transmission electron microscopy (TEM) by passing it through 400-mesh copper TEM grids. For Fourier transform infrared spectroscopy (FTIR), transparent films were produced by flattening a few milligrams of the harvested product into 3x3cm^2 plastic bags and freeze-drying. For all other characterizations, 7x3.3cm^2 films were prepared by first freeze-drying for up to 24 hours and then compression-molding into 1.0±0.4mm thick specimens using an hydraulic press operating at room temperature under 4000 psi. All products were kept in vacuumed desiccators with anhydrous calcium sulfate until characterization. Three batches of BC/PEO products were grown for each media, yielding trireplicate samples for each characterization technique. Weights were recorded at all stages of the sample preparation. Control PEO samples were also prepared by placing PEO into an aqueous solution and following the same sample preparation as for the BC/PEO products.

Transmission Electron Microscopy (TEM)

The loaded TEM grids were lightly washed with distilled water, dried and stained with 1% uranyl acetate. TEM images were acquired at 60K and at 100K magnifications on a JEOL 1200 EX operating at 100kV. Microfibril dimensions were computed from 5 to 10 measurements.

Atomic Force Microscopy (AFM)

A 5x3x0.6 mm sample was retrieved from the compression-molded product and bonded to the AFM sample disc. The sample surface was trimmed with a glass knife mounted on a cryogenic ultramicrotome (PowerTome-X, RMC Products). Imaging was then performed in tapping mode on a Veeco Multimode AFM equipped with a NanoScope IIIa controller. A silicon cantilever having a resonance frequency around 200-300 kHz and a nominal spring constant of 40 N/m was used along with a 3x3 μm J-scanner. The scan rate was 1.5 Hz and integral and proportional gains were 0.3 and 0.5 respectively. Ribbon dimensions were computed from 5 to 10 measurements.

Thermogravimetric Analysis (TGA)

To determine chemical composition and thermal stability, the control PEO, the pure BC and the composite products were characterized in accordance with ASTM E 113133 on a Rheometrics STA 625. Approximately 10 to 25 mg of powder material was retrieved from the compression molded products and placed in aluminum pans in the TGA operating under 90ml/min N_2 flow. After equilibration at 30ºC for 5 minutes, the sample was heated to 600ºC at 20ºC/minute, at which point only ashes remained. Raw and derivative weight data were used to determine decomposition temperatures and associated weight losses. Trireplicate measurements were performed.

Fourier Transform Infrared Spectroscopy (FTIR)

FTIR spectra of the neat components and the BC/PEO products were obtained in transmission mode on a Nicolet Nexus 670 FT-IR. While the freeze-dried cellulose and

BC/PEO products could be analyzed as thin films, the control PEO required pressing into KBr pellets. Forty scans were acquired in the 4000 – 600 cm^{-1} range with a resolution of 4 cm^{-1}. Samples were analyzed in duplicate.

Differential Scanning Calorimetry (DSC)

Approximately 11±4 mg of powder material from the compression molded products was loaded in aluminum pans and placed in a Mettler Toledo DSC 822e. All DSC experiments were conducted under N2 flow of 80ml/min and controlled cooling with liquid nitrogen. A first temperature program was conducted to record glass transition temperatures (T_g), melting temperature (T_m) and heat of fusion (ΔH_f). Namely, after heating to 100ºC at 20ºC/min for 5 minutes in order to erase thermal histories, the samples were cooled down to -100 ºC at a cooling rate of 30ºC/min. A second heating scan was conducted from -100ºC to 100ºC at 20ºC/min and thermal transitions were recorded. For pure bacterial cellulose, the first heating ramp was conducted to 180ºC in order to pyrolyze the proteinaceous material, followed by a similar cooling to -50ºC and a reheat scan to 200ºC.

Equilibrium melting temperatures of PEO, T_m^0, were also determined with the Hoffman-Weeks method (Hoffman and Weeks 1962) for the control PEO and for the BC/PEO product obtained when the culture medium was augmented with 1% w/w PEO. First the samples were heated to 100°C for 10 minutes to ensure complete melting of PEO, after which they were quenched to a crystallization temperature, T_c, and allowed to fully crystallize over a 30-minute period. The crystallization temperatures were 34, 36, 48, 50,

and 52ºC for control PEO, and 34, 36, 40, 42, 44ºC for the BC/PEO product. The samples were then quenched to 20ºC. Upon reheating to 100ºC at 20ºC/min, the melting temperature corresponding to each crystallization temperature was recorded and the T_m^0 PEO in both materials determined (Hoffman and Weeks 1962).

Dynamic Mechanical Analysis (DMA)

The compression molded samples were cut into strips of approximate dimensions 34x7x0.6 mm^3 and tested in tension mode on a Rheometrics RSA II. The thermal history of the samples was first erased by heating to 100°C, with the exception of the control PEO, which was heated to only 55°C. The samples were then cooled to 30°C and a dynamic strain sweep was performed at 1Hz to determine the linear viscoelastic range. The samples were further cooled (30°C/min) to -70°C. Using a dynamic strain level less than $4x10^{-4}$ within the linear viscoelatic range and a frequency of 1Hz, a temperature scan was then conducted at 2°C/min to 100°C. Duplicate measurements were performed.

Results and Discussion

Morphology of Cellulose/PEO Nanocomposites

We anticipated that the modification of the HS medium with a host polymer capable of interacting with cellulose would alter the aggregation and crystallization of glucan chains into cellulose microfibrils and ribbons, possibly resulting in smaller and more dispersed structures (Haigler et al 1982, Hirai et al 1998, Uhlin et al 1995,

Yamamoto et al 1996). To evaluate PEO's effect on cellulose crystallization into microfibrils, TEM images of the products retrieved from the standard HS medium, and from the HS medium modified with 1, 3, and 5% of PEO, were captured at 60K and 100K magnifications (Figure II-1). When grown in the standard HS medium, cellulose microfibril bundles that were 17±5nm in width formed from *Acetobacter Xylinum,* and this result was slightly larger than that previously observed under static conditions (Zaar 1977, Brown, 1996). These are referred to as nanofibers in this paper.

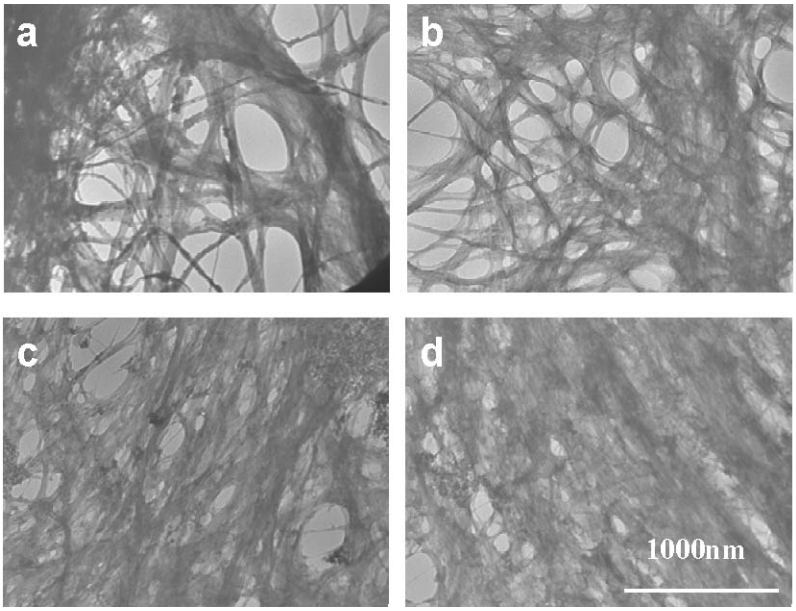

Figure II-1**.** TEM images (60K) of bacterial cellulose/polyethylene oxide (BC/PEO) products: BC grown in a) Hestrin-Shramm (HS) medium, b) HS medium with 1% PEO, c) HS medium with 3% PEO and d) HS medium with 5% PEO.

The nanofibers then aggregated into ribbons, 94±3nm in width in accordance with previous reports (Zaar 1977, Brown, 1996). As PEO was added to the HS medium, two changes in the structure and morphology of BC were apparent from the TEM images (Figure II-1). First, the nanofibers became smaller, with width of 10.0±1.6nm, 9.8±1.0nm,

and 9.7±1.5nm with addition of 1%, 3% and 5% PEO respectively. Concomitantly, the contour of the nanofibers gradually faded until they could no longer be distinguished in the TEM images when grown in a 5% PEO content HS medium. Adsorption and coating of PEO on the surface of the nanofibers could hinder the uranyl acetate from distinctively staining the BC, thereby inhibiting contrast and observation by TEM.

A second change that occurred in the structure of bacterial cellulose as the PEO content increased was the alteration of cellulose nanofibers into ribbons. With 1 % PEO in the HS medium, ribbons of 49±6nm in diameter formed, and these were approximately half the size of the neat bacterial cellulose ribbons (Figure II-1b). With the further addition of PEO in the HS medium, the aggregation into ribbons was again no longer clear from the TEM images, yet the nanofibers appeared to be held together by PEO.

While TEM provided information on the in vivo crystallization of cellulose, nanofiber dispersion in the PEO matrix was further visualized with AFM (Figure II-2). Samples changed from having a fibrous and rough surface for neat BC to having a smoother surface in the BC/PEO products, thereby facilitating AFM imaging. The smallest structures that could be distinguished with AFM were the ribbons. In neat BC, ribbons of 104±16nm in width were clearly imaged and in good agreement with the 94±3nm measured with TEM (Figure II-2a). As PEO concentration in the culture medium increased from 0.5% to 5%, the composite ribbons grew smaller, from 86±9nm to 54±4nm, until the sample became too smooth to distinguish individual ribbon contours at 5% PEO addition. At the same time, the ribbons appeared to be bonded together into aggregates,

whose width increased from 195±71nm to 204±50nm as the PEO content in the HS medium increased from 3% to 5%.

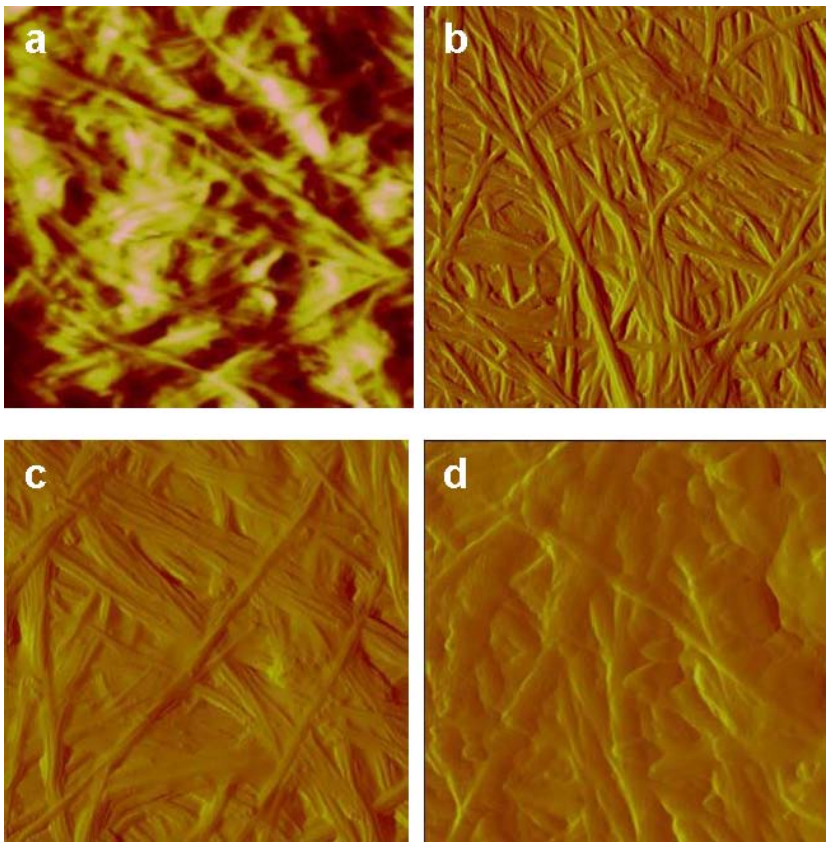

Figure II-2. Atomic force microscopy(AFM) topographical images (3x3 μm) of bacterial cellulose/ polyethylene oxide (BC/PEO) products obtained in a) Hestrin-Shramm (HS) medium, b) HS medium with 1% PEO, c) HS medium with 3% PEO and d) HS medium with 5% PEO.

The morphological changes observed with TEM and AFM corroborate the proposition that by adding PEO to the HS medium during BC synthesis, the dimensions of the microfibrils and ribbons can be tailored. This also confirms the fact that this manufacturing approach allows PEO to blend with cellulose structures, whether they aggregate in 10 nm wide cellulose nanofibers, 100 nm wide ribbons or 200 nm wide ribbon aggregates. In other words, truly dispersed cellulose/PEO nanocomposites are

manufactured. Clearly, by augmenting the culture medium with the desired matrix polymer, an excellent dispersion of high aspect ratio nanofibers can be achieved, circumventing the aggregation issue that is often encountered with other nanoscale reinforcements such as cellulose whiskers (Azizi Samir et al, 2004, Ljungberg et al, 2005). Fine dispersion of bacterial cellulose nanofibers into the thermoplastic matrix is remarkable, considering that their aspect ratio is estimated at 1000 (well above the typical cellulose whisker aspect ration of 100) (Zaar 1977, Azizi Samir et al 2005). To evaluate whether this manufacturing approach could also be used to tailor the chemical composition of cellulose/PEO nanocomposite, TGA was conducted.

Tailoring the Chemical Composition of Cellulose/PEO Nanocomposites

In Figure II-3, the TGA traces for control PEO, neat BC and one BC/PEO nanocomposites are shown along with the derivative traces. The derivative traces are best suited to determine the decomposition temperatures for each constituent, whereas the weight traces can be used to determine the weight loss associated with the decomposition of this constituent (ASTM E 1131). For PEO, a single degradation temperature was clearly observed at 410±1°C. For bacterial cellulose, decomposition involved three stages with peak temperatures at 159±4°C, 218±4°C and 346±3°C. These three weight loss stages were attributed to the loss of bound water, and loss of proteinaceous material from the bacterial cells and cellulose respectively (George et al 2005). In the BC/PEO nanocomposites, all four degradation temperatures were clearly observed, allowing calculation of the weight percent of bound water, proteinaceous material, cellulose and PEO (Figure II-3). In addition, the ash content was computed from the final weight.

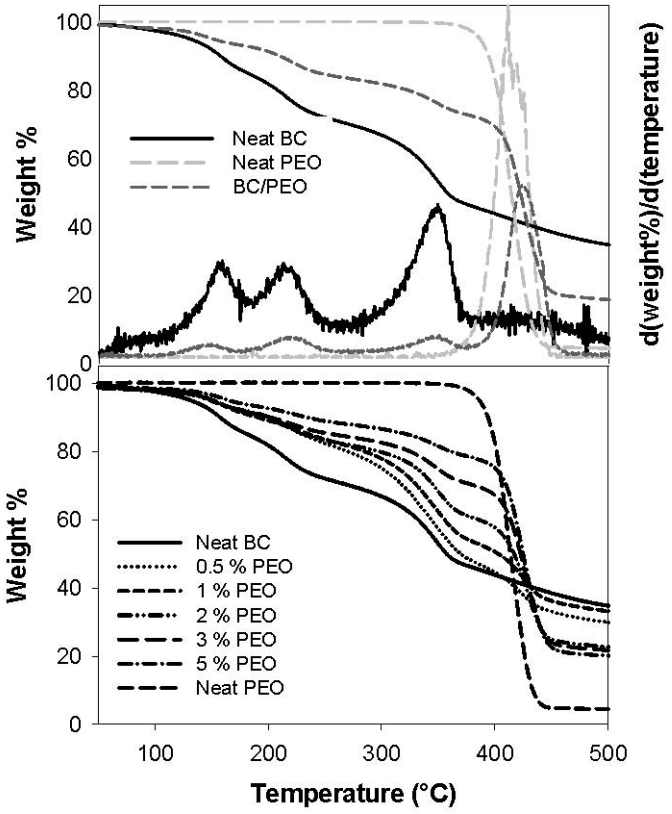

Figure II-3. Thermogravimetric analysis illustrating the original and derivative curves for the pure cellulose (BC) and polyethylene oxide (PEO) (top) and for all the BC/PEO nanocomposites as a function of the culture medium modification (bottom).

	Degradation temperature (°C)				Chemical composition (weigth %)				BC:PEO
	water	protein	cellulose	PEO	water	protein	cellulose	PEO	w/w %
Pure BC	158.5±4.1	217.9±3.5	346.4±2.4	-	18.6±4.3	19.6±3.8	61.8±11.4	-	100:0
Control PEO	-	-	-	410.3±0.7	-	-	-	100.0	0:100
BC in .5% PEO	152.3±4.0	219.4±5.3	345.7±7.0	425.9±3.2	14.8±6.4	15.7±7.0	41.1±6.4	28.4±3.1	59:41
BC in 1% PEO	157.8±2.3	210.7±25.8	350.7±2.3	428.3±3.5	17.0±2.45	13.3±6.7	37.0±8.2	32.7±3.5	53:47
BC in 2% PEO	154.6±4.0	218.0±1.6	351.4±1.8	428.6±0.6	11.1±1.5	13.2±1.2	24.8±4.3	50.9±3.7	33:67
BC in 3% PEO	159.2±5.8	222.5±3.6	351.6±1.7	427.3±1.5	11.0±2.0	11.1±1.5	17.7±4.1	60.2±6.3	23:77
BC in 5% PEO	160.8±1.0	224.9±7.5	348.3±4.3	425.3±4.8	9.5±1.7	7.8±0.5	12.0±1.8	70.7±3.5	15:85

Table II-1. Degradation temperature and chemical composition of bacterial cellulose (BC) and polyethylene oxide (PEO) and their nanocomposites.

As expected, modification of the culture medium with various concentrations of PEO resulted in a range of thermal stabilities (Figure II-3). This range stemmed in turn from a range of chemical compositions. By increasing the PEO concentration in the HS medium from 0.5wt% to 5wt%, the PEO content in the nanocomposite increased. In parallel with the reduction in the Table 1 cellulose content, the contents in bound water, proteinaceous material, and ash also decreased (Table II-1). This is expected, since the bound water is linked to the cellulose and the proteinaceous material and ash contents are linked to the bacteria cells. In fact, with the experimental conditions of this study, the BC:PEO w/w ratio in the nanocomposites varied from 59:41 to 15:85, suggesting that any blend composition could be attained by appropriately modifying the culture medium (Table II-1).

It is also interesting to note that the degradation temperature of the PEO was increased by approximately 15°C in the nanocomposite compared to the control PEO (Figure II-3 and Table II-1). In other words, dispersion of cellulose nanofibers into the PEO matrix increased the thermal stability of PEO. This increase in thermal stability may have arisen from strong intermolecular interactions between PEO and cellulose nanofibers. This thermal stabilization of PEO by cellulose contrasts with previous observations on solvent cast cellulose whiskers/PEO, possibly indicating enhanced dispersion and miscibility in the present biosynthetic approach.

With the ability to tailor chemical composition in the final nanocomposites, yields of glucose conversion into cellulose and also PEO incorporation into the composite could be computed. The conversion yield of glucose into cellulose decreased from 32% in the

standard HS medium to the 10-20% range with the addition of PEO in the culture medium. Simultaneously, PEO incorporation into the nanocomposites decreased from 40% to 16% , when PEO concentration in the HS medium increased from 0.5 to 5%.

The TGA results therefore confirm the hypothesis that the present manufacturing approach allows tailoring the chemical composition of bacterial cellulose reinforced thermoplastic nanocomposites. Altogether, it is clear that chemical composition, nanofiber dimensions and dispersion in the polymer matrix can be tailored by manipulating the growth condition of bacterial cellulose in a polymer matrix solution. This is likely also true for PEO, because cellulose and PEO can develop favorable interactions (Kondo and Sawatari 1994, Kondo et al 1994, Nishio et al 1989). CH_2 asymmetric stretching of PEO shifted from 2890 for pure PEO to 2883cm^{-1} in the BC/PEO composite, suggesting a decrease in PEO crystallinity (Bailey and Koleske 1976) (Figure II-4). Cellulose morphology was also altered, as evidenced by the change in the 750 and 710 cm^{-1} absorption bands that are characteristic of the I_α and I_β crystalline allomorphs respectively (Yamamoto et al 1996). As PEO content increased in the composite, the I_β/I_α allomorph ratio, measured from the intensity ratio of the respective absorption bands, increased from 1.01 for neat bacterial cellulose to 1.28 and 1.31 in BC/PEO composites (Table II-2). The presence of PEO in the culture medium therefore favored cellulose crystallization into the more stable I_β allomorph as previously observed with other culture modifications. The increase in production of the I_β allomorph is consistent with the observed crystallization into finer microfibrils as PEO content increased (Yamamoto et al, 1996).

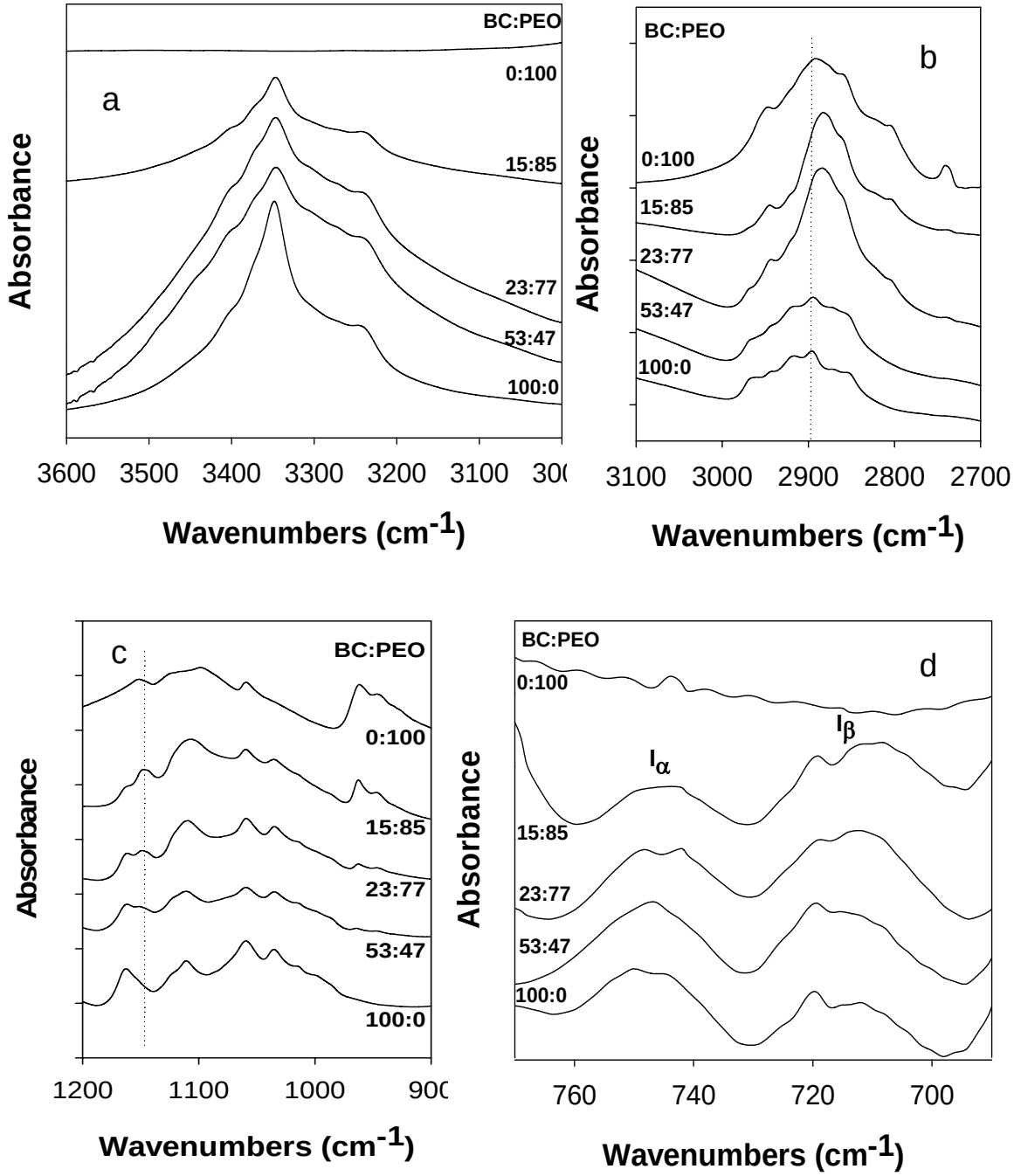

Figure II-4. FTIR spectra of bacterial cellulose (BC)/ polyethylene oxide (PEO) nanocomposites as a function of BC:PEO w/w ratio.

To further evaluate miscibility and interactions between the two polymers, the main thermal transitions, glass transition temperatures (T_g) and melting temperatures (T_m), were evaluated and compared to those of the neat components. The DSC scans of the BC/PEO composites indicated that the T_g of PEO and cellulose and the T_m of the PEO in the nanocomposites were around -50°C, 0°C and 60°C respectively (Figure II-5). The crystallinity index of the PEO in the composite material was also computed from the heat of fusion, using a ΔH_f for pure crystalline PEO of 201.2 J/g (Mark, 1999) (Table II-2). Cellulose T_g varied greatly between -20°C to 20°C as a result of the different water contents and plasticizing effects (Salmen and Back 1977) in the nanocomposites and therefore was not considered for evaluating miscibility. On the other hand, the T_g of PEO was clearly detected for all nanocomposites at around –50°C, independent of composition (Table II-2).

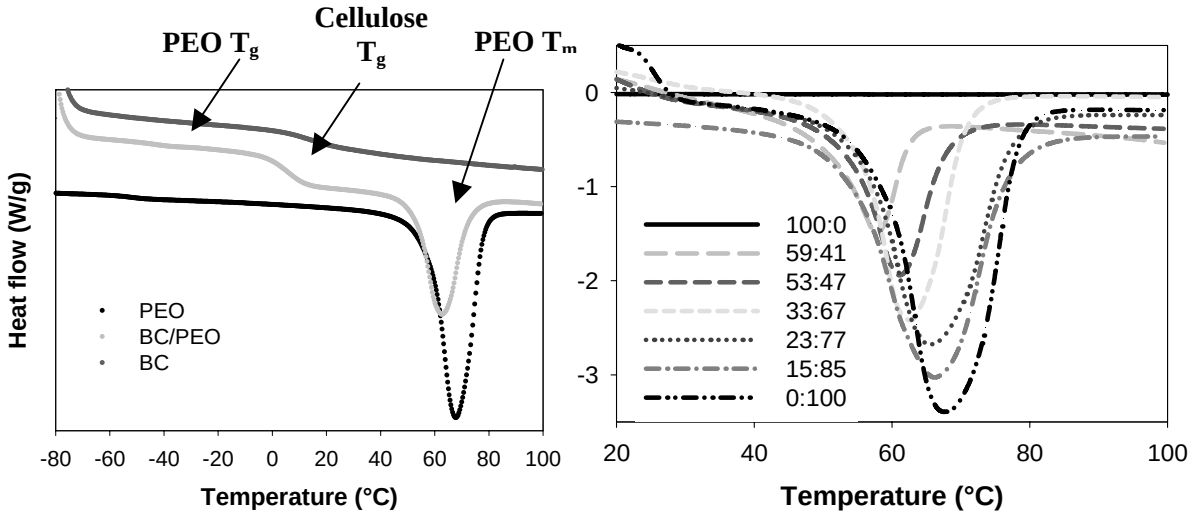

Figure II-5. Differential scanning calorimetry thermograms illustrating the determination of the glass transition and melting temperatures in the nanocomposite (left) and the variation in the melting endotherm of polyethylene oxide (PEO) as a function of the BC:PEO w/w ratio (right).

	Polyethylene oxide			Bacterial cellulose			
BC:PEO (w/w)	Tg (°C)	Tm (°C)	Xc	Iβ/Iα	nanofiber width	ribbon width	aggregate width (nm)
100:0				0.97 ± 0.02	17.1±5.2	104±16	-
59:40	-50.1±5.6	59.8±1.4	0.21±0.07	-	-	-	-
53:47	-49.7±3.7	61.7±3.1	0.36±0.22	1.06 ± 0.15	10.0±1.6	86±9	-
33:67	-48.4±1.0	63.2±1.3	0.49±0.05	-	-	-	-
23:77	-48.4±3.0	66.1±4.6	-	1.27±0.23	9.8±1.0	54±4	195±71
15:85	-51.0±2.0	68.1±2.8	0.49±0.06	1.31±0.18	9.7±1.5	-	204±50
0:100	-52.4±0.4	68.1±0.6	0.67±0.01	-	-	-	-

Table II-2. Thermal transitions and other morphological characteristics of polyethylene oxide (PEO) and bacterial cellulose (BC) in nanocomposites of varying BC:PEO ratios.

In contrast, the T_m and heat of fusion of the PEO was greatly reduced by the presence of cellulose in the nanocomposites (Figure II-5). This depression of the PEO T_m of approximately 10°C was accompanied by a large drop in crystallinity from about 67% to 21% (Table II-2). The T_m and crystallinity index of PEO decreased proportionally to the cellulose content in the nanocomposite. These results are similar to those obtained on tunicin whiskers/PEO nanocomposites (Azizi Samir et al, 2004). In PEO/tunicin whiskers composites, the T_g of PEO was unaffected by the addition of up to 30% cellulose whisker, whereas the T_m and crystallinity index of PEO were significantly depressed by the presence of cellulose. The diameter of the PEO spherulites was also found to decrease from approximately 200 microns to 10 microns with addition of 10% cellulose whiskers. This behavior was ascribed to cellulose whiskers acting has a nucleating surface for PEO, but also sterically hindering spherulitic growth due to their fine dispersion into the PEO (Azizi Samir et al, 2004). Although the PEO was of higher molecular weight (1.10^6 g/mol)

than in the present study, similar morphological effects likely contributed to the depression in melting temperature and crystallinity in the BC/PEO nanocomposites. That is, in presence of bacterial cellulose, PEO crystallization was hindered by the dispersion of cellulose nanofibers yielding smaller and less stable crystals. Aside from morphological effects, the depression in melting points may have also arisen from thermodynamic effects of miscibility between cellulose and PEO (Kondo and Sawatari 1994, Nishio et al 1989).

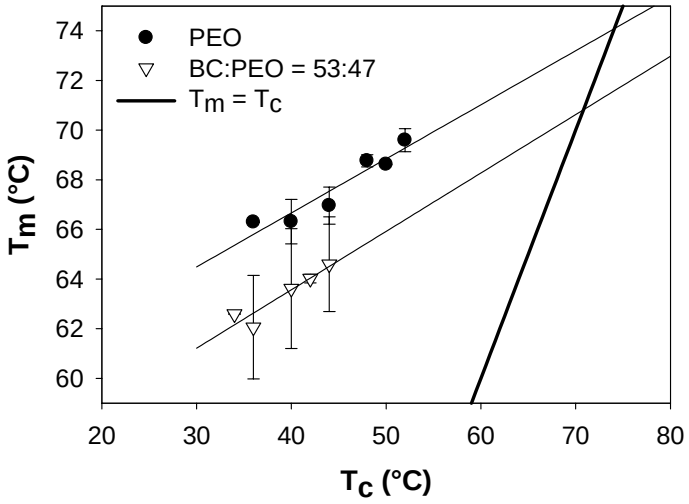

Figure II-6. Hoffman-Weeks plots for determining the equilibrium melting temperatures in control polyethylene oxide (PEO) and in a bacterial cellulose (BC)/PEO nanocomposite.

Molecular interactions and miscibility in polymer blends are best evaluated in the framework of the Flory-Huggins theory (1953) of polymer miscibility and the thermodynamic interaction parameter χ_{12} that is calculated from depression in the equilibrium melting temperature, T_m^0. In that objective, the T_m^0 of PEO in the control

PEO sample and also in the nanocomposite with BC:PEO w/w ratio of 53:47 was evaluated with the Hoffman-Weeks method (1962). As expected the melting temperature (T_m) increased linearly with the crystallization temperature (T_c) (Figure II-6). Linear regression of the data and extrapolation to $T_m=T_c$ yielded both the stability parameter, φ, and the T_m^0 according to the equation for isothermal crystallization (Hoffman and Weeks 1962, Nishi and Wang 1975):

$$T_m^0 - T_m = \phi(T_m^0 - T_c)$$

A stability parameter of 0.22±0.04 and 0.24±0.05 was thus obtained in the control PEO sample and in the nanocomposite respectively, comparable to the value of 0.24±0.07 obtained on water cast PEO with a similar molecular weight (Fuller et al, 2001). Positive stability parameters indicated relatively unstable crystals. More importantly, the similarity in stability parameters in both systems indicated that any difference in T_m^0 was due to thermodynamic rather than morphological effects. In the control PEO, T_m^0 was calculated at 74.1°C, in accordance with the literature (Fuller et al, 2001). In the nanocomposite T_m^0 was depressed to 70.1°C, supporting the hypothesis of exothermic interactions between PEO and BC in this system. To further evaluate the magnitude of the exothermic interactions in the blend, χ_{12} was estimated from equilibrium melting temperature depression:

$$1/T_m - 1/T_m^0 = -R(V_{2u}/\Delta H_{2u})[\ln v_2/V_2 + (1/V_2 - 1/V_1)v_1 + Bv_1^2/RT_m]$$

In this equation, T_m^0 is the equilibrium melting point of PEO and T_m is the observed equilibrium melting point of PEO in the nanocomposite). Subscripts 1 and 2 refer to cellulose and PEO, respectively, and v is the volume fraction, V the molar volume, V_{2u} the molar volume of the repeating units of PEO, ΔH_{2u} the enthalpy per mole of repeating units of PEO, B the interaction energy density and R the gas constant. V_1 and V_2 are large, and hence the entropic contribution to melting point depression could be neglected (Nishi and Wang, 1975), leaving only the enthalpic contribution to equilibrium melting point depression as:

$$T_m^0 - T_m = -T_m^0 (V_{2u} / \Delta H_{2u}) B v_1^2$$

The Flory-Huggins interaction parameter was then determined from B as:

$$B = RT_m (\chi_{12} / V_{1u})$$

Using densities of 1.51 and 1.09 g/cm^3 (at 75°C) for cellulose and PEO (Nishio et al 1989) respectively the volume fraction for the BC:PEO blend was computed and the melting point depression was plotted against volume fraction. The slope of the plot allowed calculating B using $\Delta H_u / V_{2u}$=240 J/cm, and finally, χ_{12} using V_{1u} = 107 cm^3/mol as determined from the molar mass and density of cellulose (Nishio et al 1989, Mark 1999). A slope of 17.3ºC was thus calculated, yielding a χ_{12} of –1.90 at 75ºC. Although this negative value should be taken with caution, considering the number of data points, it is consistent with previous observations of thermodynamic miscibility in PEO/cellulose blends with χ_{12} at -0.67 (Nishio et al, 1989) and at -0.4 (Fuller et al, 2001). In the BC/PEO

nanocomposite, however, the negative magnitude of the χ_{12} is much greater than that previously observed in solvent-cast blends (Kondo and Sawatari 1994, Nishio et al 1989), suggesting that the integrated manufacturing approach used in this study allowed for greater exothermic interactions than in solvent-cast blends. Additional Van der Waals forces and H-bonds may augment the enthalpic contribution to miscibility in the BC/PEO nanocomposites (Kondo and Sawatari, 1994). The existence of additional intermolecular interactions is also consistent with the increased thermal stability of PEO observed in the BC/PEO nanocomposites, in contrast with previous studies on water-cast blends of cellulose whiskers and PEO (Azizi Samir et al 2004).

Physical and Mechanical Properties of BC/PEO Nanocomposites

Pure bacterial cellulose dries in the form of irregular granules and fibrils that have a coarse structure and are remarkably brittle. In contrast, the nanocomposites were in the form of fibrous material that could be easily molded into resilient and bendable films. The surface topography of the nanocomposites changed with chemical composition. As the BC:PEO ratio decreased from 59:40 to 15:85, the nanocomposites became smoother, with RMS roughness dropping to the subnanometer level as measured from AFM (Figure II-7). This indicated that in the nanocomposites, the surface roughness may be tailored from chemical composition, which may be of particular interest for biomaterial applications that require specific surface properties and adhesion.

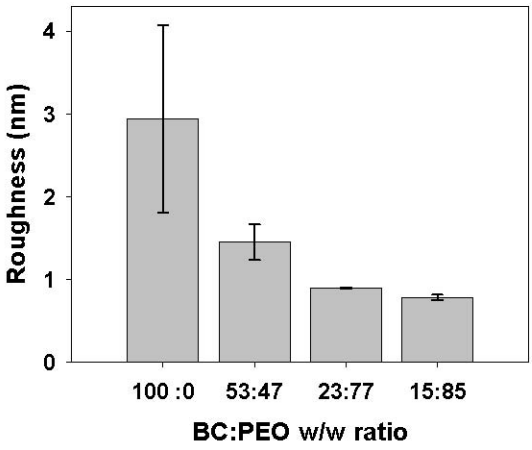

Figure II-7. Root mean square roughness bacterial cellulose (BC)/polyethylene oxide (PEO) nanocomposites as a function of BC:PEO w/w ratio.

The linear mechanical behavior of the nanocomposites was also evaluated in tensile mode under dynamic loading (Figure II-8). Note that neat bacterial cellulose was not tested, as it was too brittle to be handled. The storage modulus of both pure PEO and cellulose/PEO nanocomposites decreased slightly, from -70ºC to about 60ºC, with no apparent T_g (Figure II-8). Interestingly, the nanocomposites with higher BC content had higher sub ambient modulus, although the differences were small. As the melting point of PEO approached around 60°C, the dramatic drop in E' that was observed in the control PEO was significantly reduced by the cellulose reinforcement. Again, the modulus drop decreased with increasing cellulose content in the nanocomposites. At a BC:PEO ratio of 59:41, there was almost no noticeable drop in E' at the melting point of PEO. Clearly, cellulose provided significant thermal stabilization of PEO properties. A similar behavior has been observed in tunicin whiskers/PEO nanocomposites, and was ascribed to the formation of a rigid percolating cellulose nanocrystals network (Azizi Samir et al, 2005).

The much greater aspect ratio of bacterial cellulose (1000) compared to tunicin nanocrystals (70) may further explain the large reinforcing effect in BC/PEO nanocomposites. The lower crystallinity index in nanocomposites having higher cellulose content also likely contributed to the observed stabilization.

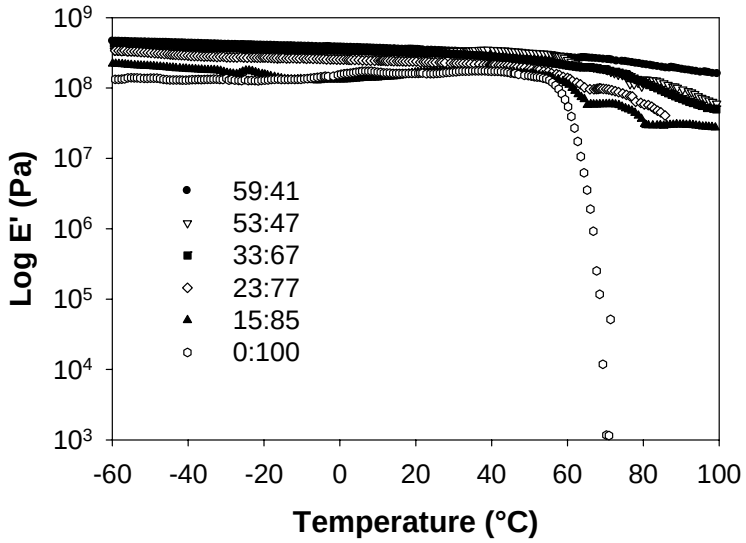

Figure II-8. Storage tensile modulus E' versus temperature at 1 Hz for nanocomposites of varying BC:PEO w/w ratios.

Conclusions

The potential of manipulating the biogenesis of bacterial cellulose to produce fiber-reinforced thermoplastic nanocomposites of controlled chemical composition, morphology and properties was demonstrated. By modifying the culture medium of bacterial cellulose with various concentrations of polyethylene oxide, nanocomposites were produced with BC:PEO w/w ratios ranging from 15:85 to 59:41. As PEO content increased, the cellulose

crystallized into smaller nanofibers (20 to 10 nm in width) and smaller ribbons (100 to 50nm in diameter) that were finely dispersed into PEO and formed 200 nm wide ribbon aggregates. At the same time, the I_β cellulose allomorph became more prominent and the crystallinity and melting temperature of PEO decreased. The morphological modifications of PEO are ascribed to the fine dispersion of cellulose nanofibers into the PEO matrix, but also to strong intermolecular interactions such as H-bonding, as demonstrated by FTIR and by the negative thermodynamic interaction parameter χ_{12}=-1.90. As expected, the thermal and mechanical properties of the nanocomposites depended on chemical composition and morphology. Regardless of cellulose content, the thermal decomposition temperature of PEO increased by 15°C. When tested in tension, BC effectively reinforced the PEO matrix in the glassy and rubbery states, and most significantly, above the melting temperature of PEO. The reinforcing effect was proportional to the cellulose content. Surface roughness was also significantly reduced with increasing PEO content.

References

American Society for Testing Materials, Standard Test Method for Compositional Analysis by Thermogravimetry. In *ASTM E1131-03*, Philadelphia, PA, 2003; Vol. 14.02.

Azizi Samir, M. A. S., Alloin, F. & Dufresne, A. (2005). Review of recent research into cellulosic whiskers, their properties and their application in nanocomposite field. *Biomacromolecules* 6, 612-626.

Azizi Samir, M.A.S., Alloin, F., Sanchez, J.Y., & Dufresne, A. (2004). Cellulose nanocrystals reinforced poly(oxyethylene). *Polymer,* 45, 4149-57.

Azizi Samir, M.A.S., Alloin, F., Sanchez, J.Y., El Kissi, N. & Dufresne, A. (2004). Preparation of cellulose whiskers reinforced nanocomposites from an organic medium suspension. *Macromolecules,* 37, (4), 1386-93.

Azizi Samir, M.A.S., Chazeau, L., Alloin, F., Cavaille, J.Y., Dufresne, A. & Sanchez, J.Y. (2005). POE-based nanocomposite polymer electrolytes reinforced with cellulose whiskers. *Electrochimica Acta,* 50, 3897-3903.

Backdahl H., Helenius G., Bodin A., Nannmark U., Johansson B.R., Risberg B., & Gatenholm, P. (2006). Mechanical properties of bacterial cellulose and interactions with smooth muscle cells. *Biomaterials, 27*, 2141-2149.

Bailey, F. E. & Koleske, J. V. (1976). *Poly(ethylene oxide)*. Academic Press: New York, 173.

Brown, R.M. Jr (1996). The biosynthesis of cellulose. *Journal of Macromolecular Science, Pure and Applied Chemistry, A33, 10*, 1345-1373.

Brown, R.M. Jr., Willison, J.H. & Richardson, C.L. (1976). Cellulose biosynthesis in *Acetobacter xylinum*: Visualization of the site of synthesis and direct measurement of the in vivo process. *Proceedings of the National Academy of Sciences, 73*, 4565-4569.

Cienchanska, D. (2004). Multifunctional bacterial cellulose/chitosan composite materials for medical applications, *Fibres and Textiles in Eastern Europe, 12*, 69-72.

Ciechanska, D., Struszczyk, H. & Guzinska, K. (1998). Modification of bacterial cellulose. *Fibres & Textiles in Eastern Europe,* 6, 61-65.

Czaja, W., Young, D.J., Kawechi, M. & Brown, R.M. Jr. (2007). The future prospects of microbial cellulose in biomedical applications, *Biomacromolecules*, 8, 1-12.

Czaja W., Krystynowicz A., Bielecki S., & Brown R.M. Jr. (2006). Microbial cellulose-the natural power to heal wounds. *Biomaterials*, 27, 145-51.

Flory, P. J. (1953). *Principles of polymer chemistry*. Cornell University Press: Ithaca, 672.

Fuller, C.S., MacRae, R.J., Walther, M. & Cameron, R.E. (2001). Interactions in poly(ethylene oxide)-hydroxypropyl methylcellulose blends. *Polymer,* 42, 9583-92.

George, J., Ramana, K.V., Sabapathy, S.N., Jagannath, J.H. & Bawa, A.S. (2005). Characterization of chemically treated bacterial (Acetobacter xylinum) biopolymer: Some thermo-mechanical properties. *International Journal of Biological Macromolecules,* 37, 189-94.

Guilak, F., Butler, D.L., Goldstein, S.A., Mooney, D.J. (2003). *Functional Tissue Engineering*. Springer: New-York, 426.

Haigler, C.H., Brown, R.M. Jr. & Benziman, M. (1980). Calcofluor White ST alters in vivo assembly of cellulose microfibrils. *Science*, 210, 903-905.

Haigler, C.H., White, A.R. & Brown, R.M. (1982). Alteration of in vivo cellulose ribbon assembly by carboxymethycellulose and other cellulose derivatives. *The Journal of Cell Biology*, 94, 64-69.

Helenius, G., Backdahl, H., Bodin, A., Nannmark, U., Gatenholm, P. & Risberg, B. (2006). In vivo biocompatibility of bacterial cellulose. *Journal of Biomedical Materials Research Part A,* 76A, 431-8.

Hestrin, S. & Schramm, M. (1954). Synthesis of cellulose by *Acetobacter Xylinum* 2. Preparation of freeze-dried cells capable of polymerizing glucose to cellulose. *Biochemical Journal*, 58, 345-352.

Hirai, A., Tsuji, M., Yamamoto, H. & Horii, F. (1998). In situ crystallization of bacterial cellulose III. Influences of different polymeric additives on the formation of microfibrils as revealed by transmission electron microscopy, *Cellulose*, 5, 201-213.

Hoffman, J.D. & Weeks, J.J. (1962). Melting process and equilibrium melting temperature of poly(chlorotrifluoroethylene). *J. Research Natl. Bur. Standards,* 66A, 13-28.

Hong, L., Wang, Y.L., Jia, S.R., Huang, Y., Gao, C. & Wan, Y.Z. (2006). Hydroxyapatite/bacterial cellulose composites synthesized via a biomimetic route. *Materials Letters,* 60, 1710-3.

Jonas, R. & Farah, L.F. (1998). Production and application of microbial cellulose. *Polymer Degradation and Stability*, 59, 101-106.

Klemm, D., Schumann, D., Udhardt, U. & Marsch, S. (2001). Bacterial synthesized cellulose - artificial blood vessels for microsurgery. *Progress in Polymer Science,* 26, 1561-1603.

Klemm, D., Udhardt, U., Marsch, S. & Schumann, D.I. (1999). Cellulose. BASYC, bacterially synthesized cellulose. Miniaturized tubes for microsurgery. *Polymer News,* 24, 377-378.

Kondo, T. & Sawatari, C. (1994). Intermolecular Hydrogen-Bonding in Cellulose Poly(Ethylene Oxide) Blends - Thermodynamic Examination Using 2,3-Di-O-Methylcelluloses and 6-O-Methylcelluloses as Cellulose Model Compounds. *Polymer,* 35, 4423-4428.

Kondo, T., Sawatari, C., Manley, R.S. & Gray, D.G. (1994). Characterization of Hydrogen-Bonding in Cellulose Synthetic-Polymer Blend Systems with Regioselectively Substituted Methylcellulose. *Macromolecules,* 27, 210-215.

Legeza, V.I., Galenko-Yaroshevskii, V.P., Zinov'ev, E.V., Paramonov, B.A., Kreichman, G.S., Turkovskii, I.I., Gumenyuk, E.S., Karnovich, A.G. & Khripunov, A.K. (2004). Effects of new wound dressings on healing of thermal burns of the skin in acute radiation disease. *Bulletin of Experimental Biology and Medicine*, 138, 311-315.

Ljungberg, N., Bonini, C., Bortolussi, F., Boisson, C., Heux, L. & Cavaille, J. Y. (2005). New nanocomposite materials reinforced with cellulose whiskers in atactic polypropylene: Effect of surface and dispersion characteristics. *Biomacromolecules,* 6, 2732-2739.

Mark, J.E. (1999). *Polymer data handbook*. Oxford University Press: New York, 1018.

Millon, L.E., Mohammadi, H. & Wan, W.K. (2006). Anisotropic polyvinyl alcohol hydrogel for cardiovascular applications. *Journal of Biomedical Materials Research Part B-Applied Biomaterials,* 79B, 305-311.

Miranda, B.T., Miranda, S.R., Chan, L.P. & Saqueton, E.R. (1965). Some studies on nata. *Nat. Appl. Sci. Bull. (Univ. Philippines),* 19, 67-79.

Nishi, T. & Wang, T.T. (1975). Melting point depression and kinetic effects of cooling on crystallization in poly(vinylidene fluoride)-poly(methyl methacrylate) mixtures. *Macromolecules,* 8, 909-915.

Nishi, Y., Uryu, M., Yamanaka, S., Watanabe, K., Kitamura, N., Iguchi, M. & Mitsuhashi, S. (1990). The Structure and Mechanical-Properties of Sheets Prepared from Bacterial Cellulose .2. Improvement of the Mechanical-Properties of Sheets and Their Applicability to Diaphragms of Electroacoustic Transducers. *Journal of Materials Science,* 25, 2997-3001.

Nishio, Y., Hirose, N. & Takahashi, T. (1989). Thermal analysis of cellulose/poly(ethylene oxide) blends. *Polymer Journal,* 21, 347-351.

Salmen, N.L. & Back, E.L. (1977). The influence of water on the glass transition temperature of cellulose. *Tappi Journal,* 60, 137-140.

Seal, B.L., Otero, T.C. & Panitch, A. (2001). Polymeric biomaterials for tissue and organ regeneration. *Materials Science & Engineering R-Reports,* 34, 147-230.

Seifert, M., Hesse, S., Kabrelian, V. & Klemm, D. (2004). Controlling the water content of never dried and reswollen bacterial cellulose by the addition of water-soluble polymers to the culture medium. *Journal of Polymer Science, Part A: Polymer Chemistry,* 42, 463-70.

Shah, J. & Brown, R.M. Jr. (2005). Towards electronic paper displays made from microbial cellulose. *Applied Microbiology and Biotechnology*, 66, 352-355.

Svensson, A., Nicklasson, E., Harrah, T., Panilaitis, B., Kaplan, D.L., Brittberg, M. & Gatenholm, P. (2005). Bacterial cellulose as a potential scaffold for tissue engineering of cartilage. *Biomaterials,* 26, 419-341.

Uhlin, K.I., Atalla, R.H. & Thompson, N.S. (1995). Influence of hemicellulose on the aggregation patterns of bacterial cellulose. *Cellulose,* 2, 129-144.

Wan, Y.Z., Hong, L., Jia, S.R., Huang, Y., Zhu, Y., Wang, Y.L. & Jiang, H.J. (2006). Synthesis and characterization of hydroxyapatite-bacterial cellulose nanocomposites. *Composites Science and Technology,* 66, 1825-32.

Watanabe K., Eto Y., Takano S., Nakamori S., Shibai H. & Yamanaka S. (1993). A new bacterial cellulose substrate for mammalian cell culture. *Cytotechnology*, 13, 107-114.

Yamamoto, H., Horii, F. & Hirai, A. (1996). In situ crystallization of bacterial cellulose II. Influences of different polymeric additives on the formation of cellulose I_α and I_β at the early stage of incubation. *Cellulose,* 3, 229-242.

Yamanaka, S., Ishihara, M. & Sugiyama, J. (2000). Structural modification of bacterial cellulose. *Cellulose*, 7, 213-225.

Yano, H., Sugiyama, J., Nakagaito, A.N., Nogi, M., Matsuura, T., Hikita, M. & Handa, K. (2005). Optically transparent composites reinforced with networks of bacterial nanofibers. *Advanced Materials***,** 17, 153-155.

Yasuda, K., Gong, J.P., Katsuyama, Y., Nakayama, A., Tanabe, Y., Kondo, E., Ueno, M. & Osada, Y. (2005). Biomechanical properties of high-toughness double network hydrogels. *Biomaterials***,** 26, 4468-75.

Zaar, K. (1977). The biogenesis of cellulose by *Acetobacter Xylinum*. *Cytobiologie European Journal Of Cell Biology*, 16, 1-15.

CHAPTER III: BIOENGINEERING OF BC/PVA NANOCOMPOSITES

Introduction

Bacterial cellulose (BC) has gained considerable attention for its very broad potential applications that include membranes, food, textile, chromatography and biomaterials (Jonas and Farah, 1998). BC's exciting application in biomedicine such as in vascular prosthetic devices (Charpentier et al, 2006), skin substitutes (Czaja et al, 2007), artificial blood vessels (Klemm, 2001) and other organ substitutes provide the motivation for this project. For BC to be suitable for such applications, some of its properties must be fine-tuned to match the essential attributes necessary for biomedical use. For example, BC's strength have to be manipulated for organ substitutes, and its porosity shall be manipulated for biological separation media (Rezwan et al, 2006).

The main objective of this research is to demonstrate that BC's unique properties, such as its fiber morphology, density, thermal and mechanical characteristics can be schemed by manipulating its biogenesis. This objective has already been demonstrated in a previous study that used poly(ethylene oxide) (PEO) to modify the growth medium of BC-producing bacterium. In the present study, poly(vinyl alcohol) (PVA) is used. PVA has OH groups and can hydrogen bond with cellulose. Also, its structure and solubility parameter is much closer to that of cellulose, suggesting that greater miscibility may be attained in the PVA/cellulose system compared to the PEO/cellulose system. Molecular structures of PEO, PVA and cellulose are shown in Figure III-1.

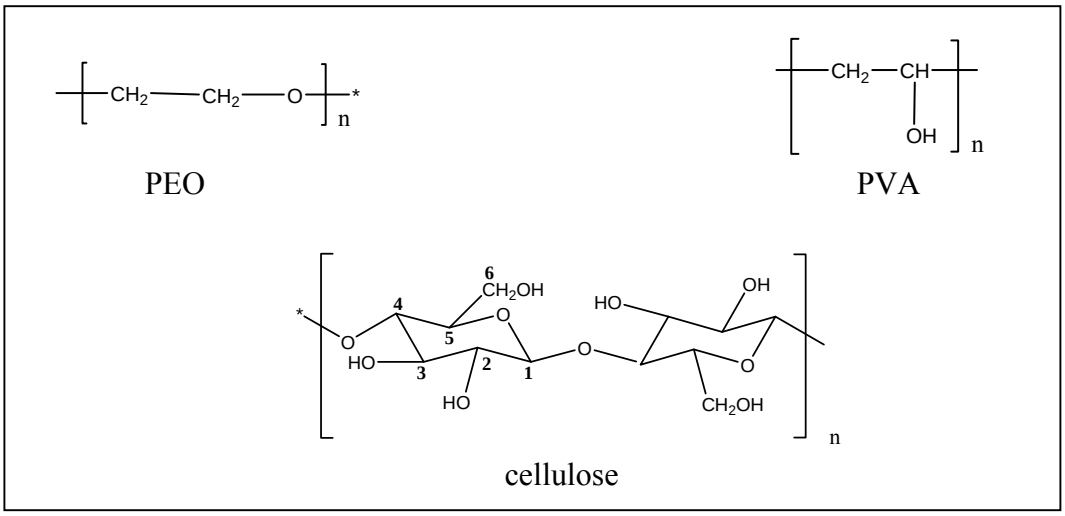

Figure III-1. Molecular Structures of cellulose and PVA.

The solubility parameter (δ), which is the square root of cohesive energy density, provides an indication of possible miscibility and intermolecular interactions between two polymers, as it accommodates three types of interaction forces: dispersion (d), polar (p) and hydrogen bonding (h). Polymers with similar solubility parameters can develop intermolecular interactions or are miscible. One approach to determine solubility parameters is to use the theory of functional group contributions (VanKrevelen and Hoftyzer, 1976). Equations and computation of (δ) and Δδ (differences in δ of BC and PEO or PVA) are detailed in Appendix C. A value of $\Delta\delta \leq 5$ means that the two polymers are miscible. Table III-1 enumerates the computed δ and Δδ, using the Hoy method (VanKrevelen and Hoftyzer 1976). The difference in the solubility parameter between PEO and BC is much larger than 5, so only minor interactions are expected between the two components. The value of Δδ for PVA and BC is only 3.9, and thus a close interaction and significant miscibility is expected when these two polymers are blended. Miscibility is

known to affect characteristics of nanocomposites, such as thermal properties (Simon, 2003).

Material	Solubility parameter (δ) $(J/cm^3)^{1/2}$	$\Delta\delta$ $(J/cm^3)^{1/2}$
BC	31.9	
PEO	21.4	15.6
PVA	28.8	3.9

Table III-1. Solubility parameters.

The objective of this study is still to demonstrate that BC/PVA nanocomposites can be engineered. The difference in interaction and miscibility between BC/PEO and BC/PVA will be investigated to see how the interactions affect the nanocomposite properties. The aim is to develop alternative methods in bioengineering BC nanocomposites. These methods include polymer amount variation and polymer type selection. To select a polymer, solubility parameters can be used to predict miscibility, which in turn shall predict the trend of property modification.

Materials and Methods

Production of the Starter Culture

Acetobacter xylinum of the strain 23769 was purchased from American Type Culture Collection. For the bacterium growth, the Hestrin-Schramm (HS) medium was prepared with 2wt% D-glucose, 0.5wt% peptone, 0.5wt% yeast extract, 0.27wt% disodium

phosphate, 0.115wt% citric acid (monohydrate) in distilled water, and the pH was adjusted to about 5.0 with hydrochloric acid (Hestrin and Schramm, 1954). The starter culture was composed of 150 grams of water, and the remaining HS reagents placed in a 250ml Erlenmeyer flask and autoclaved at 121ºC for 15 minutes. Then this was cooled down and inoculated with the bacterium strain. The inoculated medium was incubated at room temperature. The starter culture produced in this way was grown in a static environment for approximately 1 week, at which time a thin cellulose film had materialized at the air-liquid interface. The thin film was taken out, and the bacteria-rich medium was used for subsequent growth of the cellulose in the HS media, modified with PVA grown in batches. A batch consisted of 250ml Erlenmeyer flasks, each holding 150 grams of water, as well as HS reagents and varied amounts of PVA inoculated with A. xylinum bacterium that was typically grown for about 7-10 days. For every batch, a starter culture was cultivated statically to use for subsequent batches.

Production of BC in the Poly(vinyl alcohol)-Modified HS Media

Acros Organic PVA with average molecular weight of 22,000 was purchased from Fisher Scientific. In order to produce BC/PVA materials with a range of chemical compositions, the HS media were modified with 1, 2, 3, 4, 5, 7 and 9wt% PVA, amounting to 7 different media conditions. The modified media were first autoclaved in a method similar to that used with the starter culture, and bacterial incubation was then statically conducted. After 2 days of incubation, a thin pellicle had developed. This was retrieved and squeezed with long tweezers to extract and recover the bacteria-rich suspensions. These bacteria-rich suspensions were used to start magnetically stirred cultures of the PVA

modified BC. In this case, stirring is necessary to keep PVA dissolved and distributed in the liquid medium, and to promote interactions and co-crystallization with BC during its growth. Under these conditions, cloud-shaped materials started appearing on the second day of growth. After 3 to 7 days, the medium was filled with a white cotton-like substance. The product was harvested by filtering the growth medium with gauze to gather the product. A drop of the product (enough to coat the TEM grid for the TEM analysis) was added. This formed transparent, thin films that were pressed between two 3x3cm^2 plastic cellophane for the FT-IR examination. Removal of the bacteria from the product with alkali or other methods (George et al, 2005) was not attempted, as this study intends to evaluate the intact structure of the composites resulting from such incubation conditions. Instead, the products were washed thoroughly with distilled water and placed in rectangular plastic bags measuring 3.3x7cm^2. The molded products were stored in a freezer for 24 hours, and then freeze-dried for 12 to 24 hours. The dried products were weighted to obtain the conversion of glucose and PVA, then flattened into thin sheets of thickness 0.7±0.2mm in a small hydraulic press with a pressure of about 2.76 x 10^7 N/m^2 for characterizations. All products were kept dried in vacuumed desiccators with calcium sulfate until characterization. At least three batches of BC and PVA modified BC were grown, of which one batch consisted of seven media conditions, Therefore, at least three replicates of data can be obtained in the characterization of each modified BC.

Transmission Electron Microscopy (TEM)

To evaluate the cellulose fiber structure and dispersion during biosynthesis, TEM images were obtained for wet samples that were set in the 400-mesh copper TEM grid.

The loaded grid was lightly washed with distilled water, dried and stained with 1% uranyl acetate. Images were acquired at 60K magnification on a JEOL 1200 EX operating at 100kV. The diameters of cellulose nanofibers were measured and averaged from 5-10 measurements. Duplicate samples were imaged.

Atomic Force Microscopy (AFM)

To further assess the nanofiber and product morphologies, in particular the phase domain sizes and dispersion, the dry materials were imaged by AFM. Around 3 x 5 x 0.7µm rectangular-shaped sheet of freeze-dried product was glued into an AFM sample disc with Permatex PermaOxy glue. Using an RMC Products PowerTome-X ultramicrotome with a CRX cryosectioning system, the top of the sample was trimmed with a glass knife to produce a smooth surface. AFM image scanning was then performed in a tapping mode under open air on a Veeco Multimode instrument operating with NanoScope IIIa Version 5.30r3sr3 software. The scanner used was a J scanner, and the tapping tip was aVeeco MPP-11100 silicon tip with a cantilever frequency resonance of around 200-300 kHz and a nominal spring constant of 40 N/m. The scan rate was 1.5 Hz, and the scan size was 3µm x 3µm, with an aspect ratio of 1. Integral and proportional gains were 0.3 and 0.5 respectively. Two AFM images were obtained for each sample.

Fourier-Transform Infrared Spectroscopy (FT-IR)

To determine the chemical composition of the produced cellulose/PVA nanocomposites, a calibration model was developed with FTIR based on known mixtures of PVA and microcrystalline cellulose . Namely, microcrystalline cellulose obtained from

Fisher Scientific and PVA were dissolved in distilled water in known w/w % and pressed into thin transparent films between 3x3 cm^2 plastic sheets. To evaluate the composition and specific interactions developed between PVA and BC , FT-IR spectra of neat PVA and PVA modified BC products were also analyzed. Thin films of BC and PVA modified BC, prepared as described in the production section, were freeze-dried for a maximum of 8 hours, producing very thin, transparent films. PVA powder was blended with KBr to form into pellets. The samples were then frozen for 8 hours and freeze-dried for another 8 hours. The dried transparent films and pellets were analyzed in a Nicolet Nexus 670 FT-IR machine under transmission mode. For each sample, 40 scans were acquired in the 4000 – 600 cm^{-1} range with a resolution of 4 $cm^{-1.}$ Three replicates of each known mixtures were obtained.

Thermogravimetric Analysis (TGA)

To determine the degradation temperatures (T_{deg}), the dried products were characterized with TGA in accordance with ASTM E 1131 (1988). Measurements were performed on Rheometrics STA 625 equipped with RSI Orchestrator software and operating under a constant flow of nitrogen gas at a rate of 90ml/min. Samples used are the sheets of modified BC's that were previously pressed, then cut into very tiny strips and pieces. Approximately 10 to 25 mg of the dried product was placed in aluminum pans and submitted to a two-step heating program. The samples were first equilibrated at 30ºC for 5 minutes and subsequently heated to 500ºC at 10ºC/min, at which point only ashes remained. Similar measurements were performed on the neat PVA powders and pure BC sheets to determine their degradation temperature. Derivative data of temperature versus

weight percent were used to obtain $T_{deg,}$ as these were not very distinct in the raw data. Three data sets were obtained.

Dynamic Scanning Calorimetry (DSC)

Approximately 11±4 mg of dried product was loaded in a DSC aluminum pan and placed in a a Mettler Toledo DSC 822e, operating with the STARe software. The sample of BC and nanocomposite consisted of diminutive strips cut from the previously pressed sheet, and the PVA was powder. Each sample was first heated from 25ºC to 250ºC at 30ºC/min. Heating above the T_m of PVA and the T_g's of both materials allowed prior thermal histories to be erased. The sample was then cooled down to -20ºC at a 30ºC/min cooling rate. Once the prior thermal history had been erased, the sample was heated, from -20ºC to 250ºC, at a 20ºC/min heating rate, and T_g's and T_m's were recorded. T_g was taken. as the temperature corresponding to 50% of the transition or the inflection point of the heat flow, while T_m was determined from the minimum of the melting endotherm peak. Throughout the DSC experiments, the cell was purged with N2 gas at a flow rate of 80ml/min and cooled by liquid nitrogen. Three replicate data sets were obtained.

Dynamic Mechanical Analysis (DMA)

Samples that were previously pressed with a pressure of 2.76 x 10^7 N/m^2 in the small hydraulic press were cut into strips of dimensions 34±2 x 7±1 x 0.7±0.2 mm. The samples were tested in the tension mode on a Rheometrics RSA II instrument with TA Orchestrator software. First, the samples were quickly heated (30°C/min) from 20°C to 150°C to erase any previous thermal histories, and then cooled back to 30°C. A dynamic

strain sweep was performed at 1Hz to determine the linear viscoelastic range (LVE). This was defined by the strain region, which showed less than a 5% reduction in the initial E'. After the strain scan, the samples were cooled (30°C/min) to -20°C. Following a 1 min soak time at -20°C, a temperature scan of maximum strain level $3x10^{-4}$ was conducted from -20°C to 250°C at 3°C/min at 1Hz. The storage modulus (E') and tan delta traces obtained during that scan were recorded. E' before T_g was defined to be the average E' in the temperature range of -20°C to 40°C and E' after T_g was the average E' between temperatures 70°C to 250°C. Duplicate data were obtained.

Results and Discussion

Production Results

Because production of the nanocomposites was conducted to obtain just enough samples for characterization, the growth setup was cultivated only for 7 to 10 days. From this period of growth, a maximum glucose conversion of 51wt% was attained. On the other hand, for PVA, a maximum of 17wt% was developed into nanocomposite. A longer growth period or the idea of recultivating the growth medium was contemplated to produce higher conversion of the components.

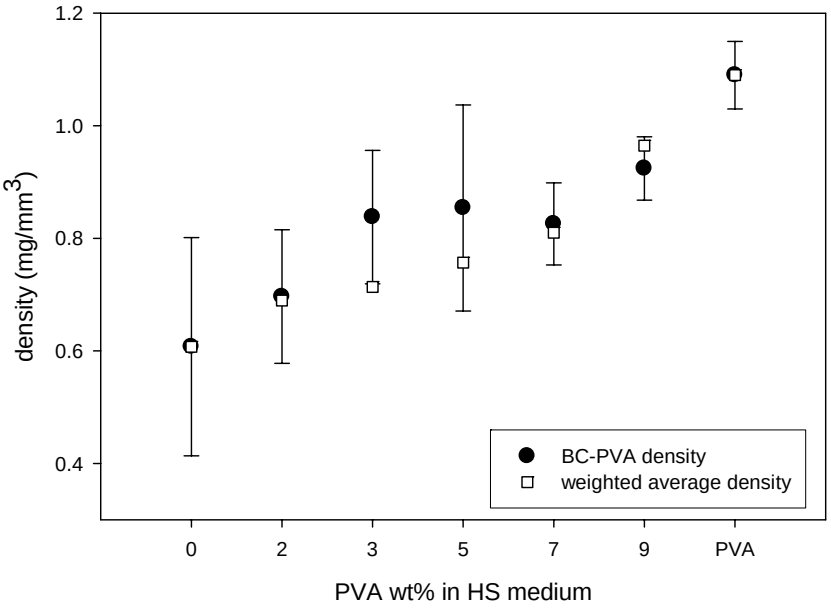

Figure III-2. Actual and calculated weighted average density vs. PVA initial amount

PVA wt% in HS medium	Density (mg/mm^3)
BC	0.61±0.19
2	0.70±0.12
3	0.84±0.12
5	0.85±0.18
7	0.83±0.07
9	0.92±0.06
PVA	1.09±0.06

Table III-2. Density of BC, PVA and BC/PVA samples.

Densities of the products were plotted vs. initial PVA values in Figure III-2, and numerical figures are listed in Table III-2. Determination of density was done by cutting a rectangular sheet from the previously pressed samples of dimensions 17±6 x 7±1 x 0.7±0.2mm and weighing it in a digital scale with 0.0mg precision. The dimensions;

length, width and thickness were acquired with a digital caliper of precision 0.00 mm. Density was taken as weight over volume. Three replicates were obtained for each sample. Densities showed increasing trend as PVA amount in the medium increased. The formation of BC with PVA formed a denser material compared to pure BC. When compared to the computed weighted average density, the data seemed to follow the trend. Going back to the solubility parameter, it was predicted that PVA would have a greater interaction than PEO, yet the result of density trend showed otherwise. BC/PEO nanocomposites densities were higher than the computed average, implying that there was closer interaction than BC/PVA. This result should be investigated further.

Investigation of BC and PVA interactions and how the nanocomposites form was done by determining product morphology, compositions, chemical interactions, and thermal and mechanical properties. Characterizations are presented in subsequent sections.

Morphology of BC/PVA Nanocomposites

It was expected that BC nanofibers would have modified morphology as PVA was added to its growth medium. Figure III-3 shows that BC grown in medium without PVA had the widest nanofibers, 17.1±5.2nm and nanofibers aggregated into ribbons of diameter 94.0±31.0nm. The individual nanofibers observed were much thicker than observed by Zaar (1977), which had the diameter of 30 to 40Å, but the ribbons were almost the same dimension as observed here. The individual nanofiber width observed could possibly be aggregated thinner fibers that Zaar observed, and this was perhaps not detected because of resolution limitation and the difference in time length of BC development. Zaar

investigated the BC fibers after 5 hours of incubation, while the fibers in this research were subjected to TEM after 10 days of development.

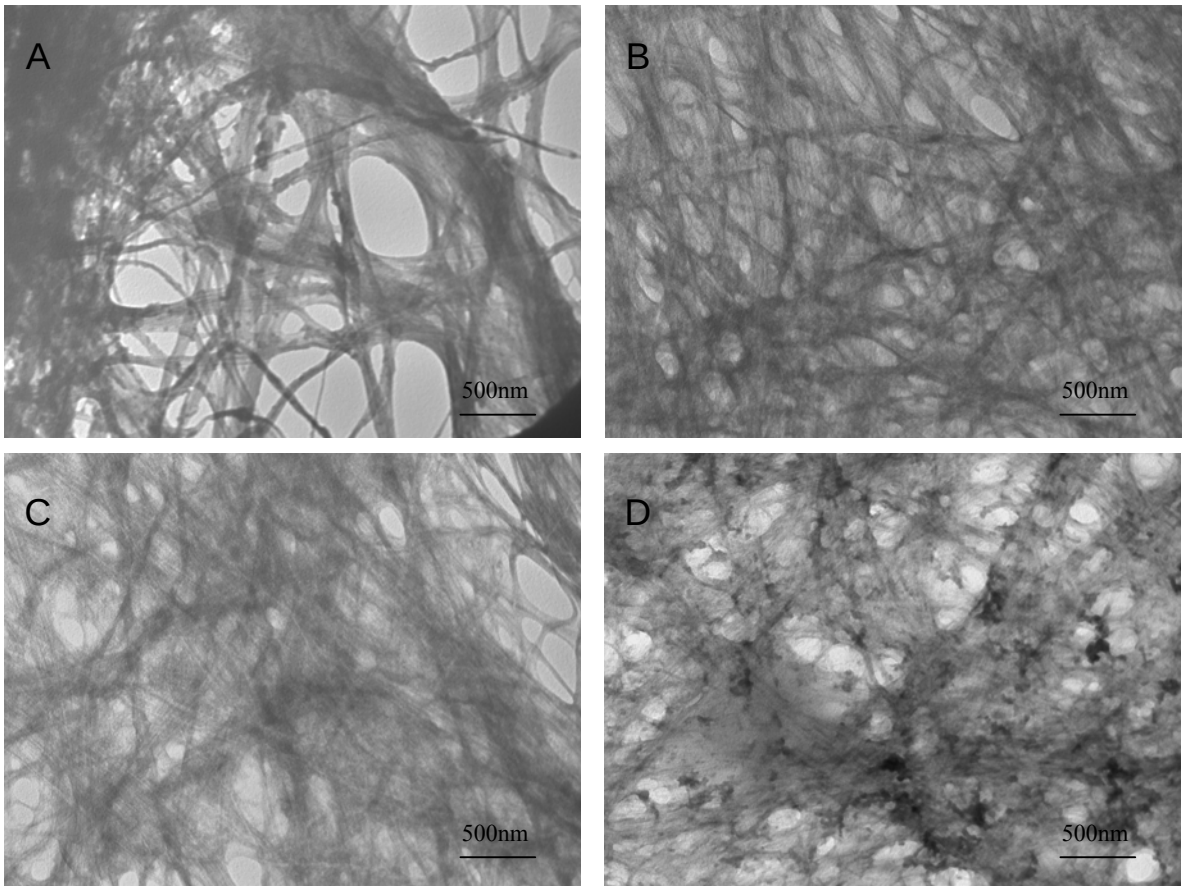

Figure III-3. TEM Images of BC and PVA modified BC. A)control BC. BC grown in medium with B)1wt% PVA C) 5wt% PVA D) 9wt% PVA.

When PVA was added into the growth medium, specifically 1, 5 and 9 wt percentages, the nanofiber diameters shrank to 10.6±1.6, 9.8±1.6, 9.7±1.2 nm for the respective PVA percentages. The smaller nanofiber widths with PVA addition confirmed that BC nanofiber formation was influenced by the addition of PVA in the medium. The aggregation of nanofibers was barely detected in Figure III-3B for BC grown in the medium with 1wt% PVA. The ribbons had a diameter of 43.4±6.8nm, half of the pure BC

ribbon size, and this size corresponded to the results obtained by Millon and Wan (2006). The nanofiber aggregation diminished when BC was grown in the medium with 5wt% and 9 wt% PVA, as seen in Figure III-3C and Figure III-3D. PVA had been predicted to interact extensively with BC, as both have the ability to hydrogen bond because of the their OH group (molecular structures in Figure III-1). This interaction can initially be seen in TEM images as PVA disrupted agglomeration of nanofibers into ribbons. Yet, considering the previous work of BC-PEO nanocomposites, the dimensions of BC diameters are almost the same, thus the predicted close interaction between BC and PVA is not evident from the nanofiber crystallization and sizes observed with TEM. To additionally inspect the morphology of BC and PVA combination, the dried products were examined with AFM. AFM images are shown in Figure III-4.

Distinguishable ribbon diameters for BC and modified BC grown with 1wt% PVA were 104±16nm and 61±6nm respectively. These dimensions are about 10-20% larger than the ribbons measurements from TEM images, but this may have been the BC ribbons wrapped by PVA in the dried state of the product. The BC grown in the medium with 1wt% PVA had ribbons oriented parallel (Figure III-4B). This phenomenon has been observed in other instances when a cellulose derivative was added to the growth medium (Ben-Hayyim and Ohad 1965). The cellulose derivative was carboxymethyl cellulose, a polymer that, like PVA, has a potential to hydrogen bond with BC. Thus, the molecular structure of the additive polymer can influence arrangement of ribbons in the dried product. As shown in Figure III-4C-D, BC grown in 5 and 9 wt% PVA did not provide significant morphological information because the surfaces were flat and smooth. Possibly

the ribbons were too small to be perceived, or that the PVA wrapped the nanofibers and covered the contours. Perhaps a new sample preparation or AFM setup should be done to get better images. BC/PEO nanocomposite seemed to be a lot more fibrous in surface when compared to BC/PVA, since BC nanofibers in PEO can be seen distinctly in AFM even with initial amount of PEO of 5wt%.

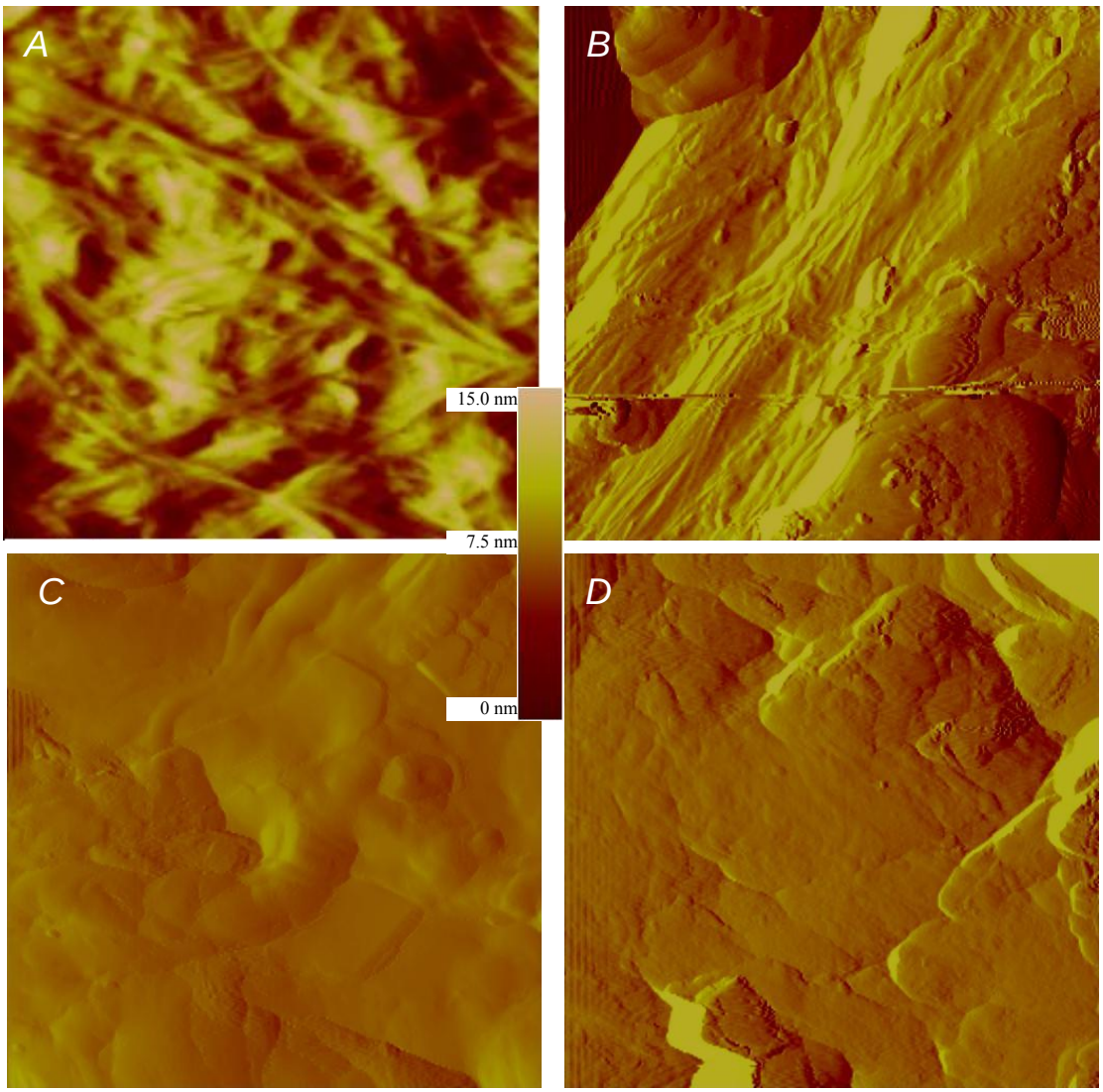

Figure III-4. AFM image. A)BC, ribbon width=104±16nm. BC grown in HS medium with B)1wt%PVA, ribbon width=61±6nm C)5wt% PVA D)9wt% PVA.

The root mean square Roughness, rms (R), was computed to determine changes in surface texture with increasing PVA content. The roughness of 2.9±1.1, 1.2±0.2nm, 0.6±0.2 and 0.8±0.0 were taken for BC grown in 1, 5 and 9wt% PVA in the HS medium respectively. In other words, the modified BC was smoother due to the addition of PVA.

TEM and AFM initially attested that PVA could have interacted with BC during BC biogenesis, as shown by the change in its physical morphology. But the questions remains as to whether a composite would be formed as a final product from this. The composition was investigated using FT-IR.

Chemical Compositions of BC/PVA Nanocomposites

In the previous study on cellulose/PEO nanocomposites, the chemical composition was determined from TGA, but TGA data of BC/PVA samples cannot provide such information, since there was only one degradation temperature that appeared for both. TGA results will be discussed in a later section.

To determine composition, characteristic IR absorption bands of each component were identified. These absorption bands, unique to bacterial cellulose and PVA, could be detected in the composite at 1160cm^{-1} and 850cm^{-1} respectively. To get the correlation between the characteristic bands and chemical composition, a plot of absorption band area ratios (A_{1160}/A_{850}) vs. composition data was obtained. The data was fitted using modified hyperbola with 2 parameters in SigmaPlot version 9software. The graph and fitted curve is shown in Figure III-5 with the equation: $y = \frac{ax}{1+bx}$ where a=268.2, b=3.086, x is $A_{1160}/A_{850,}$

where y is the wt% of cellulose and r^2 is equal to 0.960. This equation could be used to get BC wt% of the products with the assumption that the product was composed only of BC and PVA and not accounting for the bound water and proteinacious materials. The composition obtained will only be an estimation, as the cellulose used to get the standard equation is not BC. The interactions between BC with PVA and microcrystalline cellulose with PVA could likely be different. However, the fitted equation should provide a reasonable estimation of PVA and BC compositions. Computed composition of the product is enumerated in Table III-3 and also plotted in Figure III-5. Evidently, as the amount of PVA was increased in the medium, PVA composition in the dried product also increased (Table III-3).

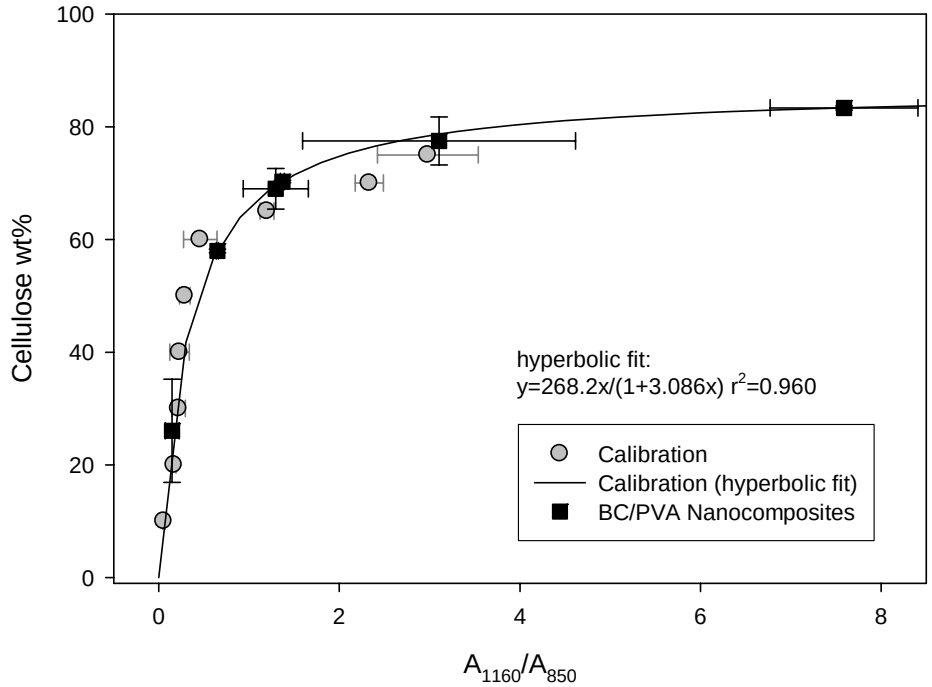

Figure III-5. Calibration and product data from FT-IR for chemical composition analysis.

PVA in HS medium (wt%)	BC final wt%	PVA final wt%	BC:PVA ratio (w:w%)
1	85.9±0.3	14.1	86:14
2	83.3±0.4	16.7	83:17
3	77.5±4.2	22.5	78:22
4	70.3±0.2	29.7	70:30
5	69.0±3.6	31.0	69:31
7	58.0±0.3	42.0	58:42
9	26.1±9.1	73.9	26:74

Table III-3. Composition of BC/PVA nanocomposites.

The compositional analysis verified the formation of composites, so in the next section, the interaction between PVA and BC will be investigated to see if a nanoscale interaction occurred in the composites.

Evaluation of Molecular Interaction and Crystallinity of BC/PVA Nanocomposites and Its Influence to Thermal Properties

The whole and expanded FT-IR spectra revealing characteristic absorption bands of BC, PVA and PVA modified BC's are shown in Figure III-6. The characteristic bands that appeared or perceived to have shifted were listed in Table III-4. BC O-H stretching is characterized by the sharp absorption band at wave number 3348cm^{-1} and the band slightly shifted to 3347cm^{-1} for all the BC/PVA samples. O-H stretching for PVA was represented with a broad absorption band centered at 3375cm^{-1}. As seen in Figure III-6, as the amount of PVA increased, the O-H stretching band broadened. This broadening was due to intermolecular hydrogen bonding between PVA and BC that was also seen in PVA-soaked

cellulose (Majumdar 2005). A big shift in the C-H stretching frequency of PVA was seen from 2943cm^{-1} to 2937cm^{-1} when BC was grown in medium with 9wt% PVA. The intensity of this absorption band had consequently dwindled and eventually became a shoulder comparable to plain BC as the amount of initial PVA decreased. This big shift of the C-H stretching absorption band, also seen in a precipitated cellulose and PVA blend (Salama et al 2004), could be a simultaneous effect of the shifting peak of the isotactic stereosequence vibration (Pritchard 1970) from 850cm^{-1} of PVA to 831cm^{-1} of the nanocomposites. This shift could indicate a change in morphology or crystallinity of PVA as its isotactic stereosequence was altered. The peak at 1730cm^{-1} is not expected from the PVA structure and it may represent a C=O stretching which may have arisen from the unpolymerized vinyl alcohol. The C=O stretching peak decreased and broadened as less PVA was added to the growth medium. The peak at 1144cm^{-1} that was assigned to skeletal motion of C-O and C-C stretching in the PVA crystal correlated to the degree of crystallinity of PVA (Pritchard 1970, Salama et al 2004). It disappeared with BC-PVA blend, likely indicating that PVA crystallinity diminished in the presence of cellulose.

BC peak (cm^{-1})	**w/ 1% initial PVA (cm^{-1})**	**w/ 5% initial PVA (cm^{-1})**	**w/ 9% initial PVA (cm^{-1})**	**PVA (cm^{-1})**	**Assignment (Oh et al 2005) (Pritchard 1970)**
3348	3347	3347	3347 (wide)	3375	O-H stretching
2942 (shoulder)	2942 (shoulder)	2942 (shoulder)	2937 (medium peak)	2943 (strong peak)	C-H stretching
-	1733	1733	1733	1733	C=O
1160	1160	1160	1160	-	COC stretching at β-glycosidic linkage
-	-	-	-	1144	C-C and C-O stretching of PVA
-	841(vague)	841 (wide)	831 (wide)	850	Skeletal vibration of isotactic PVA

Table III-4. FT-IR characteristic peaks of BC, PVA and BC/PVA samples.

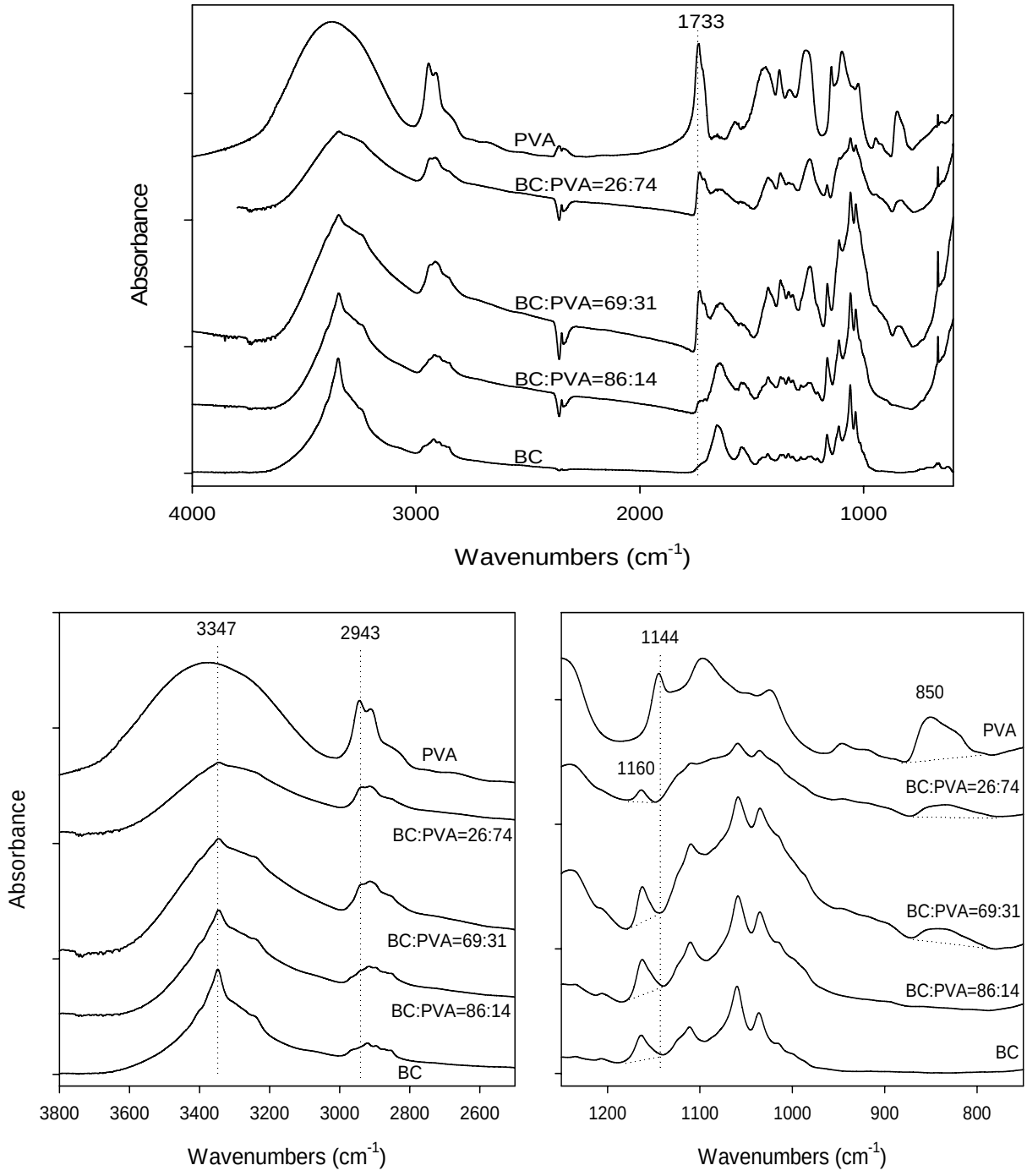

Figure III-6. FT-IR spectra of BC, PVA and BC/PVA samples. Characteristic peaks are highlighted with dotted lines.

The rest of the peak, namely 1160 and 850 cm^{-1}, corresponded to the presence or absence of BC or PVA in the sample. Since all peaks appeared in the products, it verified that composites are produced. These peaks accordingly describe the sample's composition as discussed in the previous section.

FT-IR showed molecular interactions between PVA and BC through hydrogen bonding and crystallinity change. This was observed in the change of C-H stretching and bending at the absorption bands around 2900 and 800cm^{-1}. A change in PVA crystallinity was also detected through the disappearance of an absorption band characteristic of PVA crystals.

To evaluate, verify, and analyze the effects of the assumed interactions, crystallinity changes and thermal properties were inspected with Thermal Gravimetric Analysis (TGA) and Dynamic Scanning Calorimetry (DSC).

TGA data for BC, PVA and BC/PVA nanocomposites are shown in Figure III-7, with the derivative in Figure III-8 and the list of T_{deg} in Table III-5. The bound water and proteinaceous materials evaporated and degraded at ~150ºC and ~220ºC respectively, as shown by the first two peaks in the left (Figure III-8). The T_{deg} of BC and PVA are 346.4±2.4ºC and 319.0±6.7ºC respectively. Moreover, as the amount of BC in the nanocomposites increased, its T_{deg} also increased from 319.1±1.1ºC of BC:PVA ratio 26:74 to 336.1±2.2ºC of BC:PVA ratio 87:13. This increase in T_{deg} confirmed the enhancement of thermal stability of PVA as other paper had found also that clay nanocomposite can have the same effect on PVA (Yu et al, 2003). The thermal stabilization could be induced by the interaction of BC and PVA specifically the hydrogen

bonding observed from FT-IR. The T_{deg} of PVA can therefore be adjusted by changing the amount in the growth medium.

Miscibility of cellulosic blends had been investigated by Nishioka and coworkers (1998). They noted that when there is decrease in thermal stability for cellulose, this suggests good compatibility between cellulose and polymer. They had found out that there was no alteration in T_{deg} for blend of cellulose from softwood pulp and PVA, indicating no significant miscibility, which is very different from what was seen in the result of the current research. It is obvious then that good miscibility between PVA and BC is seen here and that there should be an intimate mixing between the two to cause changes in T_{deg}.

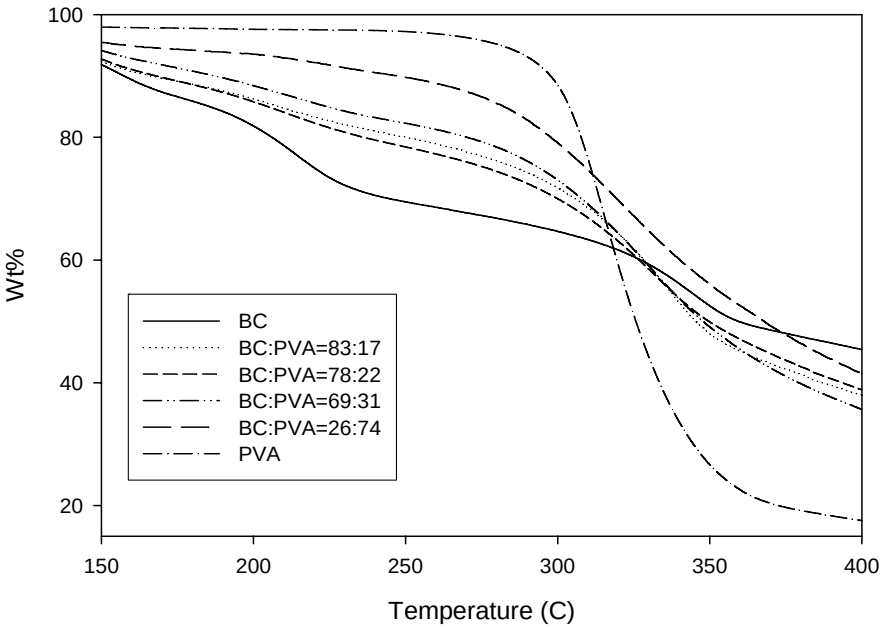

Figure III-7. TGA data of BC, PVA and BC/PVA nanocomposites.

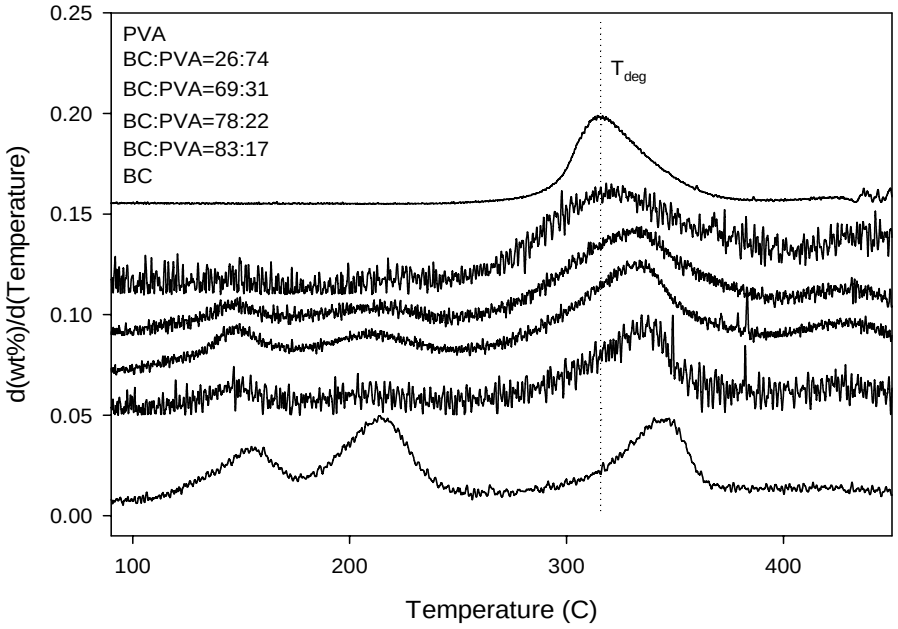

Figure III-8. Derivative data of TGA. T_{deg} of PVA is pointed out by the dotted line.

BC:PVA ratio	**Water T_{deg}**	**Proteinaceous materials T_{deg}**	**Nanocomposite T_{deg}**
BC	158.5±4.1	217.9±3.5	346.4±2.4
83:17	145.6±1.6	216.3±17.8	336.1±2.2
78:22	147.7±2.2	210.7±0.7	336.0±0.7
69:31	147.2±3.2	211.9±12.8	334.2±2.6
26:74	152.2±4.1	221.5±5.4	319.1±1.1
PVA			319.0±6.7

Table III-5. Degradation temperatures obtained from TGA for BC, PVA and BC/PVA materials.

To further evaluate miscibility and interactions between the two polymers, the main thermal transitions, T_g and T_m, were evaluated and compared with those of the neat components by DSC. A change in T_g in the blend compared to the neat component would be indicative of miscibility within the amorphous phase. Alternatively, a change in the

PVA T_m would indicate that BC fibers alter the crystalline morphology of PVA, suggesting intimate mixing in the crystalline phase.

When two polymers are blended, the thermal transitions vary depending on the type of interaction that takes place between the two polymers. The shift of glass transition temperature (T_g) is a good measure of miscibility in the amorphous phase, whereas the appearance of individual unchanged T_g indicates immiscibility (Simon 2003). As seen in Figure III-9, in the temperatures between 40-60°C together with the numerical data in Table III-6, T_g's of the nanocomposites increased with increasing amount of BC. T_g's of pure substances; BC and PVA are 198.4±2.5°C and 61.8±4.6°C respectively. The T_g's of nanocomposites increased from 78.4±1.3°C of BC:PVA=26:74 to 101.3±12.8°C of BC:PVA=86:14. This rise could be attributed to the confinement of PVA molecules due to their intimate interaction with BC that in turn prevented its segmental motions as also seen with clay nanocomposite-PVA blend (Yu et al 2003).

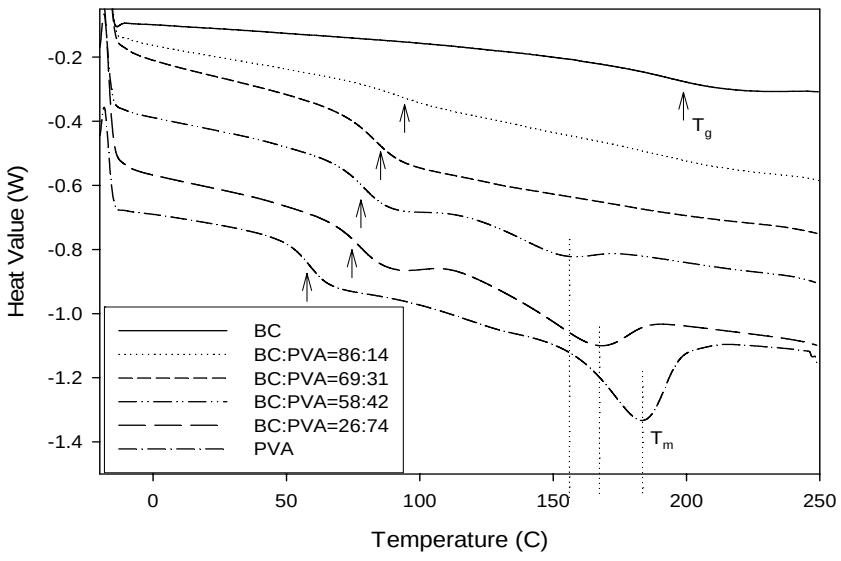

Figure III-9. DSC data of PVA, BC and BC/PVA samples. Melting temperature (T_m) is highlighted with dotted lines and glass transition temperatures (T_g) with arrows.

Sample	T_g (ºC)	T_m (ºC)	Crystallinity Index
BC	198.4±2.5	-	-
BC:PVA=86:14	101.3±12.8	-	-
BC:PVA=69:31	92.5±1.8	-	-
BC:PVA=58:42	81.6±2.3	162.7±6.2	
BC:PVA=26:74	78.4±1.3	165.4±4.1	0.09
PVA	61.8±4.6	184.5±1.8	0.14

Table III-6.T_m and T_g data from DSC.

Likewise, as BC content increased, the melting endotherm of PVA became less prominent and broader, and eventually disappeared when BC:PVA was 69:31. Additionally, T_m decreased with increasing cellulose content. Neat PVA had a distinct T_m at 184.5±1.8°C and it decreased to 165.4±4.1°C and 162.68±6.2°C in the nanocomposites with BC:PVA equal to 26:74 and 58:42 respectively. The T_m depression and the broadening of the endotherm peak denoted that the ordered association of PVA molecules into crystalline structures was hampered by BC. Depression in the melting point may arise from a morphological change (smaller and less stable crystals) or from thermodynamic favorable interactions (miscibility). In previous studies, T_m depression in similar blends investigated by Nishio and coworkers (1989) and by Park and coworkers (2001)) were also observed, and ascribed to the favorable interaction due to hydrogen bonding between cellulose and PVA.

The miscibility of BC and PVA in the amorphous phase was clearly evident in the appearance of one T_g in the nanocomposite samples as well as T_g variation with composition. Miscibility in the crystalline phase can also be assumed with T_m depression.

This means that there is a very tight interaction between the two polymers in both amorphous and crystalline phases, where hydrogen bonding could have played a major role. The disappearance of melting endotherm in the nanocomposites with higher BC contents means that the crystalline order of PVA was disrupted in the presence of BC. The crystallinity index (Table III-6) of PVA decreased from 0.14 of pure PVA to 0.09 for BC:PVA=26:74, denoting that using about 26% of BC in the nanocomposite can reduce the crystallinity of PVA by almost 65%.

To quantify the interaction in crystalline phase, the melting point depression can be analyzed to determine thermodynamic interaction parameter (χ_{12}). However, T_m appeared only on compositions with high PVA. Determining the equilibrium melting temperatures would be challenging as the melting endotherm broadened significantly with BC:PVA ratio 58:42. Nishio and coworkers (1989) did measure χ_{12} and they obtained a value of -0.948, indicating that enthalpic contributions to energy of mixing did influence the T_m depression and that this was not just due to morphological changes. From the result of χ_{12} in the BC/PEO computation, where χ_{12} of BC/PEO had a higher negative number than that of wood pulp cellulose/PEO by Nishio and coworkers (1989), it is predicted then that χ_{12} for BC/PVA would have higher negative value than –0.948. Therefore, the interaction of PVA and BC did alter the crystalline part of PVA and thermodynamic effects of miscibility is assumed.

Since there was a significant change in T_g's, amorphous interaction can be quantified with the Gordon-Taylor equation. This empirical equation (Equation 1) takes on the principle of ideal volume-mixing of the two components in a blend, and shows that the

changes in the coefficients of thermal expansion of glassy or rubbery components are constant as the blend is subjected to elevated temperatures (Gordon and Taylor, 1952). The principle applied to the amorphous component of polymer is that if the mixing of the two polymers was ideal, there would be no change on each of its volume and free volume. On the other hand, if there was interaction between polymers, its decrease in free volume would result in a change in the thermal expansion coefficients. In Equation 1, w refers to weight fraction, T_g to glass transition temperatures, 1 and 2 refers to PVA and cellulose respectively and k is $\alpha_{r2} - \alpha_{g2} \Big/ \alpha_{r1} - \alpha_{g1}$ (where α is the coefficient of thermal expansion, r and g refers to rubbery and glassy state). In the absence of α values, k can be determined by linear best fit of experimental T_g vs. $w_2 \Big/ w_1 (T_g^2 - T_g)$ (Ahn et al, 1997). The k value can be related to the strength of interaction between the components in miscible blends--the lower its value, the weaker its interaction. The determination of the Gordon-Taylor k value is shown in Figure III-10. T_g shifting in wood pulp cellulose-PVA blend observed by Nishio and Manley (1988) was plotted with BC-PVA T_g data for comparison. The BC-PVA k value was 0.11 (r^2=0.83) and wood pulp cellulose-PVA k value was 0.09 (r^2=0.99). The k values were low when compared to other polymer blends (Ahn et al 1997, Gordon and Taylor 1952), indicating that cellulose and PVA has a lower interaction than other studied blends. But the blends they investigated were chemically reacted copolymers such as butadiene/styrene (Gordon and Taylor 1952) and polybenzimidazole/polyimides, so the k values were about 0.2 to 3. Yet, when comparing BC-PVA and wood pulp cellulose-PVA interaction, it seemed that BC-PVA had a slightly higher interaction. This could be

due to the likelihood of PVA interacting with greatly dispersed and high aspect ratio BC nanofibers. Molecular weights of PVA for BC-PVA and wood pulp cellulose-PVA were 22,000 and 78,000 respectively, and this difference could also affect the interaction between PVA and cellulose.

$$w_2 = \frac{T_g - T_g^1}{k(T_g^2 - T_g) + T_g - T_g^1}$$

Equation 1. Gordon-Taylor Equation.

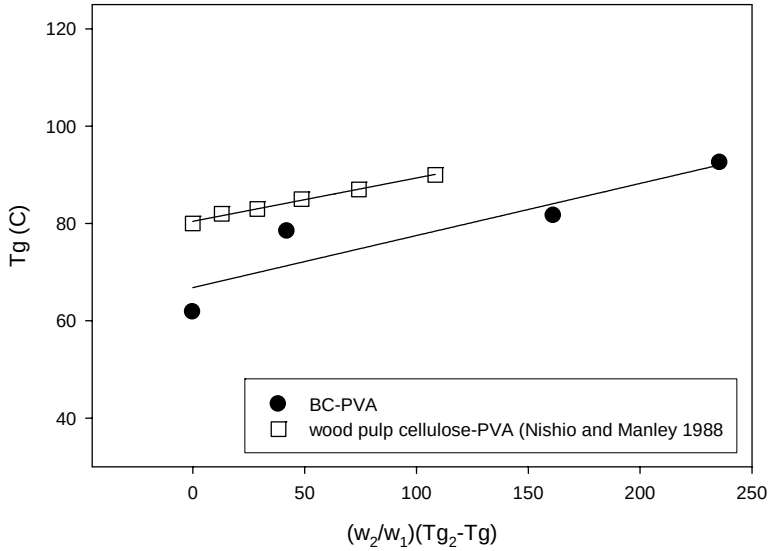

Figure III-10. Gordon-Taylor Equation fitting to BC-PVA products and Nishio and Manley (1988) wood pulp cellulose-PVA data.

Molecular interaction, crystallinity alteration and amorphous phase interaction between BC and PVA were seen by FT-IR peak, T_m and T_g shifting in different compositions of BC-PVA composites. It had been established therefore by molecular

interactions and thermal properties that as varied amounts of PVA were added to the BC growth medium, the properties of the sample diverged from the properties of pure components. In the next section, mechanical properties are investigated to see how this property changed as nanocomposite compositions changed.

Mechanical Properties of BC/PVA Nanocomposites

BC:PVA of ratios 26:74 and 78:22 were submitted to mechanical testing, as shown in Figure III-11. It can be seen that with final wt% ratio BC:PVA=26:74, the storage modulus (E') was 3.1e8±1.7e8 Pa, which is only about 30% of the BC:PVA =78:22 E' (listed in Table III-7). The pattern of E' observed is also seen in other works such as PVA blended with methyl cellulose (Park et al, 2001) and clay (Yu et al, 2003). Although the numerical values were not identical, the sudden decrease of E' at PVA T_g occurred. Nishio and Manley's (1988) blend of wood pulp cellulose and PVA obtained a higher storage modulus as their samples had E' close to 10^{10} Pa. E' values can reflect interaction of components in the blend yet the difference in instrumentation can be a factor of E' value difference since Nishio and Manley used a viscoelastometer.

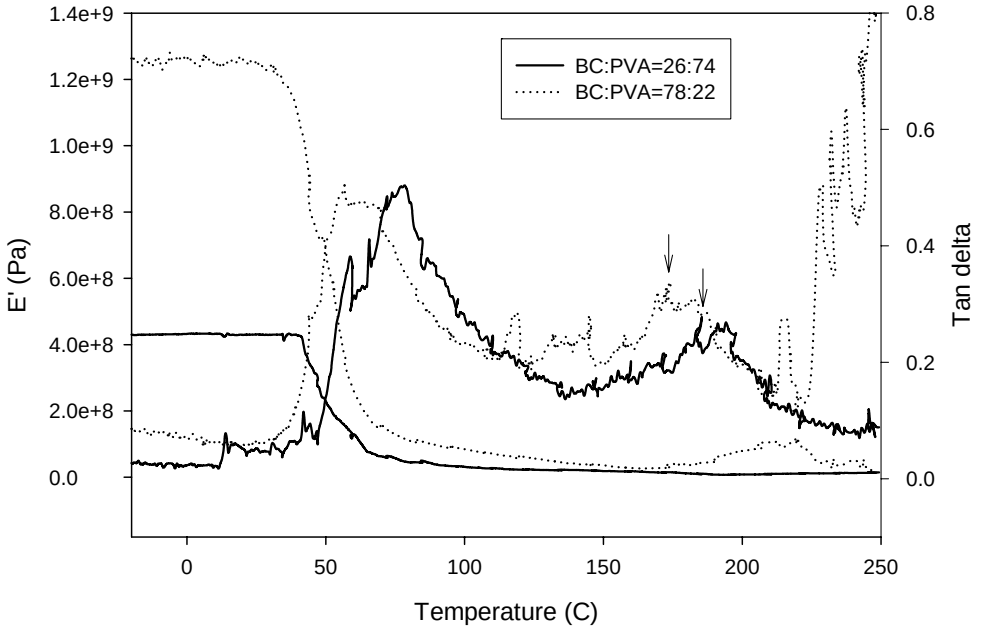

Figure III-11. DMA data of BC/PVA nanocomposites. Arrows pointed out T_m of samples.

BC:PVA	E' (Pa) before T_g	E' (Pa) after T_g	T_g (°C)	T_m (°C)
78:22	9.5e8±4.3e8	4.5e7±1.7e7	57.1±0.5	175.1±1.7
26:74	3.1e8±1.7e8	2.7e7±0.4e7	77.8±0.7	187.7+3.1

Table III-7.Storage modulus, T_g and Tm data of BC/PVA nanocomposites from DMA.

It can be noted from Table III-7 that the trend in E' after T_g was the same as before T_g, and that the nanocomposites with higher amounts of BC had higher E'. The improvement of mechanical property, as demonstrated by the increase in E', can presumably be influenced by the change in BC spherulite form (Kai and Kobayashi, 1992). This is considering that nanocomposites with approximately only 13wt% PVA unexpectedly had a high E', while E' for pure BC was unobtainable as it was too brittle to have even the slightest strain. This aforementioned spherulite change can occur when BC

is grown in a medium with PVA (Kai and Kobayashi, 1992). Thus, another aspect that can be tailored by modifying growth medium is spherulite configuration.

The peaks of tan delta data in Figure III-11 represented relaxation temperatures namely T_g exhibited by the bigger peak and T_m by the smaller peak (Park et al, 2001). These temperatures were determined by taking the highest value of each peak since the data seemed too noisy. The T_g trend in this instrumentation was opposite from DSC for it increased with an increasing amount of PVA, whereas it was the opposite in DSC. This ambiguous result could be attributed by the noisy data of tan delta. A thorough investigation of T_g with DMA would have to be performed to understand the trend seen here. Meanwhile, the T_m trend corresponded to the DSC data but the values from this instrumentation were around 20°C higher, which could presumably be a consequence of the different operating mechanisms of the two instruments. Otherwise, T_m depression was demonstrated again, verifying that there should be an alteration in the crystalline configuration of PVA as a result of BC and PVA intimate interaction.

Conclusion

One of the main objectives of this paper is to demonstrate that physical, chemical, thermal and mechanical properties can be fine-tuned by modifying the growth medium of the cellulose-producing bacterium with a varying amount of PVA. Starting with the physical attributes, TEM images verified decrease of nanofiber widths in the wet state. AFM demonstrated a parallel orientation of nanofibers in the dry state. As expected, chemical compositions varied as the amount of PVA in the medium varied. FT-IR

established hydrogen bonding between BC and PVA, which subsequently may have resulted in thermal stabilization of PVA, observed by TGA and Tg and Tm alteration of the nanocomposites. Miscibility of BC and PVA was very apparent with the alteration of $T_{deg.}$ Amorphous phase interaction was noted in the appearance of a single T_g and verified by the Gordon-Taylor equation, resulting in a k value higher than 0. Crystalline phase interaction between BC and PVA was seen in two methods. First, crystalline PVA was modified as revealed by DSC when T_m gradually vanished, and second, by FT-IR as PVA crystalline absorption peak disappeared with increasing amounts of BC in the nanocomposites. Mechanical properties increased with an increasing amount of BC in the nanocomposites. These results indicated that the properties were altered and therefore can be engineered.

Another objective of this paper is to demonstrate that with the aid of solubility parameters, interaction of BC and polymer can be approximated. That is, when two polymers are considered, values of solubility parameters should give an initial perception of how the properties will change. Here, the most significant change was in thermal properties. Solubility parameters predicted extensive interaction and miscibility for BC and PVA, as both can hydrogen-bond, hence their blend produced products having only one T_g and T_{deg}. In contrast, PEO and BC solubility parameters predicted minor interaction, which showed immiscibility as its nanocomposites had separate T_g and T_{deg}.

In effect, BC properties can be tailored by either modifying the growth medium with various amounts of polymer, or by designating the appropriate polymer. These multiple methods of tailoring provide an advantage, especially when a specific application

is implemented with two situations that could occur--that is, where either the choice of polymers is limited or unlimited. When polymer choice is limited, BC modification can be done by controlling the additive amount. When it is unlimited, solubility parameters can initially narrow down the choices.

References

Ahn, T.K., Kim, M. & Choe, S. (1997). Hydrogen-bonding strength in the blends of polybenzimidazole with BTDA- and DSDS-based polyimides. *Macromolecules*, 30, 3369-3374.

American Society for Testing Materials, Standard Test Method for Compositional Analysis by Thermogravimetry. In *ASTM E1131-03*, Philadelphia, PA, 2003; Vol. 14.02.

Ben-Hayyim, G. & Ohad, I. (1965). Synthesis of Cellulose by *Acetobacter xylinum*. *Journal of Cell Biology, 25*, 191-207.

Charpentier, P.A., Maguire, A. & Wan, W. (2006). Surface modification of polyester to produce a bacterial cellulose-based vascular prosthetic device. *Applied Surface Science 252,* 6360-6367.

Czaja, W., Young, D.J., Kawechi, M. & Brown, R.M. Jr. (2007). The future prospects of microbial cellulose in biomedical applications, *Biomacromolecules*, 8, 1-12.

George, J., Ramana, K.V., Sabapathy, S.N., Jagannath, J.H. & Bawa, A.S. (2005). Characterization of chemically treated bacterial (Acetobacter xylinum) biopolymer: Some thermo-mechanical properties. *International Journal of Biological Macromolecules,* 37, 189-94.

Gordon, M. & Taylor J.S. (1952). Ideal copolymer and the second-order transitions of synthetic rubbers. I. Non-crystalline copolymers. *Journal of Applied Chemistry*, 2, 493-500.

Hestrin, S. & Schramm, M. (1954). Synthesis of cellulose by *Acetobacter Xylinum* 2. Preparation of freeze-dried cells capable of polymerizing glucose to cellulose. *Biochemical Journal*, 58, 345-352.

Jonas, R. & Farah, L.F. (1998). Production and application of microbial cellulose. *Polymer Degradation and Stability*, 59, 101-106.

Kai, A. & Kobayashi, T. (1992). Influence of poly(vinyl alcohol) on the structure of bacterial cellulose spherulite. *Polymer Journal (Tokyo, Japan)*, 24, 131-133.

Klemm, D., Schumann, D., Udhardt, U. & Marsch, S. (2001). Bacterial synthesized cellulose - artificial blood vessels for microsurgery. *Progress in Polymer Science,* 26, 1561-1603.

Majumdar, S. & Adhikari, B. (2005). Polyvinyl alcohol-cellulose composite: A taste sensing material. *Bulletin of Materials Science*, 28, 703-712.

Millon, L.E. & Wan, W.K. (2006). The polyvinyl alcohol-bacterial cellulose system as a new nanocomposite for biomedical applications. *Journal of Biomedical Materials Research, Part B: Applied Biomaterials*, 79B, 245-253.

Nishio, Y. & Manley, R.S.J. (1988). Cellulose-poly(vinyl alcohol) blends prepared from solutions in N,N-dimethylacetamide-lithium chloride. *Macromolecules*, 21, 1270-1277.

Nishio, Y., Haratani, T. & Takahashi, T. (1989). Cellulose/poly(vinyl alcohol) blends: An estimation of thermodynamic polymer-polymer interaction by melting point depression analysis. *Macromolecules*, 22, 2547-2549.

Nishio, Y., Hirose, N. & Takahashi, T. (1989). Thermal analysis of cellulose/poly(ethylene oxide) blends. *Polymer Journal,* 21, 347-351.

Nishioka, N., Hamabe, S., Murakami, T. & Kitagawa, T. (1998). Thermal decomposition behavior of miscible cellulose/synthetic polymer blends. *Journal of Applied Polymer Science*, 69, 2133-2137.

Oh, S.Y., Yoo, D.I., Shin, Y., Kim, H.C., Kim, H.Y., Chung, Y., Park, W. & Youk, J. (2005). Crystalline structure analysis of cellulose treated with sodium hydroxide and carbon dioxide by means of x-ray diffraction and FTIR spectroscopy. *Carbohydrate Research,* 340, 2376-2391.

Park, J.S., Park, J.W. & Ruckenstein, E. (2001). A dynamic mechanical and thermal analysis of unplasticized and plasticized poly(vinyl alcohol)/methylcellulose blends. *Journal of Applied Polymer Science,* 80, 1825-1834.

Pritchard, J.G. (1970). *Poly(vinyl alcohol) Basic properties and uses*. London: Gordon and Breach, Science Publishers Ltd., 31-35.

Rezwan, K., Chen, Q.Z., Blaker, J.J. & Boccaccini, A.R. (2006). Biodegradable and bioactive porous polymer/inorganic composite scaffolds for bone tissue engineering. *Biomaterials*, 27, 3413-3431.

Salama, H., Dawny, M. & Nada, A.M.A. (2004). Studies on dielectric properties and AC-conductivity of cellulose polyvinyl alcohol blends. *Polymer-Plastics Technology and Engineering* 43, 1067-1083.

Simon, G.P. (ed) (2003). *Polymer Characterization Techniques and Their Application to Blends.* Washington DC:Oxford University Press, 42-62.

Sun, N., Das, S. & Frazier, C.E. (2004). The development of the dynamic mechanical analysis of wood for wood /adhesive research. *PMSE Preprints* 90, 552.

Van Krevelen, W. & Hoftyzer, P.J. (1976). *Properties of polymers, 2nd edition*. Elsevier, Amsterdam, 189-225.

Yu, Y.H., Lin, C.Y., Yeh, J.M. & Lin, W.H. (2003). Preparation and properties of poly(vinyl alcohol)-clay nanocomposite materials. *Polymer* 44, 3553-3560.

Zaar, K. (1977). The biogenesis of cellulose by *Acetobacter Xylinum*. *Cytobiologie European Journal Of Cell Biology*, 16, 1-15.

CHAPTER IV: CONCLUSION

Summary of Research Findings

The two expected outcomes from this research were 1) to manufacture BC fiber/thermoplastic nanocomposites having nanoscale dispersion, and 2) to gain useful knowledge on the engineering of the properties of BC nanocomposites. To achieve these objectives, BC was grown in media that were augmented with different amounts of thermoplastic polymers, polyethylene oxide (PEO) and polyvinyl alcohol (PVA).

As seen in TEM and AFM, both BC-PEO and BC-PVA nanocomposites were comprised of fibers having nanometer scale diameters and micron scale length that create a high aspect ratio (length/diameter) BC reinforcement, which is a trait favorable to nanocomposite properties. Chemical composition of the composite and morphology were therefore easily tailored from the growth conditions (Table IV-1 and Table IV-2). The ability to tailor the chemical composition and fiber morphology allowed the development of a range of material properties such as melting and softening behaviors, thermal stability, dynamic tensile behavior, surface roughness, and density (Table IV-1 and Table IV-2).

ND: Not detected

Composition	PEO in HS medium (wt%)	0	0.5	1	2	3	5	PEO
	BC:PEO ratio of dried product composition (w:w%)		59:41	53:47	33:67	23:77	15:85	
Morphology	BC fiber size in wet state (nm) (nanofiber, ribbon)	17.1, 94.0		10.0, 48.8		9.8, ND	9.7, ND	
	BC ribbon size in dry state (nm)	104		86		54	~204	
	PEO Crystallinity Index		0.21	0.36	0.49		0.49	0.67
Performance and Properties	E' before T_m (Pa)		$2.70x10^8$	$2.71x10^8$		$2.78x10^8$	$2.36x10^8$	$2.23x10^8$
	Surface Roughness (nm)	2.9		1.4		0.9	0.8	
	Density (mg/mm^3)	0.61		0.81	1.06	0.96	1.04	0.73
	T_g (°C) (PEO)		-50.1	-49.7	-48.4	-48.4	-51.0	-52.4
	T_{deg} (°C) (BC, PEO)	346.4, -	345.7, 425.9	350.7, 428.3	351.4, 428.6	351.6, 427.3	348.3, 425.3	-, 410.3
	T_m (°C) (PEO)		59.8	61.7	63.2	66.1	68.1	68.1

Table IV-1. BC-PEO nanocomposite properties.

Composition	PVA in HS medium (wt%)	0	1	2	3	4	5	7	9	PVA
	BC:PVA ratio of dried product composition (w:w%)		86:14	83:17	78:22	70:30	69:31	58:42	26:74	
Morphology	BC fiber size in wet state (nm) (nanofiber, ribbon)	17.1, 94.0	10.6, 43.4				9.8, ND		9.7, ND	
	BC ribbon size in dry state (nm)	104	61							
	PVA Crystallinity Index		ND				ND	ND	0.09	0.14
Performance and Properties	E' (Pa) (before T_g)				$9.5 x10^8$				$3.1 x10^8$	
	Surface Roughness (nm)	2.9	1.2				0.6		0.8	
	Density (mg/mm^3)	0.61		0.70	0.84		0.85	0.83	0.92	1.09
	T_g (°C)	198.4	101.3				92.5	81.6	78.4	61.8
	T_{deg} (°C)	346.4	336.1		336.0		334.2		319.1	319.0
	T_m (°C) (PVA)		ND				ND	162.7	165.4	184.5

Table IV-2. BC-PVA nanocomposite properties.

The variation of density is an illustration on how properties changed with polymer selection and concentration. The density trend was different for the two polymers and this is also pertinent to other properties, especially T_m, T_g and T_{deg}. There is a melting depression for both PEO and PVA, but T_m for PVA diminished as more BC was present in the product and subsequently, only one T_g and T_{deg} had arisen for BC/PVA materials. Chemical composition and mechanical properties followed the same trend, as they increased with an increase in the amount of BC in the nanocomposites. The variation of BC nanocomposite properties suggest that these properties could be engineered to match a desired application.

Although there has been significant work on cellulose/PEO and cellulose/PVA composites (Azizi Samir 2005, Nishio and Manley 1988) demonstrating a variation in properties with PEO content, previous work differed in the nature and dimensions of the cellulose reinforcement. In particular, the aspect ratio (length/diameter) of BC nanofibers that reinforce the thermoplastic polymers differs. The tunicin cellulose used by Azizi Samir et al (2005) has an aspect ratio of 70. The predominantly used microcrystalline cellulose produced from hydrolyzed cellulose source has a varying aspect ratio depending on the source. For example, cotton is 40 and tunicin whisker and paper is around 60 (Azizi Samir et al 2004, Podsiadlo et al 2005). With the BC produced in this research, the aspect ratios of individual nanofibers and ribbons are around 1200 and 220 respectively, assuming the 20μm length reported by Zaar (1977). The aspect ratio can be higher when BC-thermoplastic polymer nanocomposite forms as polymer disrupts the further formation of

thick ribbons. This high aspect ratio indicates very intimate interaction between the two composing polymers, which subsequently leads to advantageous engineering of the nanocomposites.

The present findings also differ from the work of Ciechanska (2004) and Seifert and coworkers (2004), which also produced BC-nanocomposites by manipulating the biogenesis of BC. In their work, static cultures were used that would likely result in heterogeneous products, and a systematic change in chemical composition and properties was not attempted. In the present research, stirring was employed that is assumed to yield homogeneously dispersed nanocomposites.

This research is therefore the first demonstration of the manufacture of BC/thermoplastic nanocomposites in which 1) cellulose fibers with an aspect ratio of over 1000 are dispersed in a thermoplastic matrix and 2) chemical composition and properties can be systematically varied, yielding a range of properties and performance.

Future Works

Of the wide potential applications of BC, its utilization in biomedicine is very promising, especially for scaffolds, implants, tissue and organ regeneration. This research is an initial step to producing functional biomaterial for these applications. A detailed diagram of requisites to achieve the biomaterial for biomedicine application is shown in Figure IV-1, taken from the review written by Seal and coworkers (2001). Using bacterial cellulose will minimize the biocompatibility challenge, as this already has been effective as a skin substitute. Also, BC is characterized by porosity and high mechanical strength in a

wet state. Thus it is only a matter of fine-tuning the degree of these characteristics to conform to the required properties.

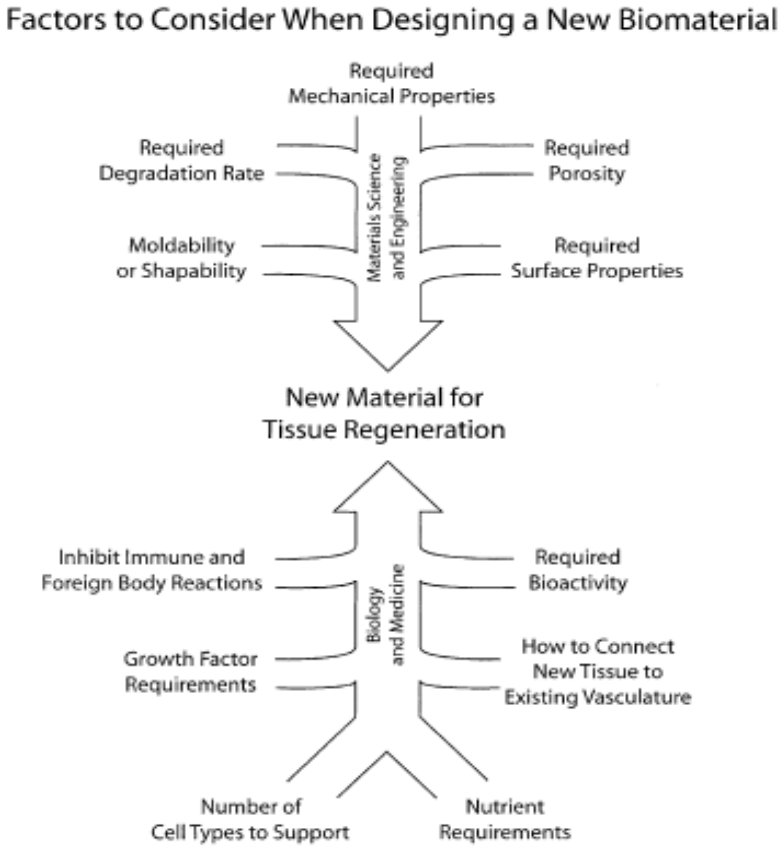

Figure IV-1. Illustration of how some material, biological, medical and engineering properties must be integrated to achieve successful biomaterials for tissue regeneration (Seal et al 2001).

There are many avenues of exploration as a result of this research, namely, i)a study for a specific application in biomedicine, such as blood vessel or dura mater application; ii) production kinetics and conversion studies of BC; iii) modeling the trend of property changes as a function of growth medium composition; iv) in-depth characterization of the products in a specific environment or state, either wet or dry; v) utilizing surfactants so non-water soluble polymers can be used, as well as many more.

One of the main questions to emerge when considering the utilization of BC in an application is the production yield. There is no mass production method for BC yet, but a few attempts for improvement are listed in Table IV-3.

Ways to improve BC production	**References**
Addition of plant extracts to medium	Webb and Colvin, 1963
Addition of endoglucanase to the medium	Tonouchi et al, 1995
Addition of insoluble microparticles such as diatomaceous earth, silica, small glass beads, and loam particles to submerged agitated culture.	Vandamme et al, 1998
Growing BC in shake flask culture with polyacrylamide-co-acrylic acid.	Joseph et al, 2003
Addition of ethanol in agitated culture.	Shoda and Sugano, 2005

Table IV-3. Ways of improving BC production.

These means of improving production would be helpful for the development of BC as a biomaterial for biomedicine applications. Currently, there has not an efficient enough production method for BC, making mass amount applications challenging. Although the target application is in the high value, materials and mass production are not a necessity, and a sufficient amount of the product must be produced for this to be economically efficient. To utilize BC for biomedicine applications, property manipulation and production improvement must be addressed.

References

Azizi Samir, M. A. S., Alloin, F. & Dufresne, A. (2005). Review of recent research into cellulosic whiskers, their properties and their application in nanocomposite field. *Biomacromolecules* 6, 612-626.

Azizi Samir, M.A.S., Alloin, F., Sanchez, J.Y. & Dufresne, A. (2005). Nanocomposite polymer electrolytes based on poly(oxyethylene) and cellulose whiskers. *Polimeros: Ciencia e Tecnologia* 15, 109-113.

Joseph, G., Rowe, G., Margaritis, A. & Wan, W. (2003). Effects of polyacrylamide-co-acrylic acid on the cellulose production by *Acetobacter xylinum*. *Journal of Chemical Technology and Biotechnology*, 78, 964-970.

Nishio, Y. & Manley, R.S.J. (1988). Cellulose-poly(vinyl alcohol) blends prepared from solutions in N,N-dimethylacetamide-lithium chloride. *Macromolecules*, 21, 1270-1277.

Podsiadlo, P., Choi, S.Y., Shim, B., Lee, J., Cuddihy, M. & Kotov, N. (2005). Molecularly engineered nanocomposites: layer-by-layer assembly of cellulose nanocrystals. *Biomacromolecules*, 6, 2914-2918.

Rezwan, K., Chen, Q.Z., Blaker, J.J. & Boccaccini, A.R. (2006). Biodegradable and bioactive porous polymer/inorganic composite scaffolds for bone tissue engineering. *Biomaterials*, 27, 3413-3431.

Seal, B.L., Otero, T.C. & Panitch, A. (2001). Polymeric biomaterials for tissue and organ regeneration. *Materials Science & Engineering R-Reports***,** 34, 147-230.

Seifert, M., Hesse, S., Kabrelian, V. & Klemm, D. (2004). Controlling the water content of never dried and reswollen bacterial cellulose by the addition of water-soluble polymers to the culture medium. *Journal of Polymer Science, Part A: Polymer Chemistry***,** 42, 463-70.

Shoda, M. & Sugano, Y. (2005). Recent advances in bacterial cellulose production. *Biotechnology and Bioprocess Engineering*, 10, 1-8.

Tonouchi, N., Tahara, N., Takayasu, T., Yoshinaga, F., Beppu, T. & Horinouchi, S. (1995). Addition of small amount of an endoglucanase enhances cellulose production by *Acetobacter xylinum*. *Biosci. Biotech. Biochem.*, 59, 805-808.

Vandamme, E.J., De Baets, S., Vanbaelen, A., Joris, K. & De Wulf, P. (1998). Improved production of bacterial cellulose and its application potential. *Polymer Degradation and Stability*, 59, 93-99.

Webb, T.E. & Colvin, R.J. (1963). The effect of bacterial cell lysis and of plant extracts on cellulose production by *Acetobacter xylinum*. *Canadian journal of biochemistry and physiology*, 41, 1691-1702.

Zaar, K. (1977). The biogenesis of cellulose by *Acetobacter Xylinum*. *Cytobiologie European Journal Of Cell Biology*, 16, 1-15.

APPENDIX A: PRODUCTION OF BC/THERMOPLASTIC POLYMER NANOCOMPOSITES

Images of Production setup

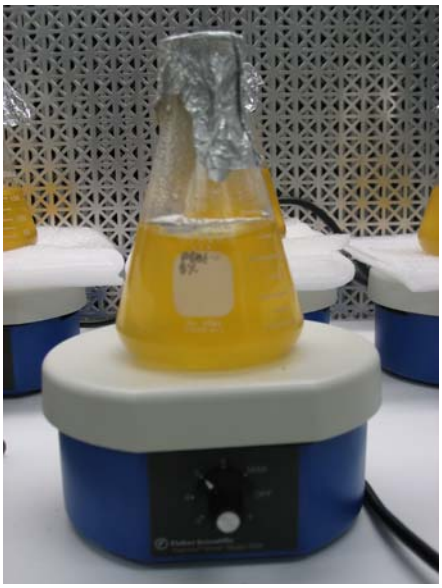

Figure A-1. Incubation in magnetically-stirred environment.

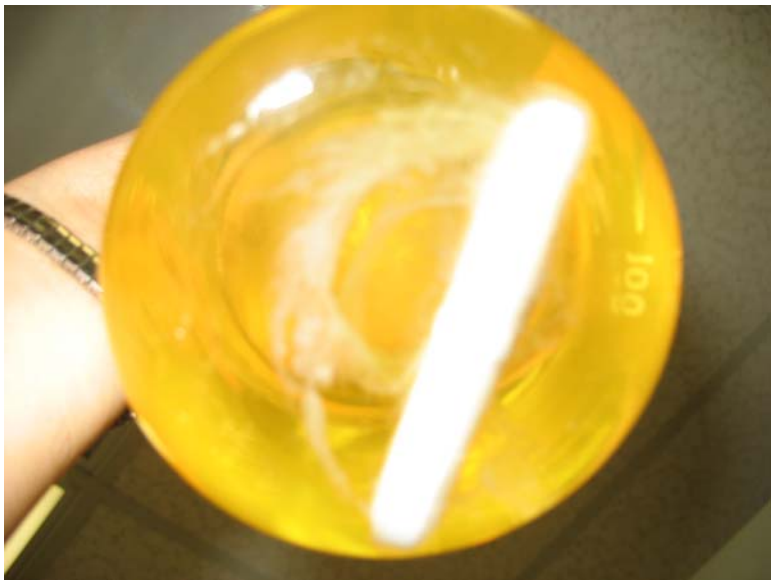

Figure A-2. Stringy material adhered to the Teflon stirrer instigate growth of product.

Figure A-3. Image of the bottom of the Erlenmeyer flask. The white cotton-like material is the product.

Figure A-4. Product ready for harvest.

Images of Dried Products

Figure A-5. Freeze-dried and flattened nanocomposites.

APPENDIX B: BC/PEO NANOCOMPOSITE DATA

TEM Images

Replicates images from TEM

	Widths(nm)
Individual fibrils	17.1±5.2
ribbons	94.0±31.0

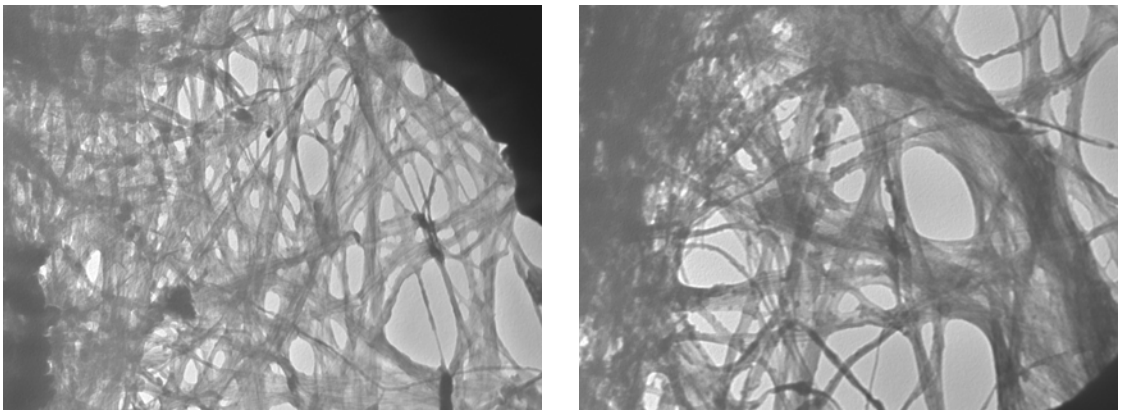

Figure B-1. TEM images of BC in unmodified HS medium.

	Widths(nm)
Individual fibrils	10.0±1.6
ribbons	48.8±6.0

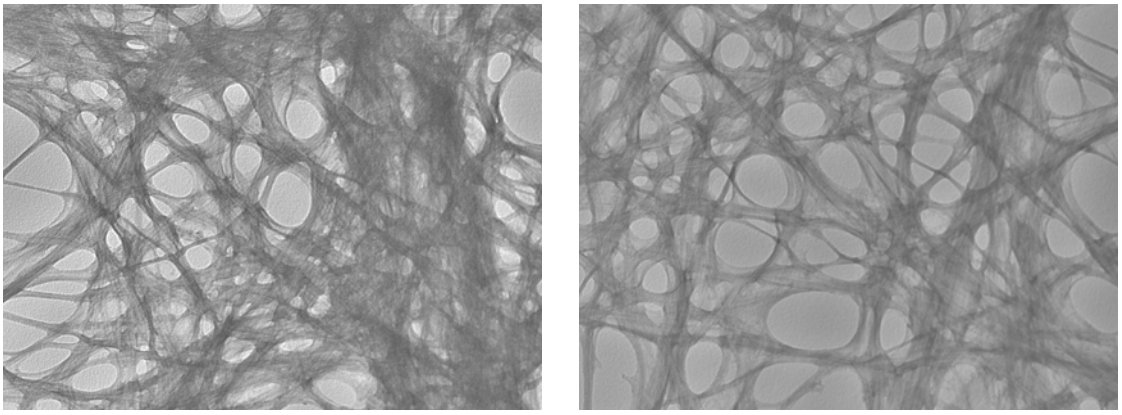

Figure B-2. TEM images of BC in 1wt% PEO1-modified HS medium.

	Widths(nm)
Individual fibrils	9.8±1.0
ribbons	-

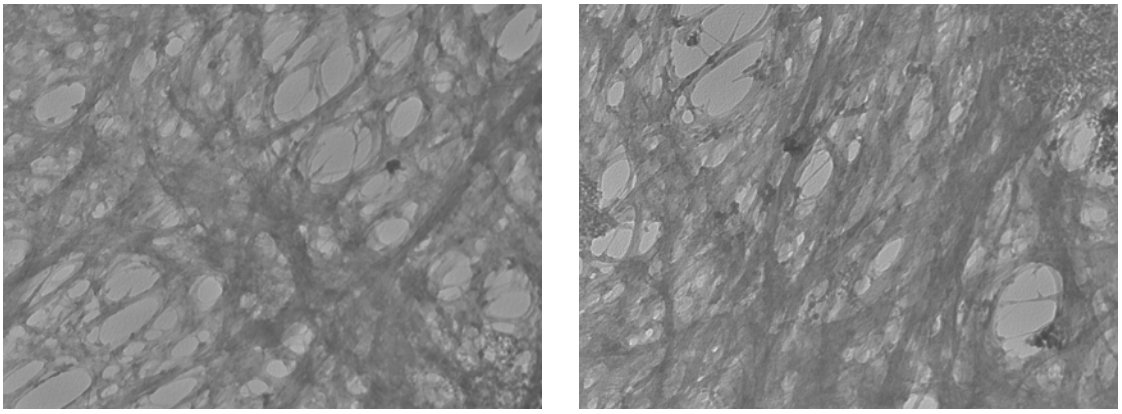

Figure B-3. TEM images of BC in 3wt% PEO1-modified HS medium.

	Widths(nm)
Individual fibrils	9.7±1.5
ribbons	-

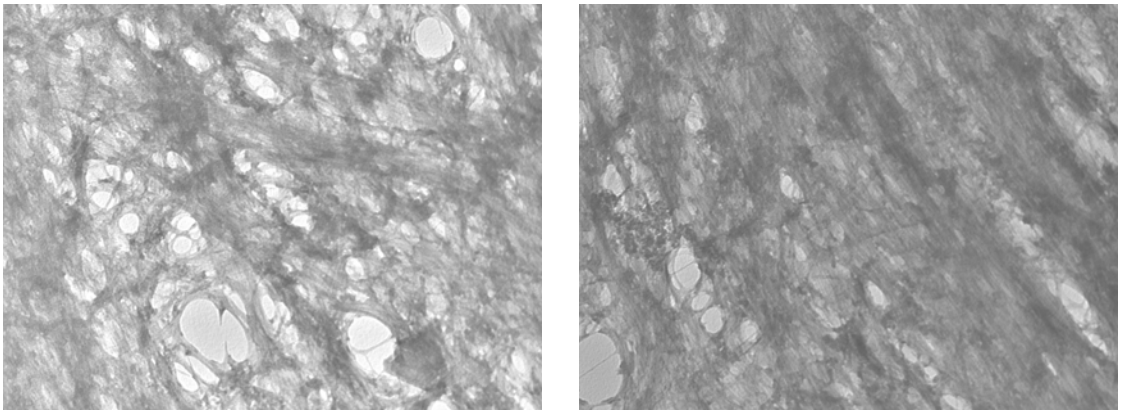

Figure B-4. TEM images of BC in 5wt% PEO1-modified HS medium.

AFM Images

Replicate images of AFM. The area inside the rectangular white outline is the region where bearing and roughness were analyzed.

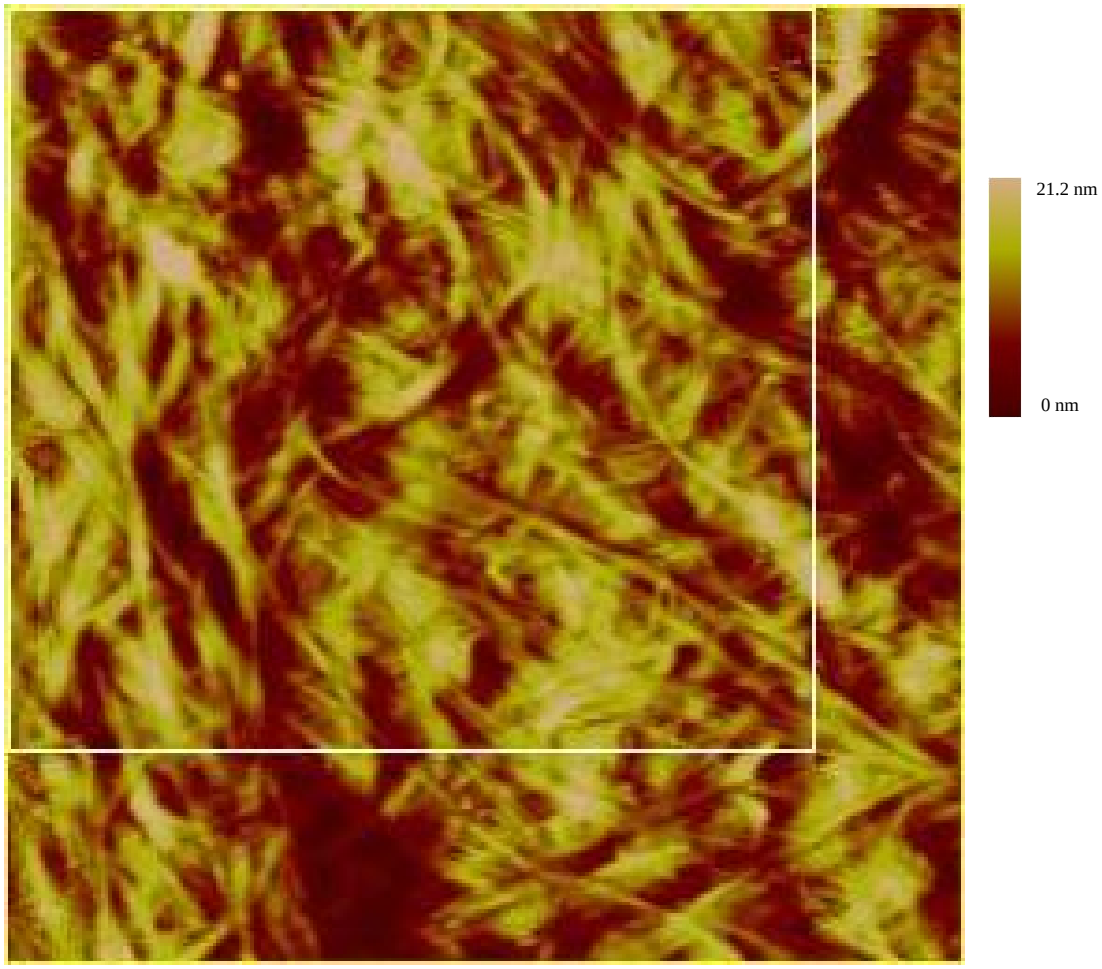

Figure B-5. AFM image of dried BC grown in unmodified HS medium.

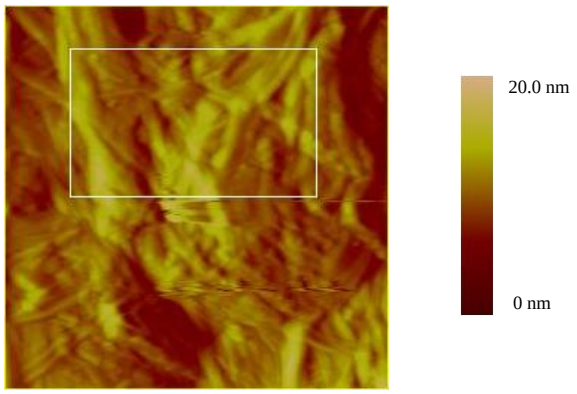

Image is 2 x 2µm

Figure B-6. AFM image of dried BC grown in unmodified HS medium.

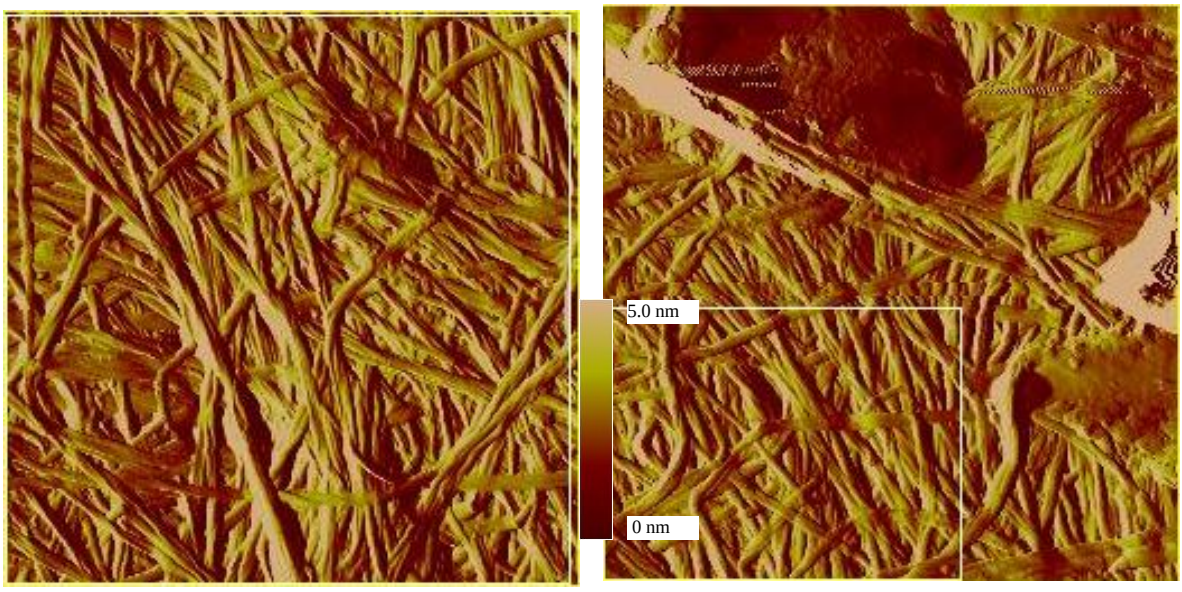

Both image are 3 x 3µm

Figure B-7. AFM Images of dried BC grown in 1wt% PEO1-modified HS medium.

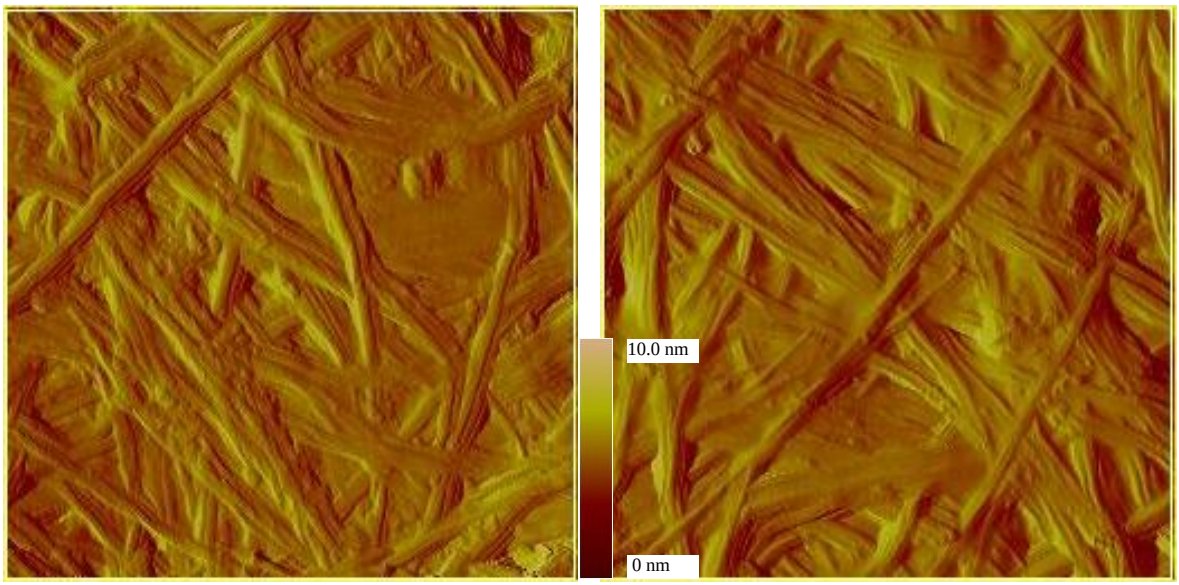

Both image are 3 x 3µm

Figure B-8. AFM Images of dried BC grown in 3wt% PEO1-modified HS medium.

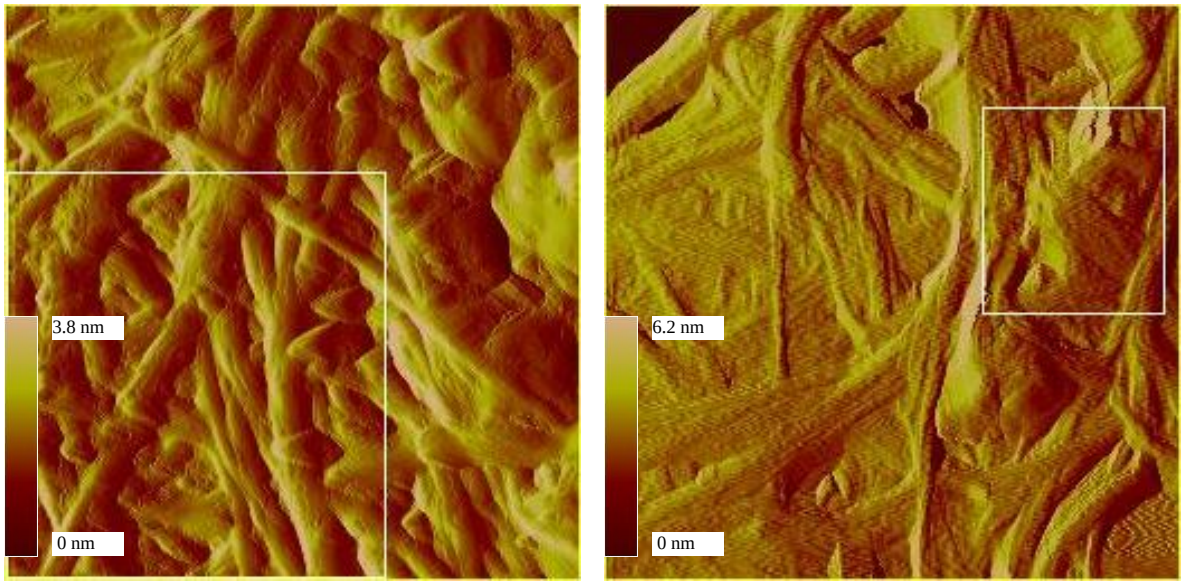

Both image are 3 x 3µm

Figure B-9. AFM Images of dried BC grown in 5wt% PEO1-modified HS medium.

Computation of Equilibrium Melting Temperature

(Using MatchCad)

From experimental line Tm vs Tc, let a1 = slope, b1 = intercept, x1 = Tc and y1 = Tm
and the line is y1 = a1*x1 +b1
From theoretical line, let y = Tm, x = Tc and the line is y = x

To determine the equilibrium temperature, the experimental line and the theretical line has to intercept or meet, thus an extrapolation has to be done so that x = a1*x1 + b1 and find x=x1

CALCULATIONS

Pure PEO1

$a1_{PEO1} := 0.217$ $b1_{PEO1} := 57.958C$ $x_{PEO1} := 1C$

Given

$a1_{PEO1} \cdot x_{PEO1} + b1_{PEO1} = x_{PEO1}$

$y_{PEO1} := \text{Find}(x_{PEO1})$

$y_{PEO1} = 74.087C$ T_{eq} of PEO1

With 1wt% initial PEO1

$a1_{BC\_PEO1} := 0.235$ $b1_{BC\_PEO1} := 54.16C$ $x_{BC\_PEO1} := 1C$

Given

$y_{BC\_PEO1} := \text{Find}(x_{BC\_PEO1})$

$y_{BC\_PEO1} = 70.816C$ T_{eq} of BC/PEO1 sample

Calculation of χ_{12}

Molecular weights of repeating units:

$T_{m0\_PEO1} := 74.1C$

$T_{m\_blend} := 70.8C$

Equilibrium Temperatures

$Mw_{BC} := 162.1\frac{gm}{mol}$ (Nishio et al 1989)

$Mw_{PEO1} := 44\frac{gm}{mol}$ (Mark 1999)

Density:

$\rho_{BC} := 1.51\frac{gm}{cm^3}$ (Nishio et al 1989)

$\rho_{PEO1} := 1.09\frac{gm}{cm^3}$ (Nishio et al 1989)

Molar volume of repeating units:

$V_{BC} := \frac{Mw_{BC}}{\rho_{BC}}$ $V_{BC} = 107.351\frac{cm^3}{mol}$

$V_{PEO1} := \frac{Mw_{PEO1}}{\rho_{PEO1}}$ $V_{PEO1} = 40.367\frac{cm^3}{mol}$

Enthalpy of fusion

$\Delta Hf_{PEO1} := 8.85\,10^3\frac{J}{mol}$ (Mark 1999)

From the blend:

Mass per 1 gram of blend:

$m_{BC} := 0.53gm$

$m_{PEO1} := 0.47gm$

Volume per of each component in 1 gram blend

$v_{BC} := \frac{m_{BC}}{\rho_{BC}}$ $v_{BC} = 0.351cm^3$

$v_{PEO1} := \frac{m_{PEO1}}{\rho_{PEO1}}$ $v_{PEO1} = 0.431cm^3$

Volume fraction of BC:

$v_{BC} := \frac{v_{BC}}{v_{BC} + v_{PEO1}}$

$v_{BC} = 0.449$

From the plot of ν_{BC}^{2} vs $\Delta T = T_{m0\_PEO1} - T_{m\_blend}$

$slope := 17.28C$

Solve B from $\Delta T = -T_{m0\_PEO1}\left(\frac{V_{PEO1}}{\Delta Hf_{PEO1}}\right)\cdot B\cdot\nu_{BC}^{2}$

B = interaction energy density characteristics

of the two components

$$B := \frac{slope}{-T_{m0\_PEO1}\left(\frac{V_{PEO1}}{\Delta Hf_{PEO1}}\right)} \qquad B = -51.126\frac{J}{cm^3} \qquad B = -12.211\frac{cal}{cm^3}$$

Solving the thermodynamic interaction parameter χ_{12}

$B = RT\cdot\left(\frac{\chi_{12}}{V_{BC}}\right)$ $T := (75 + 273)K$ at 75C same with Nishio 1989

$R := 8.31\frac{J}{K\cdot mol}$

$\chi_{12} := \frac{B\cdot V_{BC}}{R\cdot T}$

$\chi_{12} = -1.898$

Production Yield

Initial PEO wt% in HS medium	Wt% D-glucose conversion	Wt% PEO conversion
0.5	15	40
1	13	22
2	14	29
3	14	31
5	7	16

Table B-1. Wt% conversion of D-glucose to BC and PEO1 to nanocomposite.

References

Mark, J.E. (ed) (1999). *Polymer Data Handbook*. New York: Oxford University Press.

Nishio, Y., Naoto, H. & Toshisada, T. (1989). Thermal Analysis of Cellulose/Poly(ethylene oxide) Blends. *Polymer Journal* 21, 347-351.

APPENDIX C: BC/PVA NANOCOMPOSITE DATA

TEM Images

	Widths(nm)
Individual fibrils	17.1±5.2
ribbons	94.0±31.0

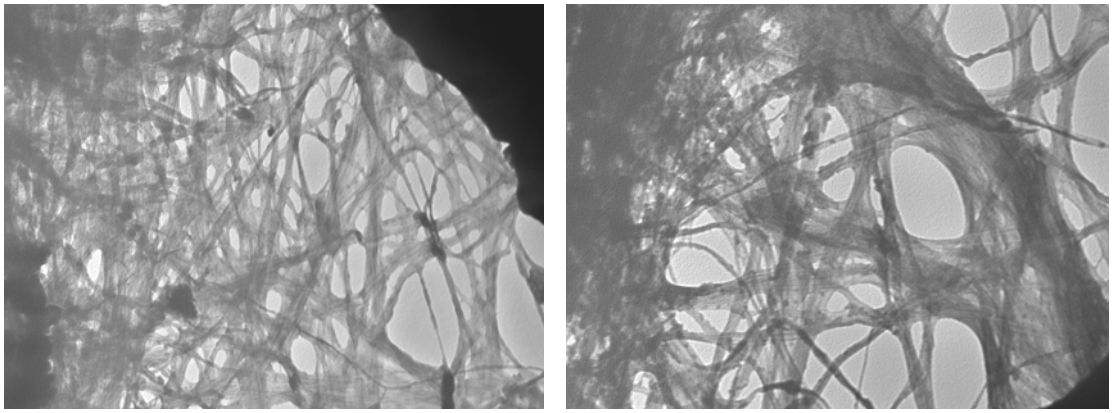

Figure C-1. TEM Images of BC grown in unmodified HS medium.

	Widths(nm)
Individual fibrils	10.6±1.6
ribbons	43.4±6.8

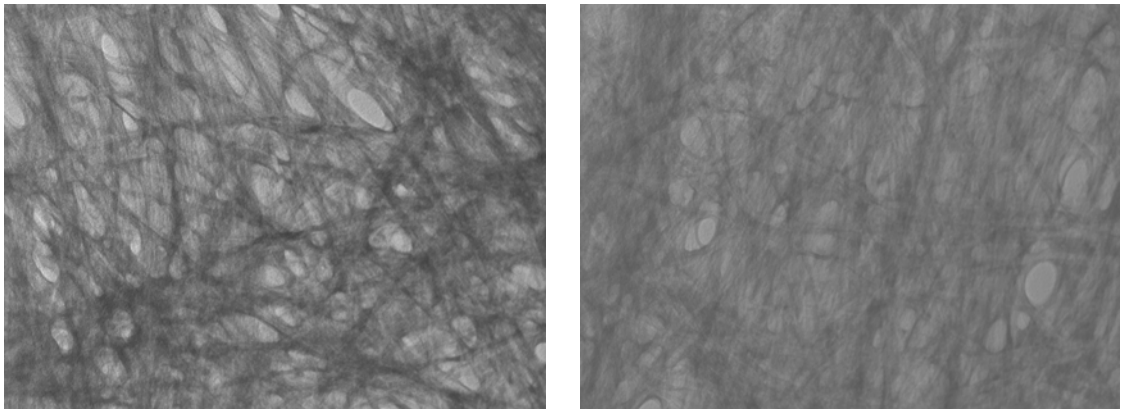

Figure C-2. TEM Images of BC grown in 1wt% PVA-modified HS medium.

	Widths(nm)
Individual fibrils	9.8±1.6
ribbons	-

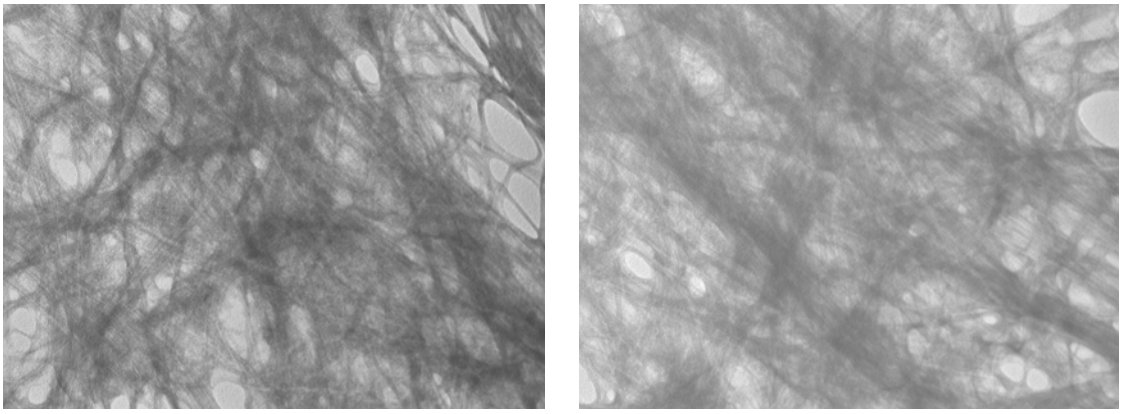

Figure C-3. TEM Images of BC grown in 5wt% PVA-modified HS medium.

	Widths(nm)
Individual fibrils	9.7±1.2
ribbons	-

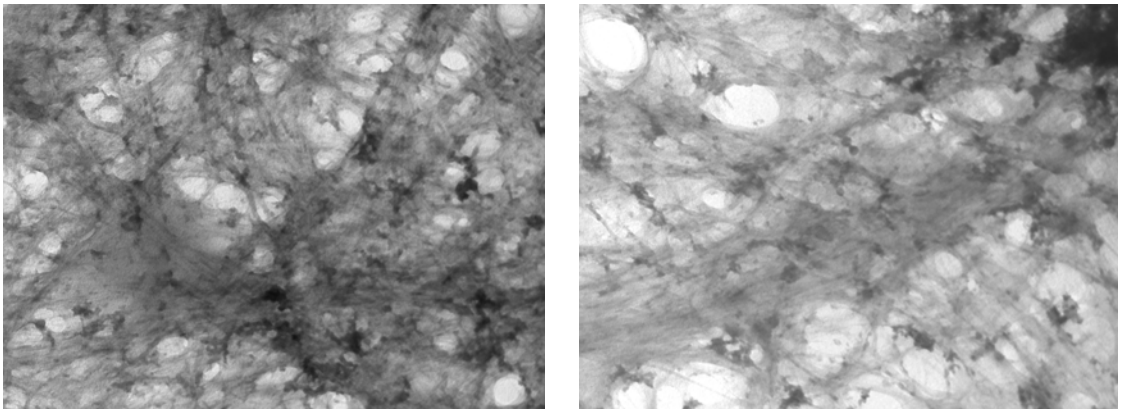

Figure C-4. TEM Images of BC grown in 9wt% PVA-modified HS medium.

AFM Images

The area inside the rectangular white outline is the region where bearing and roughness was analyzed.

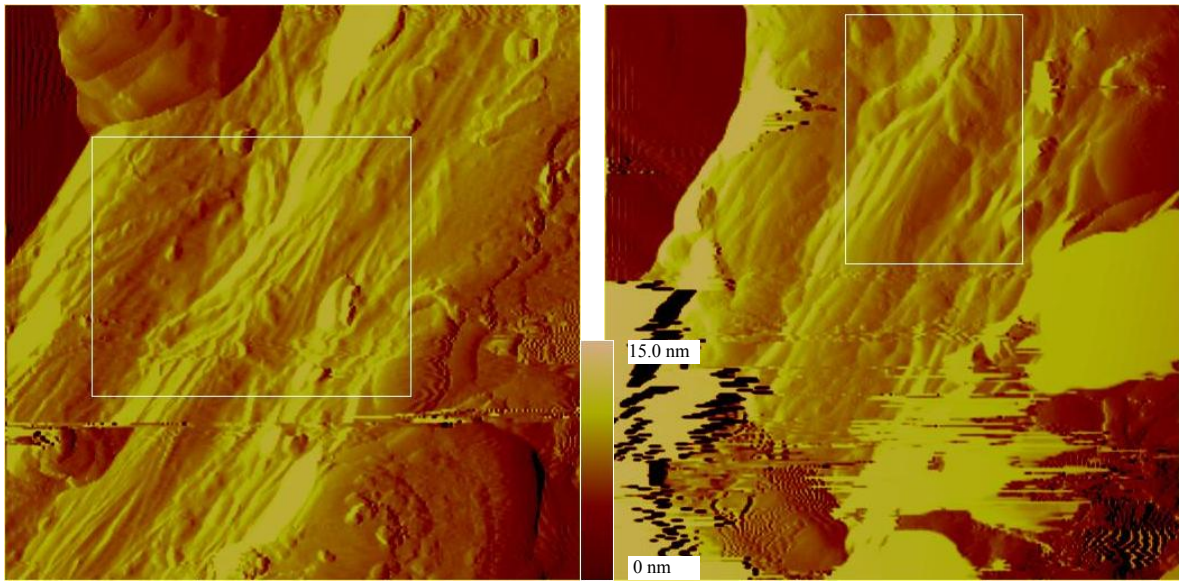

Figure C-5. AFM images of dried BC grown in 1wt% PVA-modified HS medium.

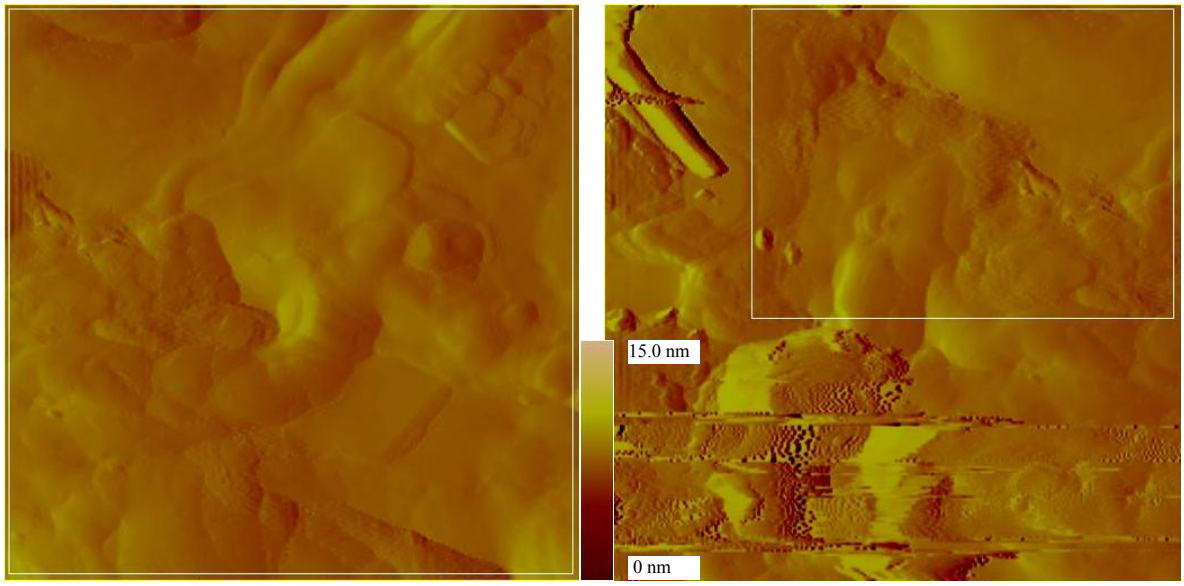

Figure C-6. AFM Images of dried BC grown in 5wt% PVA-modified HS medium.

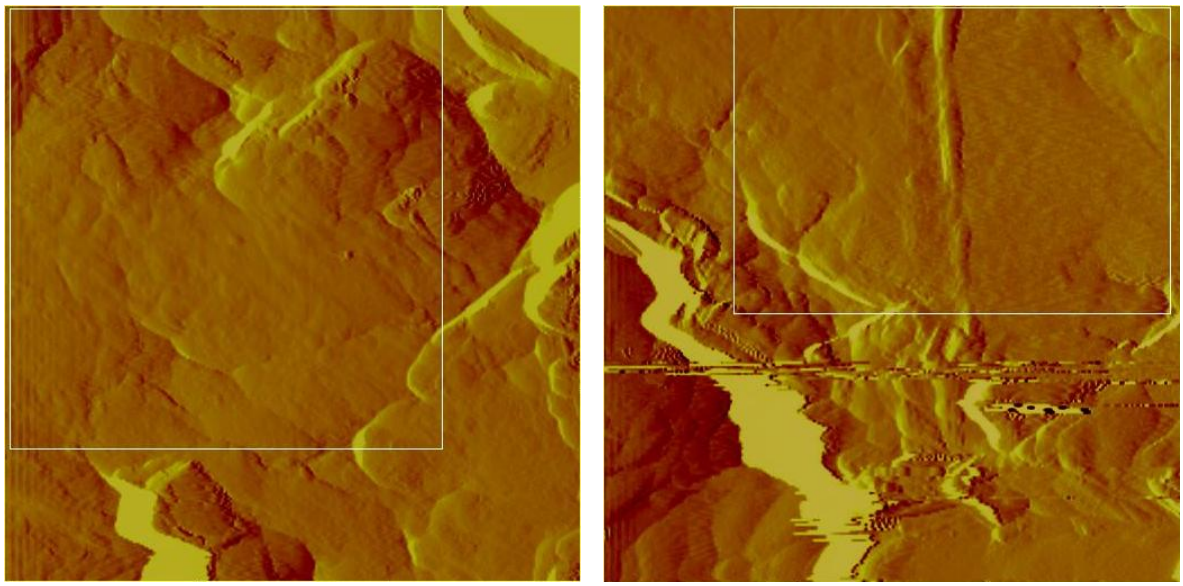

Figure C-7. AFM Images of dried BC grown in 9wt% PVA-modified HS medium.

FT-IR Data

Calibration FT-IR data (microcrystalline cellulose/PVA blend)

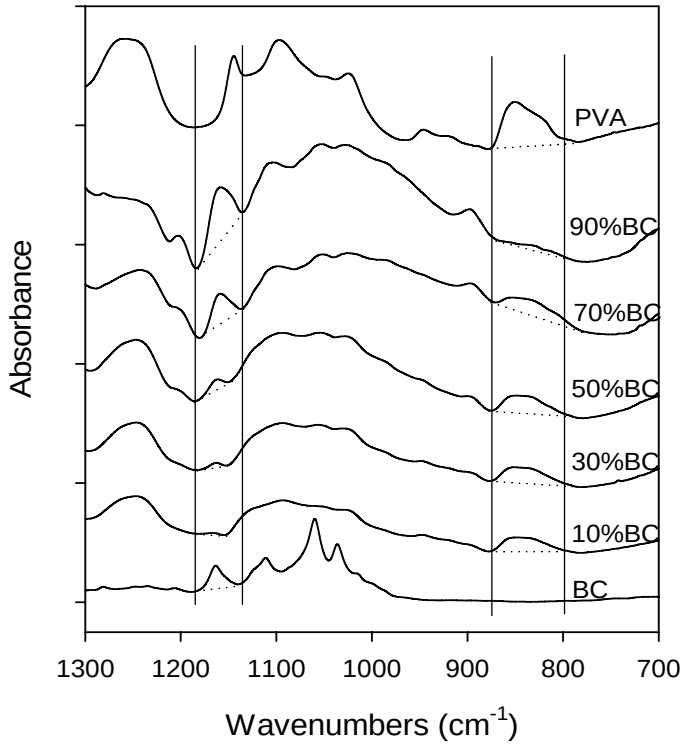

Figure C-8. A_{1165}/A_{850} from FT-IR data of microcrystalline cellulose/PVA blend as calibration to use for composition analysis of the produced BC/PVA nanocomposites.

Wt% cellulose	A_{1165}/A_{850}
10	0.022±0.006
30	0.110±0.037
50	0.159±0.049
70	0.698±0.130
90	9.476±0.447

Table C-1. Known cellulose wt% and A1165/A850 values for calibration to use for compositional analysis of produced BC/PVA nanocomposites.

Production Yield

Initial PVA wt% in HS medium	Wt% D-glucose conversion	Wt% PVA conversion
1	30	3
2	44	3
3	35	4
4	51	8
5	55	8
7	38	9
9	17	17

Table C-2. Wt% conversion of D-glucose to BC and PVA to nanocomposite.

Solubility Parameter Computations

(Using MathCad)

Cellulose

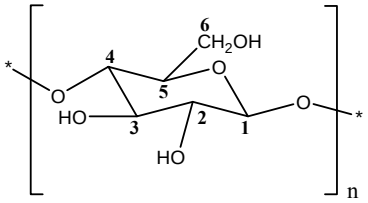

Parameters for functional groups taken from VanKrevelen and Hoftyzer 1976.

$F_{t\_CH2} := 269$
$F_{p\_CH2} := 0$
$V_{CH2} := 15.55$
$\Delta_{T\_CH2} := 0.02$
$F_{t\_OHsec} := 591$
$F_{p\_OHsec} := 591$
$V_{OHsec} := 12.45$
$\Delta_{T\_OHsec} := 0.049$

$F_{t\_CH} := 176$
$F_{p\_CH} := 0$
$V_{CH} := 9.56$
$\Delta_{T\_CH} := 0.013$
$F_{t\_O} := 235$
$F_{p\_O} := 216$
$V_{O} := 6.45$
$\Delta_{T\_O} := 0.018$

$F_{t\_OHprim} := 675$
$F_{p\_OHprim} := 675$
$V_{OHprim} := 12.45$
$\Delta_{T\_OHprim} := 0.049$

Functional groups

$CH_2 := 1$ $CH := 5$ $OH_{prim} := 1$ $OH_{sec} := 2$ $O := 2$

Hoy Calculation

$$F_t := CH_2 \cdot F_{t\_CH2} + CH \cdot F_{t\_CH} + OH_{prim} \cdot F_{t\_OHprim} + OH_{sec} \cdot F_{t\_OHsec} + O \cdot F_{t\_O}$$

$$F_p := CH_2 \cdot F_{p\_CH2} + CH \cdot F_{p\_CH} + OH_{prim} \cdot F_{p\_OHprim} + OH_{sec} \cdot F_{p\_OHsec} + O \cdot F_{p\_O}$$

$$V := CH_2 \cdot V_{CH2} + CH \cdot V_{CH} + OH_{prim} \cdot V_{OHprim} + OH_{sec} \cdot V_{OHsec} + O \cdot V_O$$

$$\Delta_T := CH_2 \cdot \Delta_{T\_CH2} + CH \cdot \Delta_{T\_CH} + OH_{prim} \cdot \Delta_{T\_OHprim} + OH_{sec} \cdot \Delta_{T\_OHsec} + O \cdot \Delta_{T\_O}$$

$$\alpha := \frac{777 \cdot \Delta_T}{V} \qquad n := \frac{0.5}{\Delta_T} \qquad B := 277$$

$$\delta_{BC} := \frac{F_t + \frac{B}{n}}{V} \qquad \delta_{h\_BC} := \delta_{BC} \cdot \left(\frac{\alpha - 1}{\alpha} \right)^{\frac{1}{2}}$$

$$\delta_{p\_BC} := \delta_{BC} \cdot \left(\frac{1}{\alpha} \cdot \frac{F_p}{F_t + \frac{B}{n}} \right)^{\frac{1}{2}} \qquad \delta_{d\_BC} := \left(\delta_{BC}^{\,2} - \delta_{p\_BC}^{\,2} - \delta_{h\_BC}^{\,2} \right)^{\frac{1}{2}}$$

$\delta_{BC} = 31.906$ $\delta_{h\_BC} = 21.509$

$\delta_{p\_BC} = 18.727$ $\delta_{d\_BC} = 14.305$

PEO

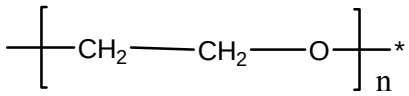

Functional groups

$CH_2 := 2$ $O := 1$

Hoy Calculation

$F_t := CH_2 \cdot F_{t\_CH2} + O \cdot F_{t\_O}$

$F_p := CH_2 \cdot F_{p\_CH2} + O \cdot F_{p\_O}$

$V := CH_2 \cdot V_{CH2} + O \cdot V_O$

$\Delta_T := CH_2 \cdot \Delta_{T\_CH2} + O \cdot \Delta_{T\_O}$

$\alpha := \frac{777 \cdot \Delta_T}{V}$ $n := \frac{0.5}{\Delta_T}$ $B := 277$

$\delta_{PEO} := \frac{F_t + \frac{B}{n}}{V}$ $\delta_{h\_PEO} := \delta_{PEO} \cdot \left(\frac{\alpha - 1}{\alpha} \right)^{\frac{1}{2}}$

$\delta_{p\_PEO} := \delta_{PEO} \cdot \left(\frac{1}{\alpha} \cdot \frac{F_p}{F_t + \frac{B}{n}} \right)^{\frac{1}{2}}$ $\delta_{d\_PEO} := \left(\delta_{PEO}^{\ 2} - \delta_{p\_PEO}^{\ 2} - \delta_{h\_PEO}^{\ 2} \right)^{\frac{1}{2}}$

$\delta_{PEO} = 21.442$ $\delta_{h\_PEO} = 8.756$

$\delta_{p\_PEO} = 10.138$ $\delta_{d\_PEO} = 16.742$

PVA

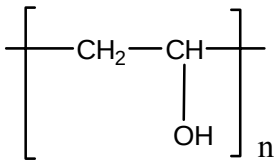

Functional groups

$CH_2 := 1$ $CH := 1$ $OH_{sec} := 1$

Hoy Calculation

$F_t := CH_2 \cdot F_{t\_CH2} + CH \cdot F_{t\_CH} + OH_{sec} \cdot F_{t\_OHsec}$

$F_p := CH_2 \cdot F_{p\_CH2} + CH \cdot F_{p\_CH} + OH_{sec} \cdot F_{p\_OHsec}$

$V := CH_2 \cdot V_{CH2} + CH \cdot V_{CH} + OH_{sec} \cdot V_{OHsec}$

$\Delta_T := CH_2 \cdot \Delta_{T\_CH2} + CH \cdot \Delta_{T\_CH} + OH_{sec} \cdot \Delta_{T\_OHsec}$

$\alpha := \frac{777 \cdot \Delta_T}{V}$ $n := \frac{0.5}{\Delta_T}$ $B := 277$

$\delta_{PVA} := \frac{F_t + \frac{B}{n}}{V}$ $\delta_{h\_PVA} := \delta_{PVA} \cdot \left(\frac{\alpha - 1}{\alpha} \right)^{\frac{1}{2}}$

$\delta_{p\_PVA} := \delta_{PVA} \cdot \left(\frac{1}{\alpha} \cdot \frac{F_p}{F_t + \frac{B}{n}} \right)^{\frac{1}{2}}$ $\delta_{d\_PVA} := \left(\delta_{PVA}^{\ 2} - \delta_{p\_PVA}^{\ 2} - \delta_{h\_PVA}^{\ 2} \right)^{\frac{1}{2}}$

$\delta_{PVA} = 28.792$ $\delta_{h\_PVA} = 18.447$

$\delta_{p\_PVA} = 16.342$ $\delta_{d\_PVA} = 14.887$

Units of δ is $\left(\frac{J}{cm^3} \right)^{1/2}$

Δδ

$$\Delta\delta_{BC\_PEO} := \left[\left(\delta_{d\_BC} - \delta_{d\_PEO}\right)^2 + \left(\delta_{p\_BC} - \delta_{p\_PEO}\right)^2 + \left(\delta_{h\_BC} - \delta_{h\_PEO}\right)^2 \right]^{\frac{1}{2}}$$

$$\Delta\delta_{BC\_PVA} := \left[\left(\delta_{d\_BC} - \delta_{d\_PVA}\right)^2 + \left(\delta_{p\_BC} - \delta_{p\_PVA}\right)^2 + \left(\delta_{h\_BC} - \delta_{h\_PVA}\right)^2 \right]^{\frac{1}{2}}$$

$\Delta\delta_{BC\_PEO} = 15.568$

$\Delta\delta_{BC\_PVA} = 3.925$

References

Van Krevelen, W., Hoftyzer, P.J. (1976). *Properties of Polymers*, 2nd Edition. Elsevier, Amsterdam, 189-225.